

UCSF

UC San Francisco Electronic Theses and Dissertations

Title

Impact of Heterotypic Interactions on Cardiomyocyte Fate and Function in 3D Microscale Models of Myocardial Tissue from Human Pluripotent Stem Cells

Permalink

<https://escholarship.org/uc/item/8w34w45p>

Author

Matthys, Oriane B.

Publication Date

2020

Peer reviewed|Thesis/dissertation

Impact of Heterotypic Interactions on Cardiomyocyte Fate and Function in 3D
Microscale Models of Myocardial Tissue from Human Pluripotent Stem Cells

by
Oriane Matthys

DISSERTATION
Submitted in partial satisfaction of the requirements for degree of
DOCTOR OF PHILOSOPHY

in
Bioengineering
in the
GRADUATE DIVISION

of the
UNIVERSITY OF CALIFORNIA, SAN FRANCISCO
AND
UNIVERSITY OF CALIFORNIA, BERKELEY

Approved:

DocuSigned by:

Todd C. McDevitt

38EF3B1D3234412...

Todd C. McDevitt

Chair

DocuSigned by:

Julie Beth Sneddon

DocuSigned by:

Aaron Streets

E246C3D2787447B...

Julie Beth Sneddon

Aaron Streets

Committee Members

Copyright 2020

by

Oriane B. Matthys

ACKNOWLEDGEMENTS

I am truly lucky to have been able to pursue my PhD in an incredibly supportive environment, and as such, I have many people to thank for pushing me through the scientific and emotional rollercoaster of graduate school.

First and foremost, I would not have come to the Bay Area if it weren't for my advisor, Dr. Todd McDevitt. I initially planned to join the Bioengineering PhD Program at Georgia Tech while Todd was still there, and 2 weeks after committing to the program, Todd emailed me to say he might be moving but couldn't tell me anything more. Luckily, I had planned to defer matriculation for a year, and a few months later, Todd told me he had accepted a position in San Francisco at the Gladstone Institutes. I moved to San Francisco in January 2015 without ever having met Todd in person, but it all worked out better than I could have hoped. I want to thank Todd for holding me to high expectations, pushing me to think critically, and continually cultivating my excitement for scientific research and big ideas. I could not have asked for a better mentor and I am excited to remain in the McDevitt family as the newest alumna. And of course, without Todd I wouldn't have met Meg, who has become my North Star for all things cooking, wine, and travel. Thank you Meg for supporting me within and outside of Gladstone, and for feeding me with leftovers when you cooked enough food for an army. And thanks for sharing Sapphire, Wrigley, Bella, and Addie, who gave me the puppy support and love necessary for surviving grad school.

I would also like to thank my committee members Dr. Julie Sneddon and Dr. Aaron Streets for their crucial feedback and support of my thesis project. They taught me how to drill down to the fundamental experiments/questions that helped determine the best research direction to pursue, and they also provided much-needed advice and support in helping me figure out my career path.

The joint nature of my PhD program, which combined UC Berkeley's engineering department with UCSF's medical programs, provided a diverse learning environment where I was able to take classes ranging from stem cell biology to biophotonics, and also opened up a number of collaborative opportunities that furthered my research projects. However, with this multi-campus program came logistical challenges; therefore, I need to thank the peers in my cohort with whom I formed a carpool/support group when we were living in Berkeley, working at UCSF's Mission Bay campus, and taking classes at UCSF's Parnassus campus.

I was fortunate in that my lab's location at the Gladstone Institutes gave me access to many additional opportunities and resources, and I am thankful to have been a part of the close-knit Gladstone community. I especially became close to other graduate students through founding the Gladstone GO organization, as well as to members of GICD, who I passed by many times per day as I walked from our lab space to the Stem Cell Core on the other side of the floor. The quality of my science was no doubt elevated because of our collaborators and facilities at Gladstone, and for that I want to especially thank the Stem Cell Core, Light Microscopy and Histology Core, Genomics Core, and Bioinformatics Core, as well as Giovanni Maki in the Gladstone art department who taught me the importance of font choice and illustrated most of the graphics that appear in my papers. I also have Gladstone to thank for hugely impacting my personal life—I met my boyfriend Gabriel Rubio when he worked for a year as a Sarnoff Fellow in the Srivastava lab.

My success in graduate school can mainly be attributed to the supportive, inclusive, and fun-loving environment of the McDevitt Lab. I started as the lab was transitioning from Georgia Tech to Gladstone, and when I first arrived Jenna Wilson was the only other person in San Francisco. She was instrumental in acclimating me to the lab and to Todd, helping me decipher my notes as I emerged confused and overwhelmed from my first few meetings with Todd. My first

lab cohort (Jenna Wilson, Josh Zimmermann, Jessie Butts, Dylan McCreedy, and Tracy Hookway) played such a special role in the beginning of my training, as we all explored our new city together and became close as a result. Our first lab manager, Amy Foley, quickly became one of my first friends in San Francisco, and still continues to support and encourage me from afar. I am thankful for the support of lab members Ashley Libby, Ariel Kauss, and David Joy, as we all went through classes, quals, conferences, and everything grad school together. Seeing the younger students in the lab (Ivana Vasic, Jasmine King, Emily Bulger, and Nick Elder) navigate their projects and grad school firsts, I was finally able to appreciate how much we all accomplish in such a short period of time (though it seems never-ending in the moment). To the postdocs in the lab (Tracy Hookway, Ana Silva, Vaishaali Natarajan, Serah Kang, Diwakar Turaga), thank you for giving me visible evidence that it's possible to make it through grad school, and for your guidance throughout many aspects of my research projects and career explorations (and Ana, thank you for greeting me with an original good morning song every day when you walked into lab). I owe a lot to Team Cardio in the lab (Tracy Hookway, Ana Silva, Ariel Kauss, Serah Kang, Sarah Rockwood, Jasmine King), who provided crucial insight into experimental planning, troubleshooting advice, and cell-sitting services whenever needed (special shout out to Ron Manlapaz for running many of my differentiations). I learned the most when I was mentoring others, and for that I am grateful to Karli Hanson, Jacqueline Yee, Beulah Dadala, Christian Lehmann, and Yohanna Gebremedhin, who all advanced my projects with their insightful questions and re-invigorated my excitement for scientific research when I witnessed their own. My swolomate, Jessie Butts: thank you for getting me out of the lab and into the gym, teaching me the craft of cocktail mixology, and spending many girls cooking/"treat yourself" days together. I also could not have succeeded without the mentorship and friendship of Tracy Hookway. Thank you Tracy for teaching me literally

everything that is in this thesis. But thank you more for sharing with me the many cooking nights, bottles of wine, ski trips, and Barley.

I would not be in science in the first place if not for my family. Both of my parents are professors at UCSB, which meant that my childhood included fun, at-home science kits and the coolest science fair experiments. They never pushed for me to major in engineering or attend graduate school, but my early exposure to the excitement of scientific discovery was enough for me to decide to do so on my own. I am also thankful that I had family close by in the Bay Area, for when I needed to escape from lab and recharge. My little sister, Madeline, moved to San Francisco after she finished college, so we were able to spend the last few years living in the same city (and both working at UCSF!). I am also lucky that my cousin Caitlin and her family (husband Dave and kids Sammy, Bennett, and Emily) live in Berkeley, so I spent a lot of time hanging out at their house, cooking holiday dinners, playing with the kids, and traveling with them. And I am thankful that I gained new family in my time here, as Gabe's parents (Yvonne and Rene) and siblings (Corrina and Kyle, Krystle and Nestor) have become my own.

Lastly, I would not have made it through grad school without my support system—childhood friends (Karina, Anjali, Kelsey, Crystal, Petra, Carly), friends from Duke (Allison, Katie, Emilie, Mel, Kim, Nichols, Steven, Angela, Mike, Noelle, Katrina), and friends I made here (Yu-Jin, Danny, Sarah, Nathan), who kept me going with texts, calls, visits, and getaways. And to my boyfriend Gabe, with whom I have created a wonderful home in San Francisco, thank you for your encouragement and patience as I navigated the many ups and down of the PhD process.

CONTRIBUTIONS

Partial text from Chapter 1 is a reprint of the material as it appears in “Design Principles for Engineering of Tissues from Human Pluripotent Stem Cells” and “Engineering Human Organoid Development Ex Vivo-Challenges and Opportunities”. Partial text from Chapter 2 is a reprint of the material as it appears in “Self-Assembled Heterotypic Cardiac Spheroids from Human Pluripotent Stem Cells”. The texts of Chapters 3, 4, and 5 are reprints of the material as it appears in “Phenotypic Variation Between Stromal Cells Differentially Impacts Cardiac Tissue Function”, “Bi-directional Impacts of Heterotypic Interactions in Engineered 3D Human Cardiac Microtissues Revealed by Single-Cell RNA-Sequencing and Functional Analysis”, and “Single Cell Determination of Cardiac Microtissue Structure and Function Using Light Sheet Microscopy”, respectively. The co-authors listed in these publications directed and supervised the research that forms the basis of this dissertation.

**IMPACT OF HETEROTYPIC INTERACTIONS ON CARDIOMYOCYTE
FATE AND FUNCTION IN 3D MICROSCALE MODELS OF
MYOCARDIAL TISSUE FROM HUMAN PLURIPOTENT STEM CELLS**

ORIANE B. MATTHYS

ABSTRACT

Native cardiac tissue is comprised of many different cell types that work cooperatively for proper tissue function. Combining self-assembled tissue engineering strategies that provide a fully-defined platform to study pairwise interactions between different cardiac cell types, with human pluripotent stem cell (hPSC) technologies, such as robust differentiation strategies and genome editing capabilities, has enabled our comprehensive studies of heterotypic interactions between cardiomyocytes and various non-myocyte sources in order to determine the specific contributions of non-myocytes to cardiac microtissue fate and function. We approached these studies in a systematic manner with narrowing focus.

We first broadly tested the most commonly-used stromal cells in cardiac tissue engineering studies and found that the different sources of stromal cells (primary human-derived vs. stem cell-derived; from different types of primary tissues) were distinct in terms of their surface marker expression, morphometry, and gene expression. These differences carried over into their ability to support engineered cardiac tissue formation and function, where only primary human cardiac fibroblasts and primary human dermal fibroblasts paired with hPSC-cardiomyocytes resulted in microtissues with the most robust tissue self-assembly and advanced calcium handling function.

Since the tissue-specific cardiac fibroblasts were able to positively support cardiac microtissue culture, we further characterized the specific contributions of different types of non-myocytes (endothelial cells, fetal human cardiac fibroblasts, adult human cardiac fibroblasts) in the context of heterotypic cardiac microtissue phenotype and function, at the single-cell and tissue-level, respectively. We found that 1 week after tissue formation, the cardiac microtissues containing the cardiac fibroblasts displayed more mature calcium handling properties relative to the tissues that contained endothelial cells and the tissues made from only cardiomyocytes, and that the cardiomyocytes paired with the cardiac fibroblasts were transcriptionally distinct from cardiomyocytes from the other tissues. However, after extended culture duration (1 month), the distinction between cardiac microtissues with cardiac fibroblasts versus without was lost, with the cardiomyocytes exhibiting similar transcriptomic profiles and the tissues displaying similar calcium transients. Furthermore, at both time points, there were no discernable differences between the different age cardiac fibroblasts, potentially because the source (isolated from primary tissue) was a bigger mismatch with stem cell-derived cardiomyocytes than the ontogenic difference.

Inspired by the pairing of different technologies to assess single-cell-level phenotype in the context of microtissue-level function, we sought to further characterize individual cell properties within intact 3D microtissues in order to better link the single cell building blocks to tissue-level properties. We used light sheet fluorescence microscopy to quantify 3D heterotypic multicellular organization as well as identify individual cardiomyocyte functional heterogeneity within heterotypic cardiac microtissues. Overall, this study demonstrated that advanced imaging techniques can be a powerful tool to dissect complex heterotypic interactions without removing the cells from their 3D environment.

Lastly, to dig deeper into the mechanisms governing the heterotypic interactions between cardiomyocyte and non-myocytes in our 3D engineered microtissues, we first had to generate cardiac tissues made from entirely stem cell-derived cellular constituents in order to take advantage of the robust genome engineering strategies developed for hPSCs. We were able to generate entirely-isogenic tissues when two differentiation protocols for the derivation of cardiac fibroblasts were published in 2019. We evaluated the different hPSC-cardiac fibroblast subtypes generated by these protocols in our heterotypic cardiac microtissue platform and found that they behaved similarly to one another and to microtissues made with primary human fetal cardiac fibroblasts in their ability to quickly self-assemble into tissues and their calcium handling function. We then knocked down one of the most-cited gap junctions that connects cardiomyocytes and cardiac fibroblasts in the heart, connexin 43, in the hPSC-derived cardiac fibroblasts using an inducible CRISPR interference method. Heterotypic cardiac microtissues generated with the knockdown fibroblasts displayed diminished calcium handling function, indicating a potential role for cardiac fibroblast support of cardiomyocyte function. Further mechanistic understanding of the interactions between cardiac cell populations can be determined in a similar manner, within the context of our fully-defined, tailored microtissue platform.

Taken together, this body of work provides a basis for the study of multicellular heterotypic interactions in 3D engineered models of myocardial tissue from human pluripotent stem cells. Future studies can build on this work by generating more complex microtissue constructs (i.e. incorporating more than two cell types, or modulating the cell types) as well as modeling cardiac diseases in tissue format. Combining genome editing, advanced imaging, and next-generation sequencing technologies enables customizable generation and comprehensive characterization of the multicellular interactions within engineered heterotypic tissue constructs.

TABLE OF CONTENTS

CHAPTER 1: INTRODUCTION	1
1.1. Overview.....	1
1.2. Cellular composition of the native human heart.....	1
1.2.1. Cardiomyocytes.....	2
1.2.2. Endothelial cells.....	3
1.2.3. Cardiac fibroblasts.....	4
1.3. Tissue engineering strategies.....	6
1.3.1. Tissue assembly considerations.....	7
1.3.2. Introducing phenotypic heterogeneity within multicellular constructs.....	9
1.3.3. Directing higher-order organization and tissue architecture.....	12
1.3.4. Engineering self-assembled, independently-merged, externally-imposed heterotypic cardiac microtissues.....	15
1.4. Advanced technological characterization of 3D heterotypic cardiac microtissues.....	17
1.4.1. Functional testing.....	18
1.4.2. Phenotypic analysis by single-cell RNA-sequencing.....	20
1.4.3. In situ characterization of 3D multicellular organization by light sheet fluorescence microscopy.....	21
1.5. Concluding remarks.....	22
1.6. Bibliography.....	23
CHAPTER 2: SELF-ASSEMBLED HETEROTYPIC CARDIAC MICROTISSUES FROM HUMAN PLURIPOTENT STEM CELLS	37
2.1. Introduction.....	37

2.2. Methods for the self-assembly of cardiac microtissue spheroids.....	37
2.2.1. Material preparation.....	37
2.2.2. Replica molding to fabricate sheets of PDMS microwell molds.....	38
2.2.3. Repeat replica molding to create arrayed circular inverse molds.....	40
2.2.4. Casting agarose microwell molds off of PDMS arrayed inverse molds.....	41
2.2.5. Cell seeding into agarose microwell molds.....	44
2.2.6. Removing microtissues from agarose microwell molds.....	46
2.2.7. Rotary suspension culture.....	48
2.3. Methods for the self-assembly of cardiac tissue rings.....	49
2.3.1. Material preparation.....	49
2.3.2. Replica molding to fabricate PDMS inverse mold.....	49
2.3.3. Casting agarose ring mold off of PDMS inverse mold.....	49
2.3.4. Cell seeding into agarose ring molds.....	50
2.4. Functional testing of engineered cardiac tissues.....	51
2.4.1. Voltage imaging.....	51
2.4.2. Calcium imaging.....	52
2.4.3. Contractile force testing.....	52
2.5. Conclusions.....	54
2.6. Bibliography.....	55

CHAPTER 3: PHENOTYPIC VARIATION BETWEEN STROMAL CELLS

DIFFERENTIALLY IMPACTS CARDIAC TISSUE FUNCTION.....	57
3.1. Introduction.....	57
3.2. Materials and methods.....	58

3.2.1. Stromal cell culture.....	58
3.2.2. Derivation of iPSC-derived fibroblasts.....	59
3.2.3. Flow cytometry.....	61
3.2.4. Immunocytochemistry.....	61
3.2.5. Image acquisition and morphometric assessment.....	61
3.2.6. Principal component analysis.....	62
3.2.7. PhenoRipper.....	62
3.2.8. RNA sequencing.....	63
3.2.9. Pluripotent stem cell culture.....	63
3.2.10. Cardiomyocyte differentiation.....	63
3.2.11. Cardiac microtissue formation.....	64
3.2.12. Gene expression analysis.....	65
3.2.13. Calcium imaging analysis.....	66
3.2.14. Histology and immunofluorescent staining.....	67
3.2.15. Statistics.....	68
3.3. Results.....	68
3.3.1. Stromal populations have distinct expression and morphological profiles....	68
3.3.2. Stromal populations have distinct transcriptomic profiles.....	74
3.3.3. Stromal cells enable variable cardiac microtissue formation.....	76
3.3.4. Stromal cell inclusion yields phenotypic variation among cardiac tissues....	80
3.3.5. Stromal cell modulation of cardiac microtissue calcium handling.....	81
3.4. Discussion.....	82
3.5. Conclusions.....	88

3.6. Bibliography.....	89
CHAPTER 4: BI-DIRECTIONAL IMPACTS OF HETEROTYPIC	
INTERACTIONS IN ENGINEERED 3D HUMAN CARDIAC MICROTISSUES	
REVEALED BY SINGLE-CELL RNA-SEQ AND FUNCTIONAL ANALYSIS.....	97
4.1. Introduction.....	97
4.2. Materials and methods.....	98
4.2.1. Pluripotent stem cell culture.....	98
4.2.2. Cardiomyocyte differentiation.....	98
4.2.3. Endothelial cell differentiation.....	99
4.2.4. Fibroblast cell culture.....	99
4.2.5. Cardiac microtissue formation.....	100
4.2.6. Histology and immunofluorescence staining.....	100
4.2.7. Calcium imaging analysis.....	101
4.2.8. Statistics.....	102
4.2.9. Single-cell RNA-sequencing sample preparation and sequencing.....	102
4.2.10. Single-cell RNA-sequencing zinbwave reduction.....	103
4.2.11. Single-cell RNA-sequencing HOPACH analysis.....	104
4.2.12. In situ hybridization.....	105
4.3. Results.....	105
4.3.1. Non-myocytes enable rapid microtissue compaction.....	105
4.3.2. Non-myocytes form a core within heterotypic cardiac microtissues.....	106
4.3.3. Cardiac fibroblasts accelerate calcium handling properties of cardiac microtissues.....	107

4.3.4. Cardiomyocyte phenotype changes as a result of cardiac fibroblast co-culture.....	110
4.3.5. Non-myocyte phenotypic changes as a result of heterotypic-co-culture.....	115
4.4. Discussion.....	120
4.5. Conclusions.....	125
4.6. Bibliography.....	127
 CHAPTER 5: SINGLE CELL DETERMINATION OF CARDIAC MICROTISSUE STRUCTURE AND FUNCTION USING LIGHT SHEET MICROSCOPY.....	
5.1. Introduction.....	133
5.2. Materials and methods.....	134
5.2.1. Cardiac fibroblast cell culture.....	134
5.2.2. Cardiomyocyte differentiation.....	134
5.2.3. Cardiac microtissue formation.....	135
5.2.4. Immunofluorescence staining.....	135
5.2.5. Structural light sheet microscopy.....	136
5.2.6. Cell classification and spatial quantification.....	137
5.2.7. Functional light sheet microscopy.....	138
5.2.8. Statistics.....	138
5.3. Results.....	139
5.3.1. Multi-view light sheet imaging enables high resolution 3D reconstruction of cardiac microtissues.....	139
5.3.2. Localization of labeled cells allows for cell identity classification and intercellular spatial analyses.....	141

5.3.3. Live light sheet calcium imaging enables detection of functional heterogeneity between engineered cardiac microtissues.....	143
5.4. Discussion.....	146
5.5. Conclusions.....	151
5.6. Bibliography.....	153
CHAPTER 6: MODULATING CARDIOMYOCYTE-CARDIAC FIBROBLAST INTERACTIONS IN ISOGENIC HETEROTYPIC CARDIAC MICROTISSUES.....	
156	
6.1. Introduction.....	156
6.2. Materials and methods.....	157
6.2.1. Cardiomyocyte differentiation from hiPSCs.....	157
6.2.2. Differentiation of hiPSC-cardiac fibroblasts from epicardial cells.....	157
6.2.3. Differentiation of hiPSC-cardiac fibroblasts from second heart field-like progenitors.....	158
6.2.4. Primary human cardiac fibroblast culture.....	159
6.2.5. DOX-inducible GJA1 knockdown in hiPSCs via CRISPRi.....	159
6.2.6. GJA1 knockdown in hiPSC-cardiac fibroblasts.....	160
6.2.7. Cardiac microtissue formation.....	160
6.2.8. Calcium imaging.....	160
6.2.9. Statistics.....	161
6.3. Results.....	161
6.3.1. Derivation of subtype-specific cardiac fibroblasts from human pluripotent stem cells.....	161
6.3.2. Cardiac fibroblasts promote robust cardiac microtissue assembly.....	162

6.3.3. Cardiac fibroblast source does not impact heterotypic cardiac microtissue calcium handling.....	164
6.3.4. GJA1 knockdown in CFs attenuates calcium handling function.....	165
6.4. Conclusions.....	166
6.5. Bibliography.....	169
CHAPTER 7: FUTURE CONSIDERATIONS.....	171
7.1. Altering the timing of cardiac heterotypic interactions.....	171
7.2. Increasing the heterogenic complexity of engineered cardiac microtissues.....	172
7.3. Concluding remarks.....	173
7.4. Bibliography.....	174
APPENDIX A: CARDIOMYOCYTE ENRICHMENT PROTOCOL.....	175

LIST OF FIGURES

Figure 1.1.	Defining characteristics of tissue formation from hPSCs.....	7
Figure 1.2.	Temporal relationship between cardiomyocyte functional measures.....	18
Figure 2.1.	Replica molding to fabricate sheets of PDMS microwell molds.....	39
Figure 2.2.	Replica molding to create arrayed circular inverse molds.....	40
Figure 2.3.	Casting microwell inverse molds off of PDMS arrayed circular inverse molds.....	42
Figure 2.4.	Slanted agarose microwell molds.....	43
Figure 2.5.	Self-assembly and long-term culture of heterotypic cardiac microtissue spheroids.....	45
Figure 2.6.	Additional cardiac microtissue constituents.....	46
Figure 2.7.	Poor tissue self-assembly.....	47
Figure 2.8.	Rotary tissue culture problems.....	48
Figure 2.9.	Self-assembled cardiac ring formation.....	51
Figure 2.10.	Functional imaging of cardiac microtissue spheroids.....	52
Figure 2.11.	Contractile force testing of cardiac rings.....	53
Figure 3.1.	Flow cytometry analysis of stromal cell surface markers.....	69
Figure 3.2.	Morphometric analysis of stromal cell populations.....	70
Figure 3.3.	Principal component analysis of morphometric measurements of F-actin- labeled stromal cells.....	72
Figure 3.4.	PhenoRipper analysis of images of F-actin-labeled stromal cells.....	73
Figure 3.5.	Additional PhenoRipper analysis of images of stromal cells.....	73

Figure 3.6.	RNA-sequencing analysis of stromal populations with cardiomyocytes included.....	74
Figure 3.7.	RNA-sequencing analysis of stromal cell populations.....	75
Figure 3.8.	Stromal cells differentially impact cardiac microtissue formation.....	77
Figure 3.9.	Immunofluorescent staining of Day 7 heterotypic cardiac microtissues.....	78
Figure 3.10.	Gene expression analysis of 3D heterotypic cardiac microtissues and 2D stromal cell populations.....	79
Figure 3.11.	Stromal cells impacted Day 7 cardiac microtissue function.....	82
Figure 4.1.	Heterotypic cardiac microtissue formation.....	106
Figure 4.2.	Histology and immunostaining of microtissue sections.....	107
Figure 4.3.	Cardiac microtissue calcium handling properties.....	108
Figure 4.4.	Calcium handling response to increasing electrical field stimulation.....	109
Figure 4.5.	Cardiac microtissue harmonic response to electrical field stimulation.....	110
Figure 4.6.	Single-cell RNA-sequencing analysis to identify cardiac cell types.....	111
Figure 4.7.	Cardiomyocyte subset analysis of single-cell RNA-sequencing data.....	112
Figure 4.8.	Cardiomyocyte subset HOPACH clusters.....	114
Figure 4.9.	Validation of top differentially expressed genes in cardiomyocytes that were cultured with cardiac fibroblasts vs. without.....	114
Figure 4.10.	Endothelial cell subset analysis of single-cell RNA-sequencing data.....	116
Figure 4.11.	Endothelial cell subset HOPACH clusters.....	117
Figure 4.12.	Cardiac fibroblast subset analysis of single-cell RNA-sequencing data.....	118
Figure 4.13.	Cardiac fibroblast subset HOPACH clusters.....	119
Figure 5.1.	Microtissue sample preparation for light sheet microscopy.....	136

Figure 5.2.	Multi-view 3D imaging of engineered cardiac microtissues.....	139
Figure 5.3.	Cell counts identified from 3D Imaris-reconstructed images.....	140
Figure 5.4.	<i>In situ</i> cell classification enables cell-specific spatial quantification of heterotypic CM+CF microtissues.....	142
Figure 5.5.	Distribution of cell counts as a function of tissue radius for empirical heterotypic cardiac microtissues and simulated heterotypic tissues.....	143
Figure 5.6.	Light sheet calcium imaging of live 3D cardiac microtissues.....	143
Figure 5.7.	Single plane calcium imaging of live cardiac microtissues.....	145
Figure 5.8.	Normalization of calcium transient profiles for individual CMs.....	145
Figure 6.1.	Differentiation protocols for cardiomyocytes and cardiac fibroblasts from hiPSCs.....	162
Figure 6.2.	Cardiac microtissue formation.....	163
Figure 6.3.	Calcium handling properties of cardiac microtissues.....	164
Figure 6.4.	GJA1 knockdown in cardiac fibroblasts attenuates calcium handling function.....	165

LIST OF TABLES

Table 3.1.	Stromal cell source and donor information.....	59
Table 3.2.	Antibody source information.....	60
Table 3.3.	Fluidigm primer sequences.....	65
Table 3.4.	Table of CD+ percentages as analyzed by flow cytometry.....	68
Table 4.1.	Antibody and in situ hybridization probe source information.....	101
Table 5.1.	Wholemout immunostaining antibody information.....	136

CHAPTER 1

INTRODUCTION

1.1. Overview

The overarching goal of the studies presented in this dissertation is to build cardiac tissue engineering models that recapitulate the multicellular composition and structure of the native myocardium in order to create human tissue constructs that can be used as substrates for biological interrogation and therapeutic discovery. To do so, we must first identify the key cardiac cellular constituents and how they interact with one another and with their environment to promote proper tissue structure, function, and phenotype. We looked to cardiac biology to better understand the native interactions of heterotypic cardiac cell types, and we leveraged controllable/customizable tissue engineering platforms for systematic pairwise studies of the parenchymal cardiomyocytes with an array of different non-parenchymal cell types in 3D self-assembled microtissues. Combining advanced technological modes of analysis further allowed us to study single-cell-level differences in the context of tissue-level properties.

1.2. Cellular composition of the native human heart

The heart is composed of multiple cell types that interact via numerous heterotypic interactions that collectively impact cardiac tissue structure and function. During normal heart development, cardiomyocytes differentiate and mature in intimate contact with non-myocytes, such as endothelial cells, cardiac fibroblasts, and immune cells, which concurrently increase in number and ultimately constitute the majority of the total number of cells in the heart (Furtado et al. 2016, Pinto et al. 2016).

1.2.1. Cardiomyocytes

Cardiomyocytes (CMs) are the parenchymal cell type of heart, responsible for facilitating the contractile force necessary to pump blood in and out of the heart and throughout the body. CMs constitute approximately 75% of the mature human heart by volume, though they only account for less than one-third of the total number of cells in the heart (Nag 1980, Banerjee et al. 2007, Bergmann et al. 2015, Zhou and Pu 2016). This numeral majority of non-parenchymal cells in the heart reflects the significance of the non-myocytes in supporting proper cardiac function.

1.2.1.1. *Human pluripotent stem cell-derived cardiomyocytes*

The ability to efficiently generate CMs from human pluripotent stem cells (hPSCs) has enabled broad use of these cells as a source for tissue engineering efforts. The differentiation of CMs from human pluripotent stem cells (hPSCs) largely follows the developmental trajectory that native CMs undergo. CMs arise early in development from two main progenitor populations: the first heart field (FHF) cardiac progenitors, which ultimately give rise to cells in the left ventricle, and the second heart field (SHF) cardiac progenitors, which yield cells populating the right ventricle and outflow tract (Kelly et al. 2014, Foglia and Poss 2016). The serum-free, small molecule-based differentiation protocol we regularly use (Lian et al. 2012, Lian et al. 2013) generates CMs by the modulation of Wnt signaling, first by introducing a high dose of GSK3 β inhibitor CHIR99021, which results in the up-regulation of endogenous BMP4 and activin/NODAL, and then by suppressing Wnt signaling with small molecule inhibitor IWP-2/IWP-4 (BurrIDGE et al. 2012). These timed cues coax the hPSCs first to a cardiac mesoderm fate before pushing the cells through the FHF cardiac progenitor state, which ultimately results in CMs thought to primarily be of a ventricular subtype.

1.2.1.2. Advancing the maturation of hPSC-derived cardiomyocytes

CMs differentiated from hPSCs are widely known to be immature, most analogous to the fetal stages of native human CMs with respect to their automaticity, ion channel expression, electrophysiology, gene expression, and ultra-structure (DeLaughter et al. 2016, Dunn and Palecek 2018, Karbassi et al. 2020). Many approaches have been explored to advance the developmental phenotype of hPSC-CMs, including extended culture duration (Kamakura et al. 2013, Lundy et al. 2013, Piccini et al. 2015), additional biochemical cues (Correia et al. 2017, Parikh et al. 2017, Yang et al. 2019), electromechanical stimulation (Chan et al. 2013, Nunes et al. 2013, Mihic et al. 2014, Ruan et al. 2015, Eng et al. 2016, Ronaldson-Bouchard et al. 2018), and three-dimensional culture (Nunes et al. 2013, Nguyen et al. 2014, Ronaldson-Bouchard et al. 2018, Beauchamp et al. 2020). However, despite these external stimuli, the cells still do not progress much past the fetal stage unless transplanted into the hearts of animal models (Chong et al. 2014, Cho et al. 2017, Kadota et al. 2017, Liu et al. 2018). This *in vivo* maturation provides further support for the importance of the heterotypic niche in advancing cellular development.

1.2.2. Endothelial cells

Endothelial cells (ECs), originating primarily from lateral plate mesoderm, are the most abundant non-myocyte population in the adult heart (Brutsaert 2003, Hsieh et al. 2006, Pinto et al. 2016). ECs communicate with CMs primarily via paracrine and endocrine signaling (i.e. release of platelet-derived growth factor-B, neuregulin, and nitric oxide), and support CM metabolism, survival, and contractility (Perbellini et al. 2018, Colliva et al. 2019). Despite the high tissue density and close proximity of ECs to CMs, ECs are physically separated from CMs by a thin

basement membrane (Yang et al. 2014), explaining why ECs primarily influence CM fate and function via secreted molecules, and not as a result of direct cell-cell interactions.

1.2.2.1. Human pluripotent stem cell-derived endothelial cells

The most common strategy for generating endothelial cells involves promoting hPSCs through a cardiac mesodermal progenitor state before endothelial specification (Williams and Wu 2019). Mesoderm is generated following the same Wnt activation treatment with GSK3 β inhibitor CHIR99021 as in the CM differentiation protocol. Treatment with cocktails of growth factors (Yang et al. 2008, Zhang et al. 2017) or small molecules (Lian et al. 2014, Liu et al. 2016) results in bi-potent endothelial progenitors, which can then differentiate into either smooth muscle cells or ECs. ECs are derived from the progenitors by continued exposure to VEGF and FGF2 as well as TGF β inhibition (James et al. 2010).

1.2.3. Cardiac fibroblasts

Cardiac fibroblasts (CFs) are in intimate physical contact with multiple neighboring CMs and constitute ~15% of non-myocytes in the heart (Pinto et al. 2016). CFs arise during embryonic development from epicardial and endocardial cells that undergo an epithelial-to-mesenchymal transition, as well as from a small population generated in the neural crest that primarily populates the outflow tract of the heart (Ali et al. 2014, Moore-Morris et al. 2014, Zhang et al. 2019). CFs derived from the epicardium constitute the majority of the fibroblast population (80-85%) in the heart (Moore-Morris et al. 2014, Zhang et al. 2019), and are typically found in the ventricular myocardium, resulting in a close spatial relationship between CFs and CMs, such that every CF is surrounded by multiple CMs (Camelliti et al. 2005, Souders et al. 2009).

As a result of their physical juxtaposition, CM-CF communication is mediated largely by direct cell-cell interactions, such as intercellular adhesions and gap junctions (Gaudesius et al. 2003, Camelliti et al. 2006, Souders et al. 2009, Ottaviano and Yee 2011, Zhang et al. 2012, Rother et al. 2015). CFs also contribute to cardiac tissue structure, function, and phenotype through the secretion of growth factors and signaling molecules (i.e. fibroblast growth factor 2, transforming growth factor-B, interleukin-1B, interleukin-6) (Kakkar and Lee 2010), as well as production of extracellular matrix (ECM) molecules and proteases responsible for cardiac remodeling (Ieda et al. 2009).

Ontogenic differences in CF morphology and ECM have also been identified between isolated fibroblasts from fetal and adult cardiac tissue (both mouse and human). Fetal CFs tend to be smaller, more proliferative, and produce ECM rich in fibronectin, periostin, and heparin-binding EGF-like growth factor, which supports CM proliferation (Ieda et al. 2009, Williams et al. 2014, Jonsson et al. 2016). In contrast, adult CFs are larger, less proliferative, and produce more structural ECM (i.e. collagen and elastin) to support CM hypertrophy (Williams et al. 2014, Jonsson et al. 2016).

1.2.3.1. Human pluripotent stem cell-derived cardiac fibroblasts

Cardiac fibroblast differentiations are the newest of the cardiac cell type derivations. Stem cell-derived fibroblasts have been previously generated via generic outgrowth methods from embryoid bodies (Huebsch et al. 2016) or teratomas (Rand et al. 2018), or by sorting CD90+ cells out of differentiations (Thavandiran et al. 2013), but the two recent cardiac-specific fibroblast differentiation protocols mimic the morphogenic cues that developing CFs receive *in vivo*. The majority of CFs in the native adult heart are derived from epicardial cells, therefore a few groups

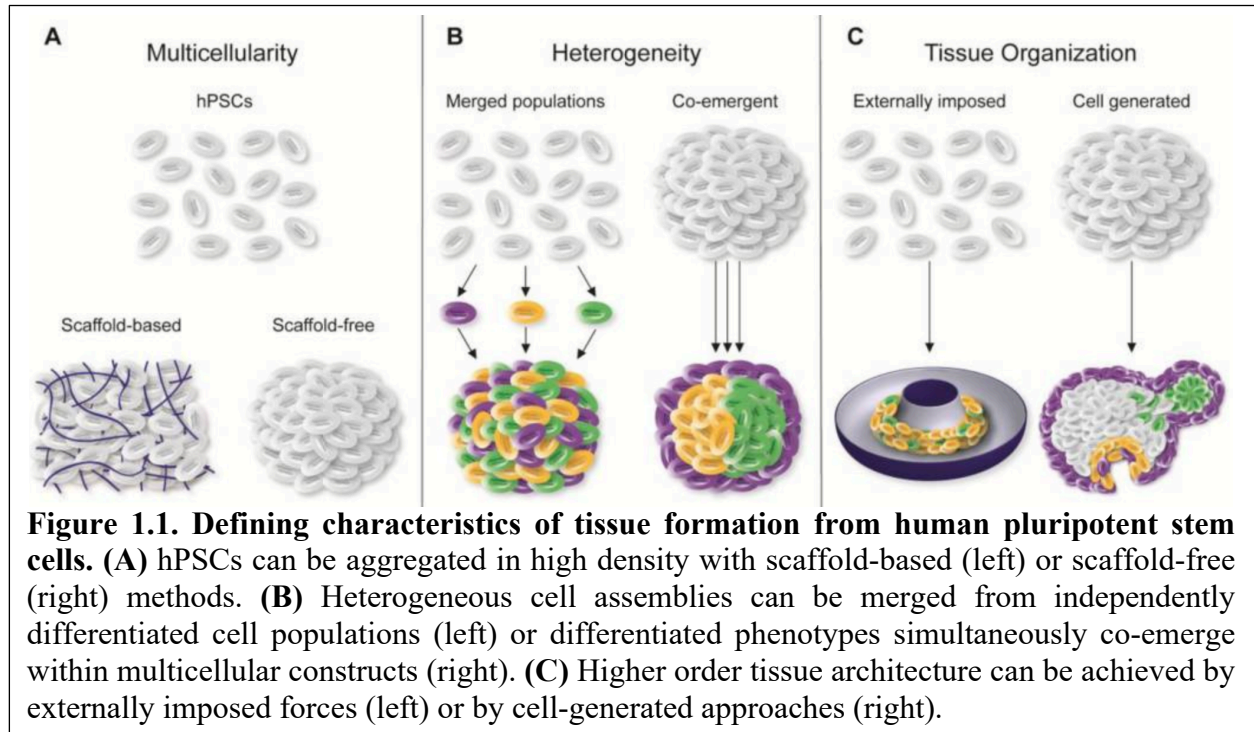
have expanded the previously-established hPSC-epicardial cell differentiation protocol (Bao et al. 2017) to generate CFs after epicardial commitment (Zhang et al. 2019, Giacomelli et al. 2020). hPSCs are first pushed to mesoderm and FHF cardiac progenitor cells, as described for the CM differentiation, before activating Wnt signaling again through the use of GSK3 β inhibitor CHIR99021 to coax cells towards an epicardial commitment. Epicardial cells can be kept in a self-renewing state with the use of a TGF β inhibitor before deriving CFs with basic fibroblast growth factor (bFGF) treatment (termed EpiC-CFs). Another avenue of CF differentiation is through second heart field progenitor cells, mimicking the endocardial-derivation of native CFs (Zhang et al. 2019). In this protocol, mesodermal progenitors are generated from hPSCs with the same Wnt activation (GSK3 β inhibitor CHIR99021) as in the CM and EpiC-CF differentiations, but instead of deriving FHF cardiac progenitors with Wnt inhibition, the cells are subjected very early on to bFGF treatment, generating CFs that progress through a second heart field-like progenitor stage (referred to as SHF-CFs).

1.3. Tissue engineering strategies

Significant advances in human pluripotent stem cell biology over the past two decades afford many new and exciting opportunities for the engineering of human tissues from hPSCs. The unique ability of hPSCs to self-renew indefinitely *in vitro* and differentiate into cell types from all three germ layers makes them an attractive cell source for engineering a wide variety of tissues.

The primary defining characteristics of a tissue include the physical assembly of multiple cells, heterogeneity of cell phenotypes, and higher-order organization of tissue architecture. Functional tissues are inherently comprised of multiple cell populations that interact within and between populations as well as with their extracellular environment to ultimately dictate tissue

form and function. These multicellular and heterogeneous cell mixtures are organized in 3D arrangements that span multiple scales and ultimately work cooperatively together to perform particular functions. Tissue engineers aim to recapitulate characteristics specific to their target model tissue, however there are many ways in which to do so, with some of the main considerations presented below.



1.3.1. Tissue assembly considerations

The first step in engineering any hPSC-derived tissue is to assemble the cells at a sufficiently high density in 3D. Generally speaking, 3D hPSC multicellular constructs can be created either by seeding on or within a scaffold material or assembling the cells in a “scaffold-free” manner by relying on intrinsic intercellular adhesion mechanisms (Figure 1A).

1.3.1.1. Scaffold-based tissue assembly

Scaffolds for hPSC assembly are made from synthetic or naturally-derived polymeric materials in the form of either highly-porous constructs or encapsulating hydrogels. The primary intent of polymeric scaffolds is to provide physical support for cell survival and growth. Cell-assembly onto scaffold materials is primarily mediated by cell-ECM adhesions such as integrins, which are transmembrane proteins on the cell surface that recognize peptide sequences found within many ECM molecules, thereby allowing cells to anchor to the surrounding scaffold (Schaller 2010, Teo et al. 2015). Scaffold-based assembly of tissues enables precise control of many aspects of the microenvironment. For example, constructing material scaffolds allows for the generation of structures that mimic aspects of the ECM specific to the target model tissue. Additional scaffold fabrication parameters to be considered when designing synthetic scaffolds are material choice, pore size, porosity, fiber diameter, fiber alignment, stiffness, scalability, etc., which may directly impact the ability of hPSCs to attach, grow, and differentiate into a desired tissue type (Lu et al. 2012, Shao et al. 2015).

1.3.1.2. Self-assembled tissue formation

In contrast to material-based approaches, scaffold-free assembly is dependent on the cells' collective ability to amass into a 3D construct. A variety of techniques exist to initiate cellular self-assembly, which differ in scale of production. The approaches range from single aggregates formed in separate vessels (individual) (Ungrin et al. 2008) to many aggregates generated in a shared volume (bulk) (Abbasalizadeh et al. 2012, Otsuji et al. 2014). The technical and logistic challenges associated with the manipulation of individual aggregates has often motivated the use of bulk methods for hPSC assembly since they are more convenient and inherently scalable when

larger numbers of aggregates are needed or desired (Kurosawa 2007). Different variations of microwell arrays provide robust platforms to force multicellular aggregation by centrifugation (Ungrin et al. 2008, Bauwens and Ungrin 2014, Pettinato et al. 2014), allowing for the generation of thousands of aggregates in parallel at high spatial density. One disadvantage of bulk tissue formation/culture, however, is that the ability to longitudinally track individual tissues is lost.

Self-assembled microtissues provide a robust platform to study the direct interactions of heterogeneous cell types in 3D. Since exogenous matrices or scaffold materials are not required for the engineering of self-assembled tissues, changes in tissue function or cell phenotype resulting from different pairings of cell types can be attributed to altered heterotypic interactions or paracrine signaling mechanisms. Furthermore, self-assembly methods of tissue engineering provide precise control over the different cell types and proportions that are seeded into the microtissues (Hookway et al. 2016). Therefore, since endogenously-driven 3D cell assembly stimulates an increase in intercellular adhesion molecules, self-assembled microtissues facilitate the study of intercellular connectivity. For example, microtissues assembled from multiple cardiac cell types provide a platform well-suited to study both physical (i.e. cadherins) and electrical (i.e. connexins) multicellular connections, and ultimately enable determination of the specific contributions of various non-myocyte populations to engineered cardiac tissue structure, function, and phenotype.

1.3.2. Introducing phenotypic heterogeneity within multicellular constructs

While multicellularity provides the starting basis for tissue formation, the cooperative interactions of organized groups of cells contribute to complex tissue function(s). The presence of two or more cell types within tissues largely arises from a need for mutually supportive co-dependence. Defined, yet heterogeneous, tissue constructs of hPSC-derived cell types can be

attained using two fundamentally different strategies, denoted here as 1) merging of independently differentiated cell populations or 2) co-emergence of differentiated phenotypes. Cells can be independently differentiated from a single source of hPSCs into specific cell types in parallel and combined after differentiation (i.e. merged populations). Alternatively, multiple cell types can be differentiated simultaneously in the same culture to form a heterotypic, multicellular tissue from a single starting population of hPSCs (i.e. co-emergence) (Figure 1B).

1.3.2.1. Merging of independently differentiated cell populations

The incorporation of multiple cell types in engineered tissues has been motivated primarily by the need for vascularization of dense multicellular constructs. Inclusion of endothelial cells enables the formation of vascular networks to assist with nutrient diffusion throughout engineered tissues. Additionally, stromal cell populations support vascular networks, provide paracrine signals to surrounding cells, and secrete extracellular matrix that supports cell functions and tissue structure, making stromal cells a very desirable population to include in engineered tissues. Methods to merge independently differentiated cell types include both extrinsically-driven scaffold-based platforms (Levenberg et al. 2005, Lesman et al. 2010, Takebe et al. 2012, Masumoto and Yamashita 2018) as well as scaffold-free approaches (Matsumoto et al. 2001, Takebe et al. 2013, Takebe et al. 2015). Many studies rely on primary isolated cells mixed with a single defined hPSC-derived cell type; however, with improved differentiation protocols for an increasing number of cell types, it is now feasible to obtain multiple distinct cell types from the same starting pluripotent population.

One advantage of merging distinct populations is that the starting stoichiometries of the independently differentiated populations can be precisely controlled at the outset. Altering the

ratios of different initial cell populations is the most direct means of varying the proportions of cells within the resulting tissues. However, an important consideration is the relative proliferative capacity of each cell type within the system. Combining cell types with drastically different proliferation rates could lead to outcomes where the ratios of cell types at the input of the experiment differ dramatically from the ratio of cells in the final functional tissue. Furthermore, different cell types can show variable survival during and/or after tissue self-assembly, potentially resulting in a final multicellular composition different from the initial input ratios. In addition to optimizing cell ratios, identifying culture media and other components that mutually support each individual cell population is also critical to the formation of functional tissue constructs.

1.3.2.2. Co-emergence of specified cell populations

In contrast to merging distinct cell populations, self-assembled hPSC aggregated can support co-emergence of multiple cell types given the proper instructive cues. The rapidly-expanding literature on organoid formation demonstrates that temporal regulation of biochemical or environmental cues in an hPSC starting population can produce *in vitro* models of human organ development (Lancaster et al. 2013, Clevers 2016, Takasato et al. 2016, Silva et al. 2020). While cellular remodeling and organization during organoid formation is largely autonomously mediated, developing effective organoid formation strategies remains an iterative process. Intercellular crosstalk and feedback mechanisms during organoid formation are relatively unknown; therefore, protocol evolution involves a systematic trial-and-error approach. Therefore, it is evident that the co-emergence approach is very much an outcome-driven process. Culture conditions for pluri-/multi-potent aggregates are manipulated until the desired outcome (or a progenitor of the desired outcome) is achieved.

Compared to the strategy of merging independently differentiated populations, the co-emergence approach lacks a level of control in the initial stages of organoid culture in that specific cell ratios and cell types are not specifically pre-determined. Despite being perhaps less well-defined at the outset, co-emergent protocols reproducibly result in functional tissue constructs where all cell types come from the same starting cell population, thereby more accurately mimicking *in vivo* embryonic developmental processes and largely achieving more advanced structural, functional, and phenotypic tissue entities than their independently-merged counterparts (i.e. cardiac organoids generated from hPSC-cardiac progenitors (Silva et al. 2020) versus merged heterotypic cardiac microtissues (Huebsch et al. 2016, Hookway et al. 2020)). Organoid engineering strategies have been reviewed in detail elsewhere (Simian and Bissell 2017, Lancaster and Huch 2019, Matthys et al. 2020).

1.3.3. Directing higher-order organization and tissue architecture

An additional level of organization within engineered tissues involves structurally assembling cells into specific multicellular arrangements that are analogous to the architecture observed in native tissues. Most approaches to achieving higher order assembly can be categorized as either exogenously imposed technologies which rely on molds or scaffolds to dictate tissue shape or endogenously driven morphogenesis in which self-organization mechanisms yield patterning without external physical guidance or instruction (Figure 1C).

1.3.3.1. Externally imposed tissue architecture

The most common approach for generating higher order tissue architecture has been to use engineered molds or scaffolds to dictate the shape of the tissue. One advantage of such techniques

is the ability to control and define the ultimate meso/macroscale size and shape of the tissues. Scaffolds can be used as a means to not only assemble cells together into multicellular constructs, but also provide dimensionality specific to the tissue being modeled. Decellularized tissues have been used as scaffolds given that they already possess the native shape and geometry of original tissues of interest. Repopulation of decellularized tissues has been examined by the perfusion of human pluripotent derived cell populations through decellularized lung (Ghaedi et al. 2013, Gilpin et al. 2014), heart (Carvalho et al. 2012, Lu et al. 2013), and kidney (Caralt et al. 2015).

As an alternative to pre-determined scaffold shape to control tissue architecture, externally-directed tissue geometries can be induced by seeding cells into physical molds that impose mechanical constraints to force assembly in particular configurations. This strategy is based on collective cell remodeling to the lowest energy state permissible given the specific boundary conditions defined by a particular mold geometry (Dahlmann et al. 2013). Molds can be generated from a variety of materials including agarose, polydimethylsiloxane, or polyacrylamide that have minimal adhesive interactions with the cells and serve mainly as a means of aggregating cells and forcing tissue shape (Youssef et al. 2011, Dahlmann et al. 2013, Bauwens and Ungrin 2014). Spheroidal shapes are the lowest energy state achieved by multicellular constructs and therefore are the easiest and most common shape to generate. Scientists have frequently exploited this concept by producing basic molds that force cells to aggregate into arrayed wells, where cell-cell adhesions drive self-assembly and condensation into spheroids (Bao et al. 2011). The resulting cell aggregates retain 3D architecture and have been generated from hPSCs or hPSC-derived cells to model embryonic development of specific tissues. Additionally, small aggregates can be used as building blocks to generate larger, more complex tissues through manual manipulation or bioprinting techniques (Faulkner-Jones et al. 2015, Skylar-Scott et al. 2019).

Generation of more complex shapes can also be achieved by producing more complex mold geometries. However, the final shape of the tissue is not dictated by physical mold boundaries, but is mediated by cell-induced tensile forces. Therefore, molds often include elements such as posts, which physically prevent the tissue from remodeling into spheroids and maintain tissues under tension (Tejavibulya et al. 2011, Bian et al. 2014). This approach may be limited, however, to tissues where cellular tension is inherently found to promote tissue function (i.e. myocardium, ligament, tendon) and not applicable to tissues that require the formation of alternative structures like epithelial sheets.

Directing tissue architecture using molding and shaping technologies enables researchers to build 3D constructs of physiologically-relevant sizes and shapes. This “top-down” approach allows the user to customize input system parameters to various design specifications. In contrast, a “bottom-up” approach that exploits cell-driven mechanisms for tissue formation provides an alternative method for achieving higher order structure and organization within tissues.

1.3.3.2. Cell-generated tissue organization

In recent years numerous reports of hPSC-derived organoids have highlighted the ability to exploit endogenous cell mechanisms to achieve well-defined multicellular architecture within tissue constructs (Nakano et al. 2012, Lancaster et al. 2013, Xia et al. 2014). This cell-programmed approach relies upon intrinsic pathways to direct a series of cellular responses such as proliferation, collective migration, and extracellular matrix assembly and remodeling to achieve tissue-specific geometries. Examples can be seen in the budding of organoids, lumen formation, vessel branching, and folding of tissue sheets (Nakano et al. 2012, Kusuma et al. 2013, Hughes et al. 2018).

Although relying upon cell-driven approaches to shape tissue structure may seem less predictable and controlled, identification of proper input cues to the system can enable hPSC morphogenesis to be highly reproducible in terms of spatial and temporal organization. This suggests that mechanisms which drive morphogenic changes act in concert with one another and are able to co-regulate not only the emergence of multiple cell populations in parallel, but also balance the appropriate interactions to coordinately develop architecture in a robust manner. Cell autonomous-driven methods to define tissue architecture afford the opportunity to gain insight into naturally arising biophysical cues that are associated with developmental morphogenesis. Information about cellular processes can be integrated into computational models to help understand the specific forces that guide self-directed morphogenesis (Libby et al. 2019). Furthermore, computational predictions of cell behaviors during tissue organization not only provide insight into developmental morphogenesis, but could also describe tissue-level changes that occur during disease.

1.3.4. Engineering self-assembled, independently-merged, externally-imposed heterotypic cardiac microtissues

Engineered cardiac tissue models have moved towards incorporating multiple cell populations in order to more accurately mimic the cellular complexity of the native heart. The majority of cardiac tissue engineering strategies acknowledge the need for including multiple heterogeneous cardiac cell populations in order to better model the cellular composition and physiology of the native tissue.

Cardiac tissue biologists have long recognized the need for using heterogeneous, non-purified CM differentiations or for including stromal or non-myocyte populations along with

enriched hPSC-CMs to enable stable tissue formation (Thavandiran et al. 2013, Huebsch et al. 2016, Giacomelli et al. 2017). A wide variety of different stromal cell types have been mixed with hPSC-CMs in engineered tissue constructs, including cardiac fibroblasts (Ravenscroft et al. 2016), dermal fibroblasts (Kensah et al. 2013, Ronaldson-Bouchard et al. 2018), mesenchymal stromal cells (Stevens et al. 2009), hPSC-derived fibroblasts (Thavandiran et al. 2013, Huebsch et al. 2016), endothelial cells (Ravenscroft et al. 2016, Giacomelli et al. 2017), and/or combinations of these cell types (Caspi et al. 2007, Tulloch et al. 2011, Nunes et al. 2013, Masumoto et al. 2016). Generally speaking, the inclusion of stromal populations increases the expression of cardiac-specific genes (Ravenscroft et al. 2016, Giacomelli et al. 2017) and improves functional properties, such as calcium handling, action potential kinetics (Giacomelli et al. 2017), and contractile force (Ravenscroft et al. 2016). However, the variability of stromal cell type has led to inconsistencies in cardiac tissue function and cardiomyocyte pharmacological responses reported by independent studies, thus limiting our understanding of the impact of different stromal cells on engineered cardiac tissues. Furthermore, despite the wide acknowledgment that stromal inclusion is necessary for cardiac tissues, the specific mechanisms by which non-myocytes impact CM fate and function have yet to be elucidated.

In the terms of the tissue engineering considerations listed above, the cardiac microtissues used throughout this dissertation follow the self-assembly method of tissue formation (Figure 1A, right), include multiple cardiac cell populations that are independently differentiated or isolated before mixing (Figure 1B, left), and employ physical molds to initiate spheroidal or ring-shaped microtissue geometries (Figure 1C, left). In order to specifically compare how different types of non-myocytes/stromal cells supported cardiac microtissue formation and function, we chose the independent mixing of cardiac-specific heterotypic cell types (that were enriched for increased

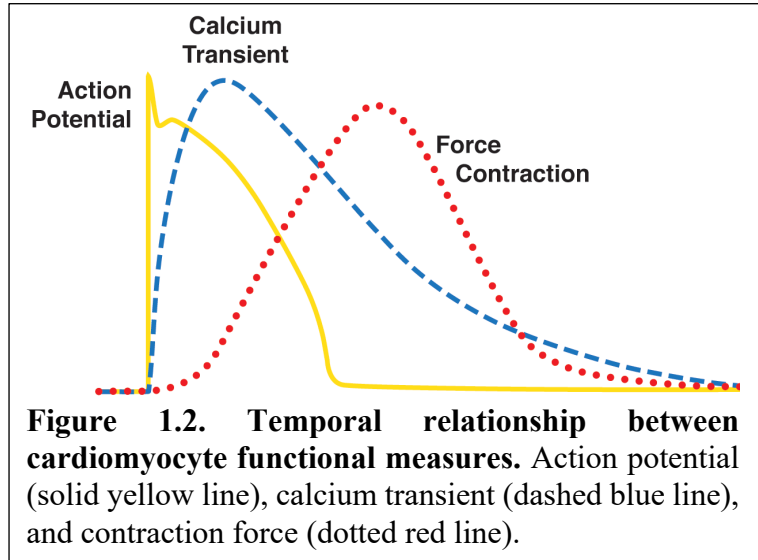
population purities), which enabled us to precisely control the identities and proportions of input cellular constituents. Furthermore, in order to better understand the mechanistic contributions of non-myocytes to cardiomyocyte fate and cardiac tissue function, we chose the self-assembly method of tissue formation that allows us to directly study intercellular interactions in 3D without the interference of exogenous material or matrix.

Lastly, we describe the generation of two different geometries of 3D cardiac microtissues—spheroids and rings—though both are built on the same principles of cellular self-assembly and independent merging of heterotypic cardiac cells. The different tissue shapes lend themselves to different types of assessments. The cardiac spheroids are microscale-sized, containing 2000 cells which produces a diameter of $\sim 150\mu\text{m}$. Therefore, these microtissues can be produced in large batches and assessed in a more high-throughput manner, especially using the video-based calcium imaging analysis pipeline. The cardiac rings are composed of 500,000 cells assembled around a 2mm-diameter post, resulting in a wall thickness of $\sim 150\text{-}200\mu\text{m}$. The size and geometry of these cardiac rings makes them amenable to contractile force testing with a myograph apparatus. Contractile force is one of the hallmark functional tests for cardiac tissue, though it is a low-throughput and labor intensive process; therefore, we utilize calcium imaging of spheroids as a first screen of cardiac tissue function before diving into contractile force testing of cardiac rings as a more direct measure of cardiac tissue function.

1.4. Advanced technological characterization of 3D heterotypic cardiac microtissues

As engineered cardiac tissue constructs are becoming increasingly complex with the incorporation of multiple heterotypic cell types, advanced technological methods are being utilized

to better determine and link the functional, phenotypic, and structural characteristics of cardiac microtissues at both the single-cell level of cardiomyocytes within the microtissues as well as at the bulk tissue-level. Here we describe the technologies used to assess cardiac



function, phenotype, and structure in self-assembled heterotypic cardiac microtissues.

1.4.1. Functional testing

Calcium transients, action potentials, and/or contractile force can be characterized (alone or in combination with one another) to assess the functional state of cardiomyocytes or cardiac tissues. Each measure reveals something slightly different about function, but they all rely on ion flux and are temporally related to one another (Figure 1.2). When sodium first enters a cardiomyocyte it causes the fast upstroke of the action potential, which in turn—with some delay—causes voltage-gated calcium channels to open. As calcium accumulates in the CM, more calcium binds to troponin, which activates the myofilaments and increases force generation (Andersson et al. 2012).

Action potential is best assessed by patch clamp, which measures resting membrane potential, action potential duration, and other kinetic parameters, but this method is labor-intensive and time-consuming, taking a full day to complete analysis on only 5-10 CMs. In response, fluorescence dyes have been developed that respond to changes in membrane potential. Video-

based imaging of these dyes enables a proxy measure of action potential that provides waveform shape, though not the absolute values of the action potential parameters. Therefore, waveform shape analysis from the fluorescence intensity of the voltage dyes enables determination of cardiac subtype specification (i.e. ventricular vs. atrial vs. nodal) in a higher-throughput manner.

While analysis of action potential waveform identifies cellular subtype, analysis of the kinetic properties of calcium transients can be used to determine the functional maturation state of CMs in cardiac tissue constructs. A more mature CM is able to take up more calcium (greater calcium transient amplitude values), and do so in a faster manner (shorter time-to-peak values and higher upstroke and downstroke velocity values). Calcium indicators in the form of fluorescence dyes (Fluo-4 AM, green; Rhodamine-3 AM, red) or constitutively-expressed genetic constructs in cell lines (GCaMP, green; RCaMP, red) have made calcium imaging a widely accessible test of cell or tissue function.

The hallmark functional characteristic of a cardiomyocyte or an engineered cardiac tissue is its ability to generate contractile forces. Direct measurement of contractile force is the most informative functional determinant, but can be challenging to acquire for individual CMs or some microtissue scales and/or geometries. Cardiac tissues have been formed in ring- or dogbone-shaped molds and transferred to an organ bath myograph testing system (Huebsch et al. 2016, Tiburcy et al. 2017), or have been formed in a tissue culture platform with integrated ability to measure contractile force—typically in the form of cells assembled around posts that are then analyzed for beam deflection (Ronaldson-Bouchard et al. 2018, Thavandiran et al. 2020). Though not as definitive as direct contractile force measurements, video-based imaging of contractile motion has been used as a proxy for studying cardiomyocyte or cardiac tissue contractility (Huebsch et al.

2015, Judge et al. 2017) and is much less labor-intensive and therefore an easier approach to screening contractility across many conditions.

1.4.2. Phenotypic analysis by single-cell RNA-sequencing

When using 3D microtissues to study how specific pairings of heterotypic cell types bi-directionally influence each other's transcriptomes, the different cell types need to be separated from one another before analysis. This becomes challenging when working with heterotypic cardiac microtissues, as cardiac cells are notoriously difficult to sort due to their lack of distinguishing surface markers (Furtado et al. 2016, Pinto et al. 2016). Therefore, single-cell-level analysis of dissociated cardiac microtissues was used in order to study how each cell type in the tissue changed after 3D heterotypic co-culture.

Single-cell RNA-sequencing has emerged as a powerful tool to dissect multicellular heterogeneity throughout tissue development (Byrnes et al. 2018, de Soysa et al. 2019) or within heterogeneous hPSC-differentiations (Butts et al. 2017, Wu et al. 2018). Applying single-cell RNA-sequencing to engineered heterotypic tissue constructs enables the determination of bi-directional multicellular phenotypes at single-cell resolution within the context of tissue-level properties. One down side, however, is that single-cell RNA-sequencing of dissociated microtissues fails to capture spatial information, and rare cell populations escape detection unless sufficient sequencing depth is obtained.

Spatial transcriptomics integrates histological tissue sectioning with RNA-sequencing to couple spatial information with gene expression (Stahl et al. 2016), but the spatial resolution is not yet at the single-cell level. We have nonetheless used this method to validate single-cell RNA-sequencing results in single planes of cardiac microtissue sections, though hundreds of serial

sections spanning the entirety of individual tissues would be required to comprehensively reconstruct 3D spatial structural/phenotypic network information.

1.4.3. *In situ* characterization of 3D multicellular organization by light sheet fluorescence microscopy

Analysis of 3D tissue structure typically requires 1) histological sectioning combined with epifluorescence microscopy, which allows for high resolution imaging of structure, but is limited by the need to physically slice the tissue, and 2) point-scanning fluorescence sectioning microscopes such as confocal or two-photon microscopes, which enable high spatial resolution imaging, but are hindered by speed limitations. In contrast, light sheet fluorescence microscopy (LSFM) allows for high resolution imaging of thick tissue samples at significantly faster speeds with low photobleaching and phototoxicity (Huisken et al. 2004, Holekamp et al. 2008, Andilla et al. 2017). A cylindrical lens is used to create a sheet of light that illuminates only the optical section of the tissue in the focal plane of the objective lens, thus allowing for a high resolution camera to image the entire 2D plane simultaneously, which improves the speed of acquisition while attenuating photobleaching and phototoxicity. LSFM has been used to image entire embryos with single cell resolution over multiple hours (Huisken et al. 2004, Keller et al. 2008) as well as to image the function of hundreds of neurons simultaneously (Holekamp et al. 2008, Turaga and Holy 2012, Greer and Holy 2019, Wan et al. 2019).

We analyzed the multicellular organization of 3D engineered cardiac microtissues by combining immunofluorescence staining and LSFM to dissect cell-type specific localization and calcium handling function of the engineered tissue constructs at high spatial and temporal fidelity. Coupling single-cell structural and functional information of 3D engineered tissues will advance

understandings of cell type-specific contributions to tissue properties as well as enable further insights into developmental- or disease-specific biological events that can be interrogated in 3D tissue models.

1.5. Concluding remarks

This dissertation applies bioengineering principles for tissue design to systematically study how cellular heterogeneity impacts elements of cardiac tissue function, phenotype, and structure. Understanding of cardiac development has led to robust differentiation protocols to generate cardiomyocytes, endothelial cells, and cardiac fibroblasts from human pluripotent stem cells, creating an unlimited source of genetically-perturbable, tissue-specific cell types. Heterogeneity is widely appreciated as necessary for cardiac tissue engineering studies, but this body of work aimed to determine the importance of non-parenchymal cell type identity/source as well as the specific contributions that non-parenchymal cells impart on cardiac fate and function.

1.6. Bibliography

- Abbasalizadeh, S., et al. (2012). "Bioprocess development for mass production of size-controlled human pluripotent stem cell aggregates in stirred suspension bioreactor." Tissue Eng Part C Methods **18**(11): 831-851.
- Ali, S. R., et al. (2014). "Developmental heterogeneity of cardiac fibroblasts does not predict pathological proliferation and activation." Circ Res **115**(7): 625-635.
- Andersson, D. C., et al. (2012). Excitation–Contraction Coupling in the Heart. Fundamental Biology and Mechanisms of Disease. Muscle. **1**: 153-159.
- Andilla, J., et al. (2017). "Imaging tissue-mimic with light sheet microscopy: A comparative guideline." Sci Rep **7**: 44939.
- Banerjee, I., et al. (2007). "Determination of cell types and numbers during cardiac development in the neonatal and adult rat and mouse." Am J Physiol Heart Circ Physiol **293**(3): H1883-1891.
- Bao, B., et al. (2011). "Connexon-mediated cell adhesion drives microtissue self-assembly." FASEB J **25**(1): 255-264.
- Bao, X., et al. (2017). "Directed differentiation and long-term maintenance of epicardial cells derived from human pluripotent stem cells under fully defined conditions." Nat Protoc **12**(9): 1890-1900.
- Bauwens, C. L. and M. D. Ungrin (2014). "Scalable cardiac differentiation of human pluripotent stem cells as microwell-generated, size controlled three-dimensional aggregates." Methods Mol Biol **1181**: 15-25.

- Beauchamp, P., et al. (2020). "3D Co-culture of hiPSC-Derived Cardiomyocytes With Cardiac Fibroblasts Improves Tissue-Like Features of Cardiac Spheroids." Front Mol Biosci **7**: 14.
- Bergmann, O., et al. (2015). "Dynamics of Cell Generation and Turnover in the Human Heart." Cell **161**(7): 1566-1575.
- Bian, W., et al. (2014). "Robust T-tubulation and maturation of cardiomyocytes using tissue-engineered epicardial mimetics." Biomaterials **35**(12): 3819-3828.
- Brutsaert, D. L. (2003). "Cardiac endothelial-myocardial signaling: its role in cardiac growth, contractile performance, and rhythmicity." Physiol Rev **83**(1): 59-115.
- Burridge, P. W., et al. (2012). "Production of de novo cardiomyocytes: human pluripotent stem cell differentiation and direct reprogramming." Cell Stem Cell **10**(1): 16-28.
- Butts, J. C., et al. (2017). "Differentiation of V2a interneurons from human pluripotent stem cells." Proc Natl Acad Sci U S A **114**(19): 4969-4974.
- Byrnes, L. E., et al. (2018). "Lineage dynamics of murine pancreatic development at single-cell resolution." Nat Commun **9**(1): 3922.
- Camelliti, P., et al. (2005). "Structural and functional characterisation of cardiac fibroblasts." Cardiovasc Res **65**(1): 40-51.
- Camelliti, P., et al. (2006). "Structural and functional coupling of cardiac myocytes and fibroblasts." Adv Cardiol **42**: 132-149.
- Caralt, M., et al. (2015). "Optimization and critical evaluation of decellularization strategies to develop renal extracellular matrix scaffolds as biological templates for organ engineering and transplantation." Am J Transplant **15**(1): 64-75.

- Carvalho, J. L., et al. (2012). "Characterization of Decellularized Heart Matrices as Biomaterials for Regular and Whole Organ Tissue Engineering and Initial In-vitro Recellularization with Ips Cells." J Tissue Sci Eng Suppl **11**: 002.
- Caspi, O., et al. (2007). "Tissue engineering of vascularized cardiac muscle from human embryonic stem cells." Circ Res **100**(2): 263-272.
- Chan, Y. C., et al. (2013). "Electrical stimulation promotes maturation of cardiomyocytes derived from human embryonic stem cells." J Cardiovasc Transl Res **6**(6): 989-999.
- Cho, G. S., et al. (2017). "Neonatal Transplantation Confers Maturation of PSC-Derived Cardiomyocytes Conducive to Modeling Cardiomyopathy." Cell Rep **18**(2): 571-582.
- Chong, J. J., et al. (2014). "Human embryonic-stem-cell-derived cardiomyocytes regenerate non-human primate hearts." Nature **510**(7504): 273-277.
- Clevers, H. (2016). "Modeling Development and Disease with Organoids." Cell **165**(7): 1586-1597.
- Colliva, A., et al. (2019). "Endothelial cell-cardiomyocyte crosstalk in heart development and disease." J Physiol.
- Correia, C., et al. (2017). "Distinct carbon sources affect structural and functional maturation of cardiomyocytes derived from human pluripotent stem cells." Sci Rep **7**(1): 8590.
- Dahlmann, J., et al. (2013). "The use of agarose microwells for scalable embryoid body formation and cardiac differentiation of human and murine pluripotent stem cells." Biomaterials **34**(10): 2463-2471.
- de Soysa, T. Y., et al. (2019). "Single-cell analysis of cardiogenesis reveals basis for organ-level developmental defects." Nature **572**(7767): 120-124.

- DeLaughter, D. M., et al. (2016). "Single-Cell Resolution of Temporal Gene Expression during Heart Development." Dev Cell **39**(4): 480-490.
- Dunn, K. K. and S. P. Palecek (2018). "Engineering Scalable Manufacturing of High-Quality Stem Cell-Derived Cardiomyocytes for Cardiac Tissue Repair." Front Med (Lausanne) **5**: 110.
- Eng, G., et al. (2016). "Autonomous beating rate adaptation in human stem cell-derived cardiomyocytes." Nat Commun **7**: 10312.
- Faulkner-Jones, A., et al. (2015). "Bioprinting of human pluripotent stem cells and their directed differentiation into hepatocyte-like cells for the generation of mini-livers in 3D." Biofabrication **7**(4): 044102.
- Foglia, M. J. and K. D. Poss (2016). "Building and re-building the heart by cardiomyocyte proliferation." Development **143**(5): 729-740.
- Furtado, M. B., et al. (2016). "View from the heart: cardiac fibroblasts in development, scarring and regeneration." Development **143**(3): 387-397.
- Gaudesius, G., et al. (2003). "Coupling of cardiac electrical activity over extended distances by fibroblasts of cardiac origin." Circ Res **93**(5): 421-428.
- Ghaedi, M., et al. (2013). "Human iPS cell-derived alveolar epithelium repopulates lung extracellular matrix." J Clin Invest **123**(11): 4950-4962.
- Giacomelli, E., et al. (2017). "Three-dimensional cardiac microtissues composed of cardiomyocytes and endothelial cells co-differentiated from human pluripotent stem cells." Development **144**(6): 1008-1017.

- Giacomelli, E., et al. (2020). "Human-iPSC-Derived Cardiac Stromal Cells Enhance Maturation in 3D Cardiac Microtissues and Reveal Non-cardiomyocyte Contributions to Heart Disease." Cell Stem Cell.
- Gilpin, S. E., et al. (2014). "Enhanced lung epithelial specification of human induced pluripotent stem cells on decellularized lung matrix." Ann Thorac Surg **98**(5): 1721-1729; discussion 1729.
- Greer, C. J. and T. E. Holy (2019). "Fast objective coupled planar illumination microscopy." Nat Commun **10**(1): 4483.
- Holekamp, T. F., et al. (2008). "Fast three-dimensional fluorescence imaging of activity in neural populations by objective-coupled planar illumination microscopy." Neuron **57**(5): 661-672.
- Hookway, T. A., et al. (2016). "Aggregate formation and suspension culture of human pluripotent stem cells and differentiated progeny." Methods **101**: 11-20.
- Hookway, T. A., et al. (2020). "Bi-directional Impacts of Heterotypic Interactions in Engineered 3D Human Cardiac Microtissues Revealed by Single-Cell RNA-Sequencing and Functional Analysis." bioRxiv: 2020.2007.2006.190504.
- Hsieh, P. C., et al. (2006). "Endothelial-cardiomyocyte interactions in cardiac development and repair." Annu Rev Physiol **68**: 51-66.
- Huebsch, N., et al. (2016). "Miniaturized iPSC-Cell-Derived Cardiac Muscles for Physiologically Relevant Drug Response Analyses." Sci Rep **6**: 24726.
- Huebsch, N., et al. (2015). "Automated Video-Based Analysis of Contractility and Calcium Flux in Human-Induced Pluripotent Stem Cell-Derived Cardiomyocytes Cultured over Different Spatial Scales." Tissue Eng Part C Methods **21**(5): 467-479.

- Hughes, A. J., et al. (2018). "Engineered Tissue Folding by Mechanical Compaction of the Mesenchyme." Dev Cell **44**(2): 165-178 e166.
- Huisken, J., et al. (2004). "Optical sectioning deep inside live embryos by selective plane illumination microscopy." Science **305**(5686): 1007-1009.
- Ieda, M., et al. (2009). "Cardiac fibroblasts regulate myocardial proliferation through beta1 integrin signaling." Dev Cell **16**(2): 233-244.
- James, D., et al. (2010). "Expansion and maintenance of human embryonic stem cell-derived endothelial cells by TGFbeta inhibition is Id1 dependent." Nat Biotechnol **28**(2): 161-166.
- Jonsson, M. K. B., et al. (2016). "A Transcriptomic and Epigenomic Comparison of Fetal and Adult Human Cardiac Fibroblasts Reveals Novel Key Transcription Factors in Adult Cardiac Fibroblasts." JACC Basic Transl Sci **1**(7): 590-602.
- Judge, L. M., et al. (2017). "A BAG3 chaperone complex maintains cardiomyocyte function during proteotoxic stress." JCI Insight **2**(14).
- Kadota, S., et al. (2017). "In Vivo Maturation of Human Induced Pluripotent Stem Cell-Derived Cardiomyocytes in Neonatal and Adult Rat Hearts." Stem Cell Reports **8**(2): 278-289.
- Kakkar, R. and R. T. Lee (2010). "Intramyocardial fibroblast myocyte communication." Circ Res **106**(1): 47-57.
- Kamakura, T., et al. (2013). "Ultrastructural maturation of human-induced pluripotent stem cell-derived cardiomyocytes in a long-term culture." Circ J **77**(5): 1307-1314.
- Karbassi, E., et al. (2020). "Cardiomyocyte maturation: advances in knowledge and implications for regenerative medicine." Nat Rev Cardiol **17**(6): 341-359.

- Keller, P. J., et al. (2008). "Reconstruction of zebrafish early embryonic development by scanned light sheet microscopy." Science **322**(5904): 1065-1069.
- Kelly, R. G., et al. (2014). "Heart fields and cardiac morphogenesis." Cold Spring Harb Perspect Med **4**(10).
- Kensah, G., et al. (2013). "Murine and human pluripotent stem cell-derived cardiac bodies form contractile myocardial tissue in vitro." Eur Heart J **34**(15): 1134-1146.
- Kurosawa, H. (2007). "Methods for inducing embryoid body formation: in vitro differentiation system of embryonic stem cells." J Biosci Bioeng **103**(5): 389-398.
- Kusuma, S., et al. (2013). "Self-organized vascular networks from human pluripotent stem cells in a synthetic matrix." Proc Natl Acad Sci U S A **110**(31): 12601-12606.
- Lancaster, M. A. and M. Huch (2019). "Disease modelling in human organoids." Dis Model Mech **12**(7).
- Lancaster, M. A., et al. (2013). "Cerebral organoids model human brain development and microcephaly." Nature **501**(7467): 373-379.
- Lesman, A., et al. (2010). "Transplantation of a tissue-engineered human vascularized cardiac muscle." Tissue Eng Part A **16**(1): 115-125.
- Levenberg, S., et al. (2005). "Engineering vascularized skeletal muscle tissue." Nat Biotechnol **23**(7): 879-884.
- Lian, X., et al. (2014). "Efficient differentiation of human pluripotent stem cells to endothelial progenitors via small-molecule activation of WNT signaling." Stem Cell Reports **3**(5): 804-816.

- Lian, X., et al. (2012). "Robust cardiomyocyte differentiation from human pluripotent stem cells via temporal modulation of canonical Wnt signaling." Proc Natl Acad Sci U S A **109**(27): E1848-1857.
- Lian, X., et al. (2013). "Directed cardiomyocyte differentiation from human pluripotent stem cells by modulating Wnt/beta-catenin signaling under fully defined conditions." Nat Protoc **8**(1): 162-175.
- Libby, A. R. G., et al. (2019). "Automated Design of Pluripotent Stem Cell Self-Organization." Cell Syst **9**(5): 483-495 e410.
- Liu, X., et al. (2016). "Differentiation of functional endothelial cells from human induced pluripotent stem cells: A novel, highly efficient and cost effective method." Differentiation **92**(4): 225-236.
- Liu, Y. W., et al. (2018). "Human embryonic stem cell-derived cardiomyocytes restore function in infarcted hearts of non-human primates." Nat Biotechnol **36**(7): 597-605.
- Lu, H. F., et al. (2012). "A 3D microfibrinous scaffold for long-term human pluripotent stem cell self-renewal under chemically defined conditions." Biomaterials **33**(8): 2419-2430.
- Lu, T. Y., et al. (2013). "Repopulation of decellularized mouse heart with human induced pluripotent stem cell-derived cardiovascular progenitor cells." Nat Commun **4**: 2307.
- Lundy, S. D., et al. (2013). "Structural and functional maturation of cardiomyocytes derived from human pluripotent stem cells." Stem Cells Dev **22**(14): 1991-2002.
- Masumoto, H., et al. (2016). "The myocardial regenerative potential of three-dimensional engineered cardiac tissues composed of multiple human iPS cell-derived cardiovascular cell lineages." Sci Rep **6**: 29933.

- Masumoto, H. and J. K. Yamashita (2018). "Human iPS cell-engineered three-dimensional cardiac tissues perfused by capillary networks between host and graft." Inflamm Regen **38**: 26.
- Matsumoto, K., et al. (2001). "Liver organogenesis promoted by endothelial cells prior to vascular function." Science **294**(5542): 559-563.
- Matthys, O. B., et al. (2020). "Engineering Human Organoid Development Ex Vivo-Challenges and Opportunities." Current Opinion in Biomedical Engineering.
- Mihic, A., et al. (2014). "The effect of cyclic stretch on maturation and 3D tissue formation of human embryonic stem cell-derived cardiomyocytes." Biomaterials **35**(9): 2798-2808.
- Moore-Morris, T., et al. (2014). "Resident fibroblast lineages mediate pressure overload-induced cardiac fibrosis." J Clin Invest **124**(7): 2921-2934.
- Nag, A. C. (1980). "Study of non-muscle cells of the adult mammalian heart: a fine structural analysis and distribution." Cytobios **28**(109): 41-61.
- Nakano, T., et al. (2012). "Self-formation of optic cups and storable stratified neural retina from human ESCs." Cell Stem Cell **10**(6): 771-785.
- Nguyen, D. C., et al. (2014). "Microscale generation of cardiospheres promotes robust enrichment of cardiomyocytes derived from human pluripotent stem cells." Stem Cell Reports **3**(2): 260-268.
- Nunes, S. S., et al. (2013). "Biowire: a platform for maturation of human pluripotent stem cell-derived cardiomyocytes." Nat Methods **10**(8): 781-787.
- Otsuji, T. G., et al. (2014). "A 3D sphere culture system containing functional polymers for large-scale human pluripotent stem cell production." Stem Cell Reports **2**(5): 734-745.

- Ottaviano, F. G. and K. O. Yee (2011). "Communication signals between cardiac fibroblasts and cardiac myocytes." J Cardiovasc Pharmacol **57**(5): 513-521.
- Parikh, S. S., et al. (2017). "Thyroid and Glucocorticoid Hormones Promote Functional T-Tubule Development in Human-Induced Pluripotent Stem Cell-Derived Cardiomyocytes." Circ Res **121**(12): 1323-1330.
- Perbellini, F., et al. (2018). "Heterocellularity and Cellular Cross-Talk in the Cardiovascular System." Front Cardiovasc Med **5**: 143.
- Pettinato, G., et al. (2014). "ROCK inhibitor is not required for embryoid body formation from singularized human embryonic stem cells." PLoS One **9**(11): e100742.
- Piccini, I., et al. (2015). "Human pluripotent stem cell-derived cardiomyocytes: Genome-wide expression profiling of long-term in vitro maturation in comparison to human heart tissue." Genom Data **4**: 69-72.
- Pinto, A. R., et al. (2016). "Revisiting Cardiac Cellular Composition." Circ Res **118**(3): 400-409.
- Rand, T. A., et al. (2018). "MYC Releases Early Reprogrammed Human Cells from Proliferation Pause via Retinoblastoma Protein Inhibition." Cell Rep **23**(2): 361-375.
- Ravenscroft, S. M., et al. (2016). "Cardiac Non-myocyte Cells Show Enhanced Pharmacological Function Suggestive of Contractile Maturity in Stem Cell Derived Cardiomyocyte Microtissues." Toxicol Sci **152**(1): 99-112.
- Ronaldson-Bouchard, K., et al. (2018). "Advanced maturation of human cardiac tissue grown from pluripotent stem cells." Nature **556**(7700): 239-243.
- Rother, J., et al. (2015). "Crosstalk of cardiomyocytes and fibroblasts in co-cultures." Open Biol **5**(6): 150038.

- Ruan, J. L., et al. (2015). "Mechanical Stress Promotes Maturation of Human Myocardium From Pluripotent Stem Cell-Derived Progenitors." Stem Cells **33**(7): 2148-2157.
- Schaller, M. D. (2010). "Cellular functions of FAK kinases: insight into molecular mechanisms and novel functions." J Cell Sci **123**(Pt 7): 1007-1013.
- Shao, Y., et al. (2015). "On human pluripotent stem cell control: The rise of 3D bioengineering and mechanobiology." Biomaterials **52**: 26-43.
- Silva, A. C., et al. (2020). "Developmental co-emergence of cardiac and gut tissues modeled by human iPSC-derived organoids." bioRxiv: 2020.2004.2030.071472.
- Simian, M. and M. J. Bissell (2017). "Organoids: A historical perspective of thinking in three dimensions." J Cell Biol **216**(1): 31-40.
- Skylar-Scott, M. A., et al. (2019). "Biomanufacturing of organ-specific tissues with high cellular density and embedded vascular channels." Sci Adv **5**(9): eaaw2459.
- Souders, C. A., et al. (2009). "Cardiac fibroblast: the renaissance cell." Circ Res **105**(12): 1164-1176.
- Stahl, P. L., et al. (2016). "Visualization and analysis of gene expression in tissue sections by spatial transcriptomics." Science **353**(6294): 78-82.
- Stevens, K. R., et al. (2009). "Physiological function and transplantation of scaffold-free and vascularized human cardiac muscle tissue." Proc Natl Acad Sci U S A **106**(39): 16568-16573.
- Takasato, M., et al. (2016). "Generation of kidney organoids from human pluripotent stem cells." Nat Protoc **11**(9): 1681-1692.
- Takebe, T., et al. (2015). "Vascularized and Complex Organ Buds from Diverse Tissues via Mesenchymal Cell-Driven Condensation." Cell Stem Cell **16**(5): 556-565.

- Takebe, T., et al. (2012). "Generation of functional human vascular network." Transplant Proc **44**(4): 1130-1133.
- Takebe, T., et al. (2013). "Vascularized and functional human liver from an iPSC-derived organ bud transplant." Nature **499**(7459): 481-484.
- Tejavibulya, N., et al. (2011). "Directed self-assembly of large scaffold-free multi-cellular honeycomb structures." Biofabrication **3**(3): 034110.
- Teo, A., et al. (2015). "Embryonic stem cells growing in 3-dimensions shift from reliance on the substrate to each other for mechanical support." Journal of Biomechanics **48**(10): 1777-1781.
- Thavandiran, N., et al. (2013). "Design and formulation of functional pluripotent stem cell-derived cardiac microtissues." Proc Natl Acad Sci U S A **110**(49): E4698-4707.
- Thavandiran, N., et al. (2020). "Functional arrays of human pluripotent stem cell-derived cardiac microtissues." Sci Rep **10**(1): 6919.
- Tiburcy, M., et al. (2017). "Defined Engineered Human Myocardium With Advanced Maturation for Applications in Heart Failure Modeling and Repair." Circulation **135**(19): 1832-1847.
- Tulloch, N. L., et al. (2011). "Growth of engineered human myocardium with mechanical loading and vascular coculture." Circ Res **109**(1): 47-59.
- Turaga, D. and T. E. Holy (2012). "Organization of vomeronasal sensory coding revealed by fast volumetric calcium imaging." J Neurosci **32**(5): 1612-1621.
- Ungrin, M. D., et al. (2008). "Reproducible, ultra high-throughput formation of multicellular organization from single cell suspension-derived human embryonic stem cell aggregates." PLoS One **3**(2): e1565.

- Wan, Y., et al. (2019). "Single-Cell Reconstruction of Emerging Population Activity in an Entire Developing Circuit." Cell **179**(2): 355-372 e323.
- Williams, C., et al. (2014). "Young developmental age cardiac extracellular matrix promotes the expansion of neonatal cardiomyocytes in vitro." Acta Biomater **10**(1): 194-204.
- Williams, I. M. and J. C. Wu (2019). "Generation of Endothelial Cells From Human Pluripotent Stem Cells." Arterioscler Thromb Vasc Biol **39**(7): 1317-1329.
- Wu, H., et al. (2018). "Comparative Analysis and Refinement of Human PSC-Derived Kidney Organoid Differentiation with Single-Cell Transcriptomics." Cell Stem Cell **23**(6): 869-881 e868.
- Xia, Y., et al. (2014). "The generation of kidney organoids by differentiation of human pluripotent cells to ureteric bud progenitor-like cells." Nat Protoc **9**(11): 2693-2704.
- Yang, H., et al. (2014). "Role of the basement membrane in regulation of cardiac electrical properties." Ann Biomed Eng **42**(6): 1148-1157.
- Yang, L., et al. (2008). "Human cardiovascular progenitor cells develop from a KDR+ embryonic-stem-cell-derived population." Nature **453**(7194): 524-528.
- Yang, X., et al. (2019). "Fatty Acids Enhance the Maturation of Cardiomyocytes Derived from Human Pluripotent Stem Cells." Stem Cell Reports **13**(4): 657-668.
- Youssef, J., et al. (2011). "Quantification of the forces driving self-assembly of three-dimensional microtissues." Proc Natl Acad Sci U S A **108**(17): 6993-6998.
- Zhang, H., et al. (2019). "Generation of Quiescent Cardiac Fibroblasts From Human Induced Pluripotent Stem Cells for In Vitro Modeling of Cardiac Fibrosis." Circ Res **125**(5): 552-566.

Zhang, J., et al. (2017). "Functional characterization of human pluripotent stem cell-derived arterial endothelial cells." Proc Natl Acad Sci U S A **114**(30): E6072-E6078.

Zhang, J., et al. (2019). "Functional cardiac fibroblasts derived from human pluripotent stem cells via second heart field progenitors." Nat Commun **10**(1): 2238.

Zhang, P., et al. (2012). "Cross talk between cardiac myocytes and fibroblasts: from multiscale investigative approaches to mechanisms and functional consequences." Am J Physiol Heart Circ Physiol **303**(12): H1385-1396.

Zhou, P. and W. T. Pu (2016). "Recounting Cardiac Cellular Composition." Circ Res **118**(3): 368-370.

CHAPTER 2

SELF-ASSEMBLED HETEROTYPIC CARDIAC MICROTISSUES FROM HUMAN PLURIPOTENT STEM CELLS

2.1. Introduction

Engineered cardiac tissue models aim to recapitulate the multicellular composition of the native myocardium by incorporating multiple tissue-relevant cell populations. Here we describe the process of generating self-assembled cardiac microtissues comprised of heterotypic cardiac cell types. The absence of exogenous extracellular matrix (ECM) or scaffolding makes microtissue assembly dependent upon intercellular adhesion interactions over cell-ECM interactions, analogous to early development. Furthermore, the ability to generate these tissues in multiple geometries—such as micro-scale spheroids (Nguyen et al. 2014, Hookway et al. 2016) and meso-scale rings (Gwyther et al. 2011, Strobel et al. 2018)—enables complementary modes of analysis, particularly with respect to functional assessments. Therefore, this approach of self-assembled tissue engineering creates a 3D platform to study how multicellular heterotypic interactions impact tissue structure, function, and phenotype.

2.2. Methods for the Self-assembly of Cardiac Microtissue Spheroids

2.2.1. Material preparation

1. PDMS (SYLGARD 184): Weigh base and curing agents and mix thoroughly at a 10:1 ratio of base to curing agent.

NOTE: Ensure that PDMS base and curing agents are mixed well; the curing agent is cytotoxic on its own, but becomes safe for use with cells when thoroughly mixed.

2. 3% Agarose: Weigh 3g of agarose and add to glass storage container. Pour in 100mL of Dulbecco's Modified Eagle Medium (DMEM). Microwave and stir to dissolve agarose in DMEM. Autoclave.

2.2.2. Replica molding to fabricate sheets of PDMS microwell molds

1. Place microfabricated silicon wafer (Figure 2.1A) in a vacuum chamber contained within a chemical fume hood. Place a few drops of silane into a weigh boat lined with aluminum foil, and set in the vacuum chamber beside the wafer. Leave under vacuum overnight.

NOTE: The chemically-etched silicon wafer contains 400 μ m x 400 μ m inverted pyramidal microwells.

NOTE: Silane surface treatment prevents PDMS from adhering to the silicon wafer as well as to itself (Ratner and Hoffman 2013).

NOTE: We recommend dedicating a vacuum chamber solely for silanization because the chamber also gets coated during the surface treatment.

NOTE: Silane wafer can be used indefinitely for replica molding, but silanization should be repeated every ~5 uses.

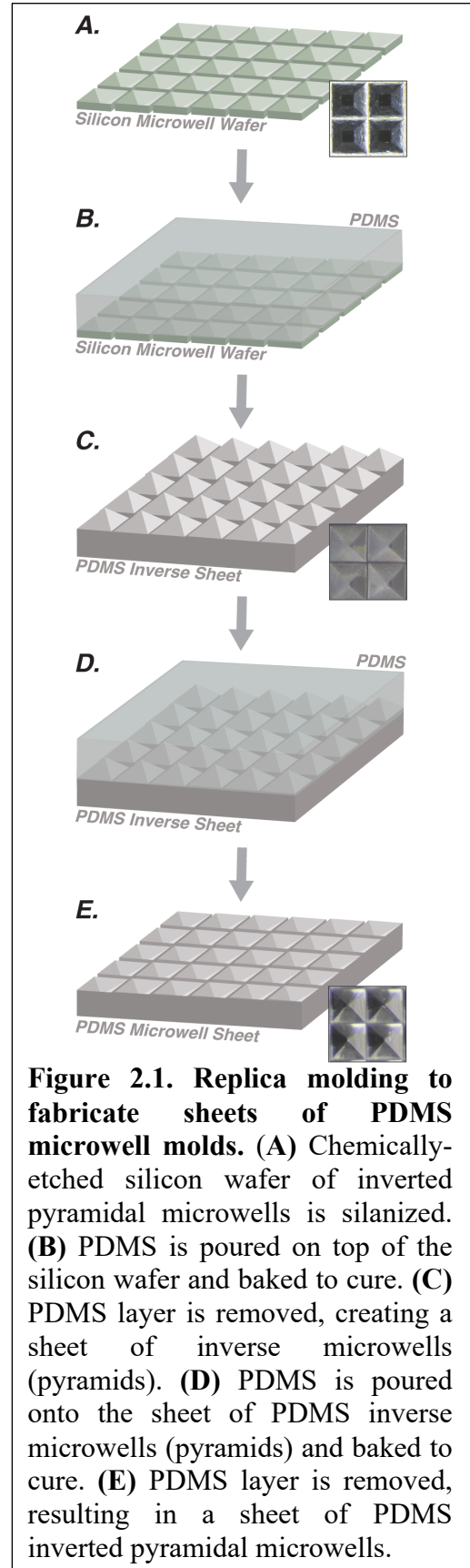
2. De-gas mixed PDMS solution (2.2.1.1) by placing under vacuum until most bubbles have disappeared (~30 minutes). Can be performed in a vacuum chamber set up on a benchtop.
3. Pour de-gassed PDMS onto silane-treated silicon wafer (Figure 2.1B). De-gas PDMS again by placing under vacuum until all bubbles have disappeared, or at least raised up to the top surface, away from the microwell interface. Place in 60°C oven for a minimum of 1 hour, or until cured (no longer viscous or sticky to the touch).

NOTE: The desired PDMS thickness for this step is ~6-8mm. In a 10cm plate, 50g of mixed PDMS results in a thickness of ~6mm and 75g of PDMS yields a thickness of ~9mm.

NOTE: For bubbles to completely disappear in the PDMS once it has been poured onto the silicon wafer or microwells usually takes a minimum of 2 hours under vacuum, but PDMS can be left under vacuum overnight.

NOTE: Bubbles at the PDMS-silicon wafer interface will result in defects at the microwell surface that will persist throughout replica molding and result in tissue assembly impurities.

- Using a razor blade or scalpel, free PDMS from the edges of the container, being careful not to score or scratch the silicon. Peel the PDMS layer away from the silicon wafer, working slowly so as to not tear the PDMS. This process results in a PDMS sheet of pyramids (i.e. inverse microwells; Figure 2.1C).



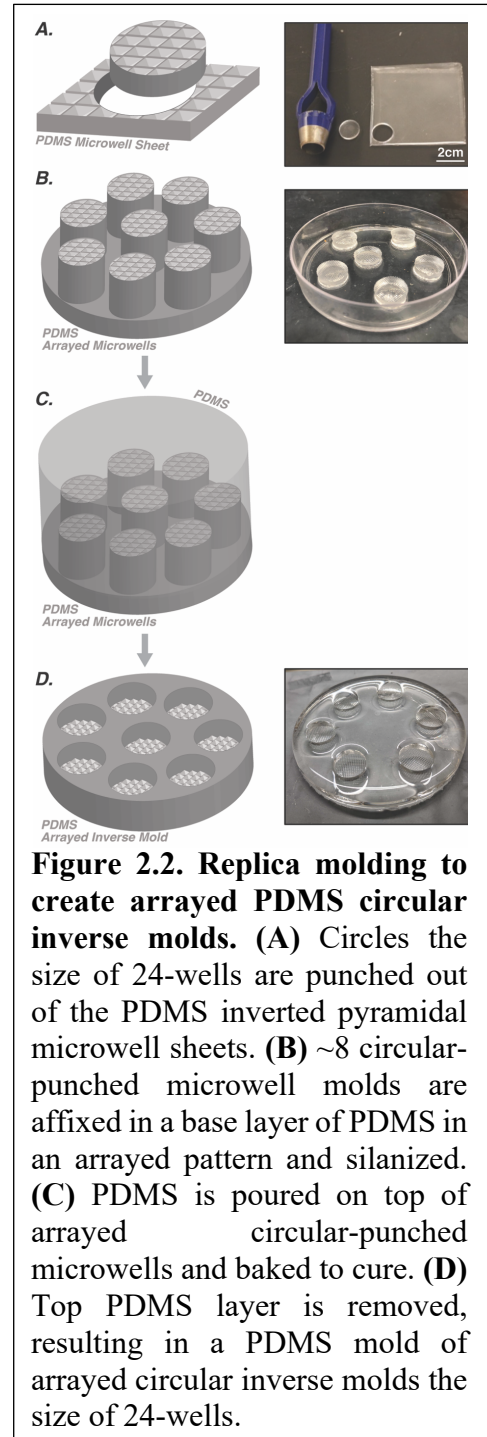
5. Perform silane surface treatment on the sheet of PDMS inverse microwells as described in 2.2.2.1. Place mixed PDMS under vacuum until most of the bubbles have disappeared and then pour on top of PDMS inverse sheet (Figure 2.1D). De-gas and cure as described in 2.2.2.2 and 2.2.2.3. Carefully peel top PDMS layer off of the bottom inverse layer as described in 2.2.2.4. This results in a PDMS sheet of inverted pyramidal microwells (Figure 2.1E).

NOTE: For this step, you need a thicker layer of PDMS (~12mm) because this layer will be cut and adhered in another layer of PDMS. You want the microwell surface of thicker, cut PDMS to be sitting >5mm above the adherent PDMS layer.

2.2.3. Repeat replica molding to create arrayed circular inverse molds

1. Punch the PDMS microwell sheet into circles sized for a 24-well plate (Figure 2.2A).

NOTE: To punch the PDMS microwell sheet into circles that fit in a 24-well plate, we use a 15mm steel hole punch (C.S. Osborne Industrial Tools, Arch Punch; Figure 2.2A). Cutting at this size produces ~1000 microwells (and therefore 1000



microtissues) per 24-well mold. The microwell sheet can also be punched in a diameter that fits additional well-plate sizes; a punched circle sized for a 6-well plate contains ~5000 microwells.

2. To create an array of circular-punched microwell molds that fit into a 24-well plate, pour a 6-8mm-thick layer of de-gassed PDMS into a 10cm plate and arrange ~8 cut microwell molds into the de-gassed PDMS with the microwell surface facing upward, as illustrated in Figure 2.2B. Allow to cure in 60°C oven for a minimum of 1 hour.
3. Silanize the PDMS array of microwell molds as described in 2.2.2.1. Pour de-gassed PDMS into the 10cm dish holding the arrayed molds (Figure 2.2C). De-gas and cure as described in 2.2.2.2 and 2.2.2.3. Carefully peel top PDMS layer off of bottom layer. This results in the final PDMS mold, containing an array of circular wells with inverse microwells (i.e. extruded pyramids) covering the bottom surface (Figure 2.2D, Figure 2.3A).

NOTE: Pour enough PDMS to ensure that the tops of the circular-punched microwell molds are covered >2mm (~8-10mm thick altogether).

4. Autoclave PDMS arrayed circular inverse mold before use.

NOTE: The PDMS inverse molds can be reused indefinitely. To clean, follow a series of wash steps performed in a sonicating bath: 20 minutes in 90% EtOH, 20 minutes in 70% EtOH, 20 minutes in DI water. Then autoclave.

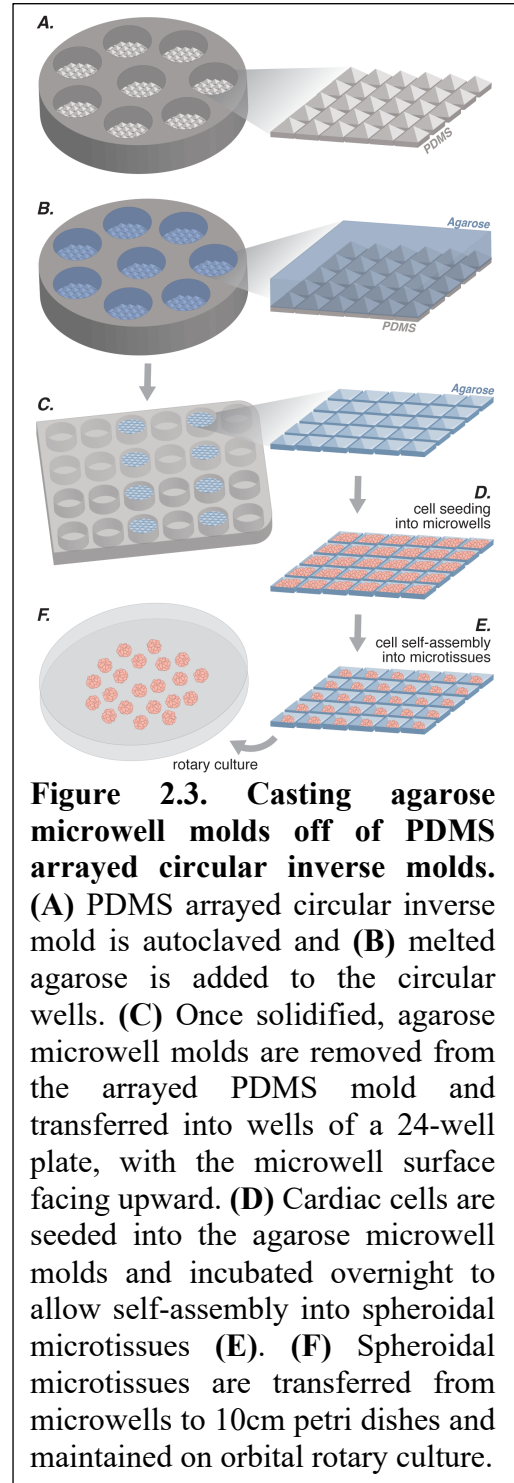
2.2.4. Casting agarose microwell molds off of PDMS arrayed circular inverse molds

1. Microwave 3% agarose (see 2.2.1.2) until liquid.

NOTE: In order to keep the agarose sterile while microwaving, loosen the lid but do not remove. Batch of agarose can be microwaved ~3 times before a fresh batch should be made and autoclaved.

- In a biosafety cabinet, slowly pipette (using stripette or wide-bore P1000 pipette tip) melted agarose into the circular wells of the PDMS arrayed circular inverse mold (Figure 2.3B), being careful not to introduce bubbles. Let the agarose cool until solid (~5-10 min).

NOTE: When pipetting agarose into the circular wells of the PDMS arrayed circular inverse mold, make sure to fill up the wells exactly to the top, such that the agarose creates a flat surface. Any concavity or convexity will prevent the agarose microwell mold from sitting flat against the bottom of the 24-well plate, creating slanted microwells (Figure 2.4).



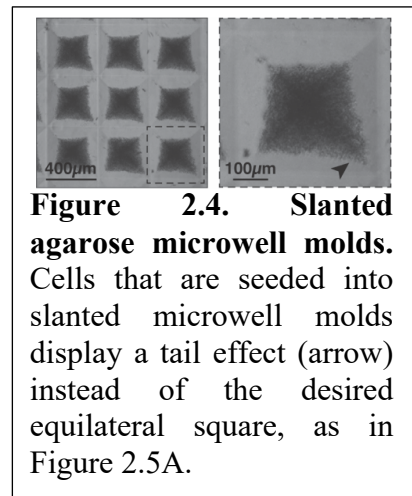
- Remove agarose microwell molds by carefully bending the PDMS arrayed circular inverse mold to release the agarose microwell molds. Make sure to release the agarose microwell molds onto a sterile surface, such as an empty 10cm or 15cm round tissue culture plate.

- Using sterile forceps, carefully place the agarose microwell molds into a 24-well plate, ensuring that the microwell surface is facing up (Figure 2.3C). Using the forceps, gently push the agarose microwell mold down into the well until it lays flat along bottom of plate.

NOTE: Be careful not to touch the forceps to the top microwell surface of the agarose microwell mold. Forceps can easily scratch the agarose, which mars the microwells and creates defects that the cells will settle into. Only touch the sides of the agarose microwell molds when guiding them into the plate.

- Add 0.5mL of media or PBS into the wells that contain agarose microwell molds. Centrifuge the plate at 2000g for 5 minutes in order to force the agarose molds flat against the bottom of the plate and to remove air bubbles from the microwells of the molds.

NOTE: If the thickness of the agarose microwell molds is not uniform, the top microwell surface of the agarose molds will sit at a slant in the 24-well plate. In these instances, the cells cannot fill up the entirety of the microwell when seeded, which alters the self-assembly and size of the microtissues (Figure 2.4).



- Agarose microwell molds can be cast and set into 24-well plates up to 24 hours before cell seeding. Store in an incubator with 0.5-1mL PBS or media in the wells in order to prevent agarose from drying out.

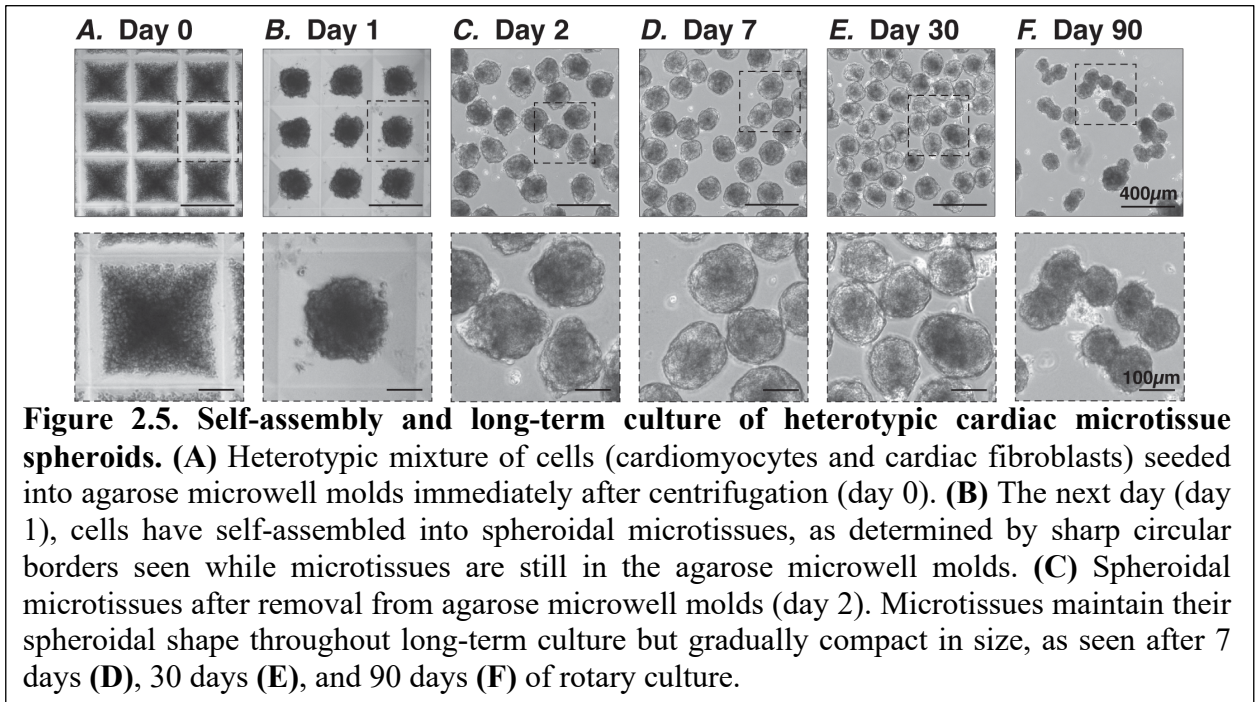
2.2.5. Cell seeding into agarose microwell molds

1. In a biosafety cabinet, rinse adherent cultures of cardiomyocytes (CMs) and cardiac fibroblasts (CFs) with PBS. Incubate cells in 0.25% Trypsin at 37°C for 5-10 min, or until cells have lifted off of the plate in a single-cell suspension. Collect CMs and CFs in a conical tube and quench 1:1 volumetrically with 20% FBS in DMEM. Centrifuge at 200g for 3 minutes. Aspirate supernatant and resuspend in cardiac maintenance medium (RPMI1640 plus B27 supplement with insulin) and 10 μ M ROCK inhibitor (ROCKi).

NOTE: Stem cell-derived cardiomyocytes (Lian et al. 2012, Lian et al. 2013) were lactate-purified (Tohyama et al. 2013) in order to achieve higher purity of CMs. Using enriched cells ensures that the desired ratio of mixed cell types is accurate.

NOTE: Commercially-available primary human cardiac fibroblasts were used in these studies. hiPSC-derived cardiac fibroblasts can also be used (Zhang et al. 2019, Zhang et al. 2019).

2. Count CMs and CFs using a hemocytometer. To make 2000-cell microtissues, seed 2x10⁶ total cells per 24-well sized agarose microwell mold. For heterotypic cardiac microtissues at a ratio of 3:1 CMs:CFs, mix 1.5x10⁶ CMs with 0.5x10⁶ CFs in a conical tube. Centrifuge conical tube with cell mixture at 200g for 3 minutes. Aspirate and resuspend in cardiac maintenance media supplemented with 10 μ M ROCKi at a concentration of 1mL media per agarose microwell mold.
3. Pipette 1mL of cardiac cell mixture (2x10⁶ total cells) into each agarose microwell mold. Centrifuge at 200g for 3 minutes but reduce the acceleration and brake settings (acceleration = 0, brake = 3). Check by microscopy that cells have settled into the microwells (Figure 2.3D, Figure 2.5A).



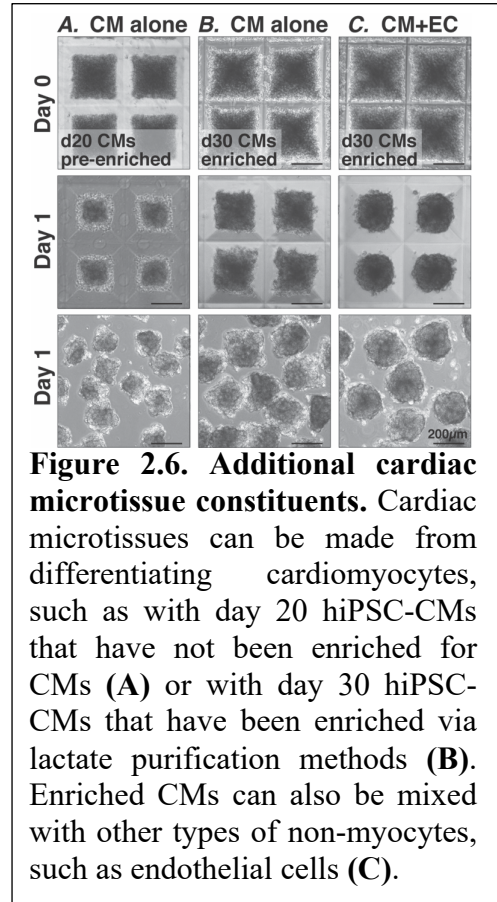
NOTE: To punch the PDMS microwell sheet into circles that fit in a 24-well plate, we use a 15mm steel hole punch (C.S. Osborne Industrial Tools, Arch Punch; Figure 2.2A). Cutting at this size produces ~1000 microwells (and therefore 1000 microtissues) per 24-well mold. The microwell sheet can also be punched in a diameter that fits additional well-plate sizes; a punched circle sized for a 6-well plate contains ~5000 microwells.

NOTE: Additional cell types and/or combinations of cell types can be incorporated into the cardiac microtissues, for example by mixing endothelial cells in with cardiomyocytes (Figure 2.6C). However, in order for tissues to self-assemble, the starting CM population need to contain or be mixed with >10% non-myocytes (Hookway et al. 2019). Therefore, microtissues can be made from heterogeneous cardiac differentiations, which usually contain ~60-80% CMs (Figure 2.6A) or

from enriched CM differentiations that still contain a small non-myocyte fraction (~85-95% CMs; Figure 2.6B).

NOTE: For example, if seeding 4 agarose microwell molds-worth of heterotypic cardiac microtissues, combine 6×10^6 CMs and 2×10^6 CFs in a conical tube, centrifuge, and resuspend in 4mL media.

4. Transfer to incubator, being careful not to jostle the plate. Leave in incubator overnight without disturbing (18-24 hours).



2.2.6. Removing microtissues from agarose microwell molds

1. After 18-24 hours, check that the cells have self-assembled into microtissues in the agarose microwell molds. This will be evident by a sharp spheroidal boundary indicating successful tissue assembly (Figure 2.3E, Figure 2.5B).

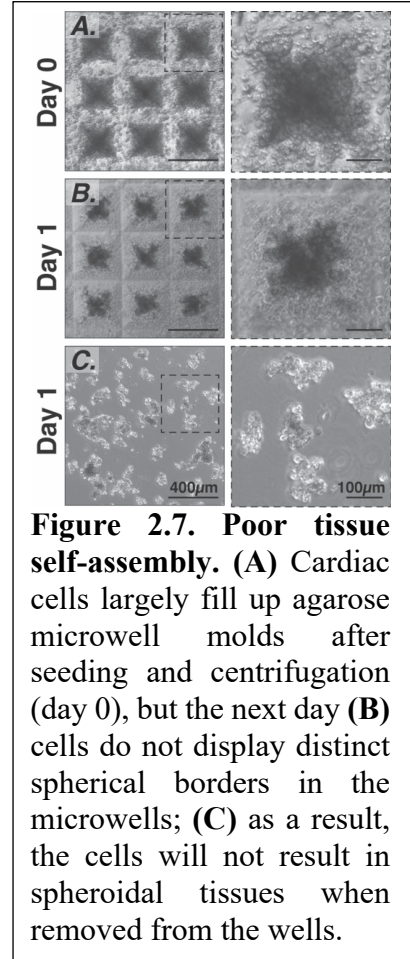
NOTE: Microtissues that do not self-assemble after 18 hours lack distinct spherical borders in the microwells (Figure 2.7).

2. Using P1000 wide-bore pipette tips, gently pipette up and down over the agarose microwell molds to dislodge the microtissues from their microwells. Transfer microtissues to conical tubes. Add 1mL PBS to the agarose microwell molds and gently pipette up and down to

collect remaining microtissues. Repeat until all of the microtissues have been collected in the conical tubes, checking by microscope between rinses.

3. Allow the microtissues to settle to the bottom of the conical tube via gravitational force (~5 minutes). Carefully aspirate the excess supernatant, taking care not to aspirate the pellet of microtissues.

NOTE: In the case that microtissues do not settle down to the bottom of the conical tubes on their own, it is possible to gently centrifuge at ~80g for 1-3 minutes (acceleration = 0, brake = 3). If microtissues are centrifuged too fast or for too long, they will agglomerate.

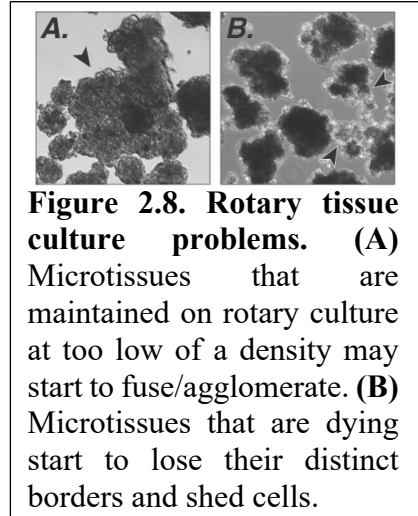


4. Add fresh cardiac maintenance media to the microtissues in the conical tubes and transfer tissues to 10cm petri dish, combining microtissues from 2-4 agarose microwell molds per 10cm dish in a final volume of 10mL media per 10cm plate (Figure 2.3F, Figure 2.5C).

NOTE: Non-tissue culture-treated petri dishes, as opposed to tissue culture polystyrene (TCPS) plates, are utilized in order to minimize cell or tissue attachment to the plates. Ultra-low adherent (ULA) plates can be used as well.

NOTE: Smaller sized plates (i.e. ULA 6-well plates) can be used in place of 10cm petri dishes, however the scaled-down number of microtissues maintained in each well will need to be optimized.

NOTE: When too few microtissues are cultured in a 10cm petri dish, the microtissues may begin to agglomerate (Figure 2.8A) or start to dissociate and eventually fall apart (Figure 2.8B) (Hookway et al. 2016).



2.2.7. Rotary suspension culture

1. Place 10cm dish on a rotary orbital shaker in an incubator rotating at 65rpm.

NOTE: Using an incubator-grade rotary orbital shaker (we use the Benchmark Scientific Orbi-Shaker CO2 with a 0.75” orbital offset distance) will increase the lifetime of the shaker in the humid incubator environment.

NOTE: Adjusting the rotation speed of the rotary orbital shaker changes the hydrodynamic forces in the suspension culture, altering tissue parameters such as agglomeration, size, or cell survival (Kinney et al. 2011, Hookway et al. 2016).

2. Re-feed microtissues every 3 days with cardiac maintenance medium. To feed, use a stripette to transfer the 10mL of media with microtissues to a 15mL conical tube. Allow the microtissues to settle to the bottom of the conical tube (via gravitational force; ~5 minutes). Carefully aspirate the spent media and add fresh cardiac maintenance media. Transfer the microtissues and fresh media back to the 10cm petri dish (can use the same dish or a new one) using a stripette or wide-bore P1000 pipette tip.

NOTE: Other types of microtissues may need to be fed more or less frequently, depending on the metabolic activity of the cultures.

3. Microtissues can be maintained on the rotary for months (Figure 2.5C-F).

2.3. *Methods for the Self-assembly of Cardiac Tissue Rings*

2.3.1. Material preparation

1. Prepare PDMS as described in **2.2.1.1**.
2. Prepare Agarose as described in **2.2.1.2**.

2.3.2. Replica molding to fabricate PDMS inverse mold

1. Silanize 3D-printed plastic annular ring mold as described in **2.2.2.1**.

NOTE: Each ring mold fits a 6-well plate and contains 5 ring wells.

2. De-gas mixed PDMS solution as described in **2.2.2.2**.
3. Pour PDMS onto 3D-printed plastic mold; de-gas and cure as described in **2.2.2.3**.
4. Remove PDMS inverse mold from 3D-printed plastic mold as described in **2.2.2.4**.
5. Autoclave PDMS inverse molds before use.

2.3.3. Casting agarose ring mold off of PDMS inverse mold

1. Microwave 3% agarose until liquid (see **2.2.4.1**).
2. In a biosafety cabinet, slowly pipette melted agarose into PDMS inverse mold, being careful not to introduce bubbles. Let cool until the agarose is solid (~5-10 minutes).

NOTE: In order for the agarose posts to properly form, all of the air from the inverse post molds needs to be removed. One of the most efficient ways to do this before

the agarose cools is by placing a P-20 pipette tip at the bottom of each inverse post mold and removing the air so that the agarose fills the entire inverse post.

3. Remove agarose ring mold by carefully picking up (with sterile gloves) the PDMS inverse mold and use thumbs to bend/press up on the bottom of the inverse mold until the agarose is pushed out of the PDMS inverse. The posts are the most susceptible to tearing or sticking in the inverse molds.
4. Place agarose ring molds into 6-well plate.
5. Add media or PBS into the wells that contain the agarose ring molds to “pre-wet” the agarose before cell seeding. If preparing molds the day before cell seeding, add enough media or PBS to agarose molds such that they won’t dry out in the incubator.

2.3.4. Cell seeding into agarose ring molds

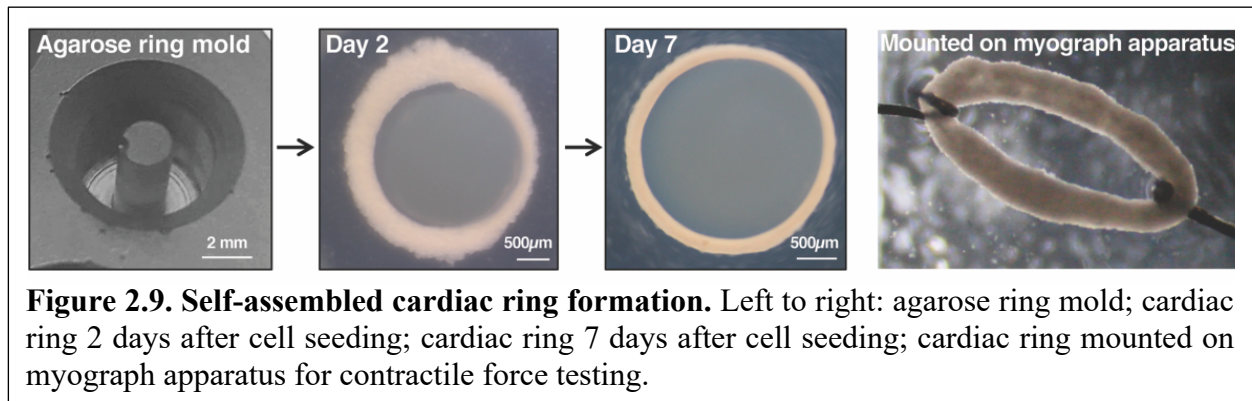
1. Dissociate, count, and mix cardiac cells at desired ratio, as described in **2.2.5.1** and **2.2.5.2**.

NOTE: Seed 500,000 cells per cardiac ring.

NOTE: Suspend the 500,000 cells in a media volume of 75 μ L (concentration of 6.67 $\times 10^6$ cells/mL).

2. Remove media from the ring wells where the cells will be seeded (Figure 2.9A).
3. Add the 75 μ L of 500,000 cardiac cells to each ring well.
4. Do not add media on top of the seeded rings, as this may displace the cells. Instead, fill the wells of the plate around the agarose mold.
5. 18-24h later, gently add more media to the plate, fully submerging the seeded cells.

- Maintain ring tissues in the agarose molds until use for contractile for testing, refreshing media every 2-3 days (Figure 2.9B,C).



2.4. *Functional Testing of Engineered Cardiac Tissues*

Methods to determine the function of engineered tissue constructs have been typically limited to bulk tissue-level measures, as functional analyses at single-cell resolution typically necessitate removing cells from their 3D environment prior to analysis. Video-based modalities to assess function (calcium transients, membrane potential, contractile motion) are a relatively easy and high-throughput approach to characterize microtissue functional properties, and are primarily limited by sample number and data storage capacity as opposed to time for image acquisition or analysis. Direct contractile force measurement is the hallmark functional test, but it requires larger tissue constructs and is much more labor-intensive and therefore lower-throughput.

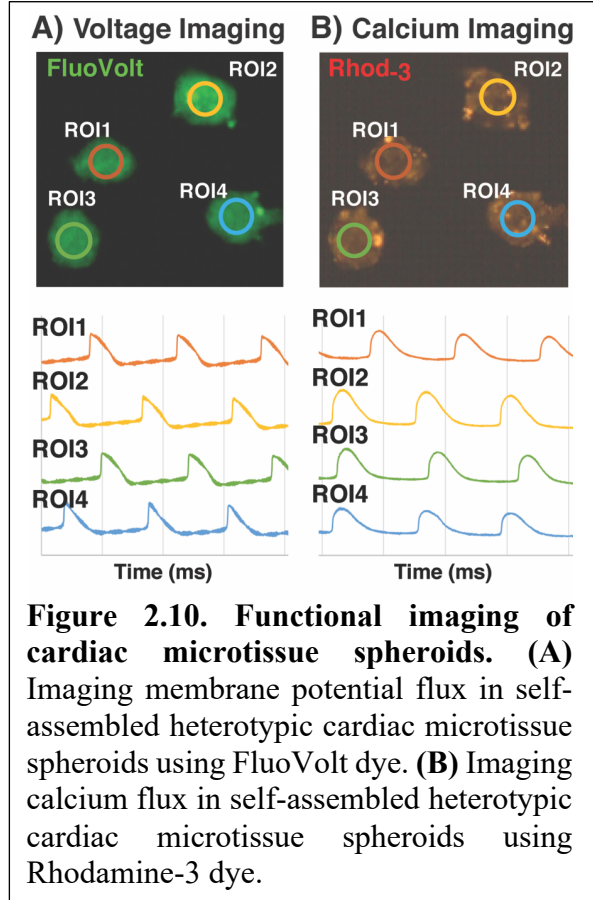
2.4.1. **Voltage imaging**

We used FluoVolt membrane potential dye to plot the waveform of spheroidal cardiac microtissues paced at 1Hz electrical field stimulation. A slight plateau phase was evident in the membrane potential waveform (Figure 2.10A), indicative of a ventricular-like CM phenotype

(Kane and Terracciano 2017), which makes sense given that the standard hPSC-CM differentiation yields largely ventricular-like CMs.

2.4.2. Calcium imaging

In order to compare calcium transients with membrane potential waveforms, the same cardiac microtissues were incubated in both FluoVolt and Rhodamine-3, a red calcium flux dye. The microtissues were stimulated at 1Hz and mean fluorescence intensity was plotted over time to visualize calcium transient waveforms (Figure 2.10B). The shape difference between calcium

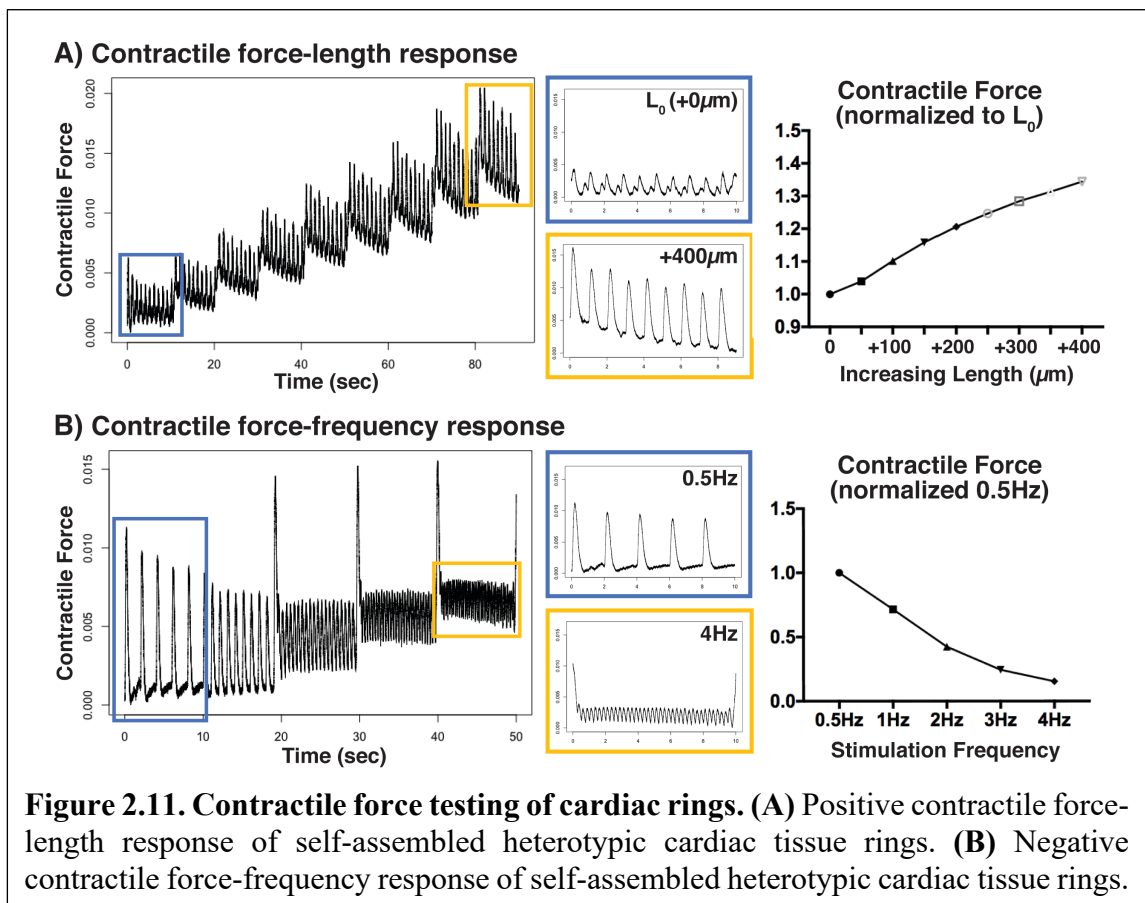


transient and membrane potential waveforms was evident, indicating that the dyes can be used in conjunction with one another.

2.4.3. Contractile force testing

Direct contractile force measurements cannot be acquired with the spheroidal cardiac microtissues, as they are too small to mount on a myograph apparatus. Therefore, the larger-scale, ring-shaped cardiac tissues were generated to enable the determination of contractile force. Cardiac rings were mounted between two pin-hooks, one a force transducer and the other an actuator, submerged in a 37°C bath of Tyrode's solution (a physiologic salt solution) (Figure 2.9). Two types of tests were performed, looking at the force-length and force-frequency responses. For the

force-length testing regiment, the cardiac rings were stretch $50\mu\text{m}$ every 10 seconds and the resultant contractile force was read out. As the tissues were increasingly stretched, the contractile force increased, as demonstrated by the increased force amplitudes with time/stretch (Figure 2.11A); this positive force-length response is consistent with native heart physiology. For the force-frequency testing regiment, the electrical field stimulation was increased every 10 seconds, from 0.5Hz to 1Hz, 2Hz, 3Hz, and finally 4Hz. As the frequency increased, the contractile force decreased, as demonstrated by the smaller force amplitudes at later stages (Figure 2.11B). This negative force-frequency response is inconsistent with native tissue physiology; however, most engineered cardiac tissues display the same negative response, a sign of their immaturity compared to native tissue.



2.5. Conclusions

In conclusion, this chapter details the protocols for forming and testing self-assembled 3D heterotypic cardiac microtissues in two different geometries: a smaller-scale spheroidal tissue amenable to high-throughput video-based functional analyses and a meso-scale ring construct that allows for direct measurement of contractile force. These functional assays demonstrate that the self-assembled cardiac microtissues exhibit physiologic attributes consistent with the state of the cardiac tissue engineering field; for example, with the spheroidal microtissues able to respond to electrical stimulation and the cardiac rings displaying a posting force-length relationship (hallmark of native cardiac tissue) and a negative force-frequency relationship (inconsistent with native tissue function, but consistent with engineered cardiac tissues derived from pluripotent stem cells). The studies in the following chapters primarily utilize calcium imaging of spheroidal microtissues as a functional screen of heterotypic tissue conditions in a higher-throughput manner.

2.6. *Bibliography*

- Gwyther, T. A., et al. (2011). "Directed cellular self-assembly to fabricate cell-derived tissue rings for biomechanical analysis and tissue engineering." J Vis Exp(57): e3366.
- Hookway, T. A., et al. (2016). "Aggregate formation and suspension culture of human pluripotent stem cells and differentiated progeny." Methods **101**: 11-20.
- Hookway, T. A., et al. (2019). "Phenotypic Variation Between Stromal Cells Differentially Impacts Engineered Cardiac Tissue Function." Tissue Eng Part A **25**(9-10): 773-785.
- Kane, C. and C. M. N. Terracciano (2017). "Concise Review: Criteria for Chamber-Specific Categorization of Human Cardiac Myocytes Derived from Pluripotent Stem Cells." Stem Cells **35**(8): 1881-1897.
- Kinney, M. A., et al. (2011). "The multiparametric effects of hydrodynamic environments on stem cell culture." Tissue Eng Part B Rev **17**(4): 249-262.
- Lian, X., et al. (2012). "Robust cardiomyocyte differentiation from human pluripotent stem cells via temporal modulation of canonical Wnt signaling." Proc Natl Acad Sci U S A **109**(27): E1848-1857.
- Lian, X., et al. (2013). "Directed cardiomyocyte differentiation from human pluripotent stem cells by modulating Wnt/beta-catenin signaling under fully defined conditions." Nat Protoc **8**(1): 162-175.
- Nguyen, D. C., et al. (2014). "Microscale generation of cardiospheres promotes robust enrichment of cardiomyocytes derived from human pluripotent stem cells." Stem Cell Reports **3**(2): 260-268.

- Ratner, B. D. and A. S. Hoffman (2013). "Physicochemical Surface Modification of Materials Used in Medicine." Biomaterials Science: An Introduction to Materials: Third Edition: 259-275.
- Strobel, H. A., et al. (2018). "Fabrication of Custom Agarose Wells for Cell Seeding and Tissue Ring Self-assembly Using 3D-Printed Molds." J Vis Exp(134).
- Tohyama, S., et al. (2013). "Distinct metabolic flow enables large-scale purification of mouse and human pluripotent stem cell-derived cardiomyocytes." Cell Stem Cell **12**(1): 127-137.
- Zhang, H., et al. (2019). "Generation of Quiescent Cardiac Fibroblasts From Human Induced Pluripotent Stem Cells for In Vitro Modeling of Cardiac Fibrosis." Circ Res **125**(5): 552-566.
- Zhang, J., et al. (2019). "Functional cardiac fibroblasts derived from human pluripotent stem cells via second heart field progenitors." Nat Commun **10**(1): 2238.

CHAPTER 3

PHENOTYPIC VARIATION BETWEEN STROMAL CELLS DIFFERENTIALLY IMPACTS CARDIAC TISSUE FUNCTION

3.1. *Introduction*

Throughout heart development, cardiomyocytes differentiate and mature in direct contact with non-parenchymal cell types, such as cardiac fibroblasts. Thus, when modeling myocardial tissue *in vitro*, tissue engineers include a supporting stromal cell population that is necessary for tissue formation, although the source of stromal cells has varied widely. This study systematically characterized the phenotype of commonly used stromal cell populations and analyzed the differential impacts of stromal phenotype on cardiac microtissue phenotype and function. Quantitative morphometric analysis, flow cytometry, unbiased morphological feature clustering, and RNA sequencing of the different stromal populations revealed variable cell morphologies, surface marker expression, and gene signatures, with primary adult stromal populations exhibiting more similar phenotypes to each other than to stem cell-derived and progenitor populations. The ability of self-assembled cardiac microtissues to consistently form tissues was highly dependent on the stromal population mixed with stem cell-derived cardiomyocytes, with cardiac fibroblasts and dermal fibroblasts forming the most robust tissues as compared to mesenchymal stromal cells and induced pluripotent stem cell-derived fibroblasts. Cardiac and dermal fibroblasts also resulted in cardiac microtissues displaying a more mature calcium handling profile, with increased amplitude and upstroke velocity. These results demonstrate the breadth of phenotypic variation across stromal populations due to cell and tissue source, with certain primary populations, such as

cardiac fibroblasts and dermal fibroblasts, supporting cardiac microtissue phenotype and improved calcium handling function.

3.2. *Materials and Methods*

3.2.1. Stromal cell culture

See Table 3.1 for cell source and donor information. Human fetal cardiac fibroblasts (fCF) were purchased from Cell Applications (San Diego, CA) and human adult cardiac fibroblasts (aCF) were purchased from Cell Applications and PromoCell (aCF_{PC}) (Heidelberg, DE). Cardiac fibroblasts were seeded at a concentration of 1×10^4 cells/cm² and expanded in Cardiac Fibroblast Growth Medium (Cell Applications) or Fibroblast Growth Medium 3 (PromoCell) for up to 10 passages. Human bone marrow-derived mesenchymal stromal cells (MSC) were purchased from RoosterBio (Frederick, MD), maintained in Rooster-Nourish MSC Medium, replated at 1×10^4 cells/cm², and cultured for up to 10 passages. Human dermal fibroblasts (DF) were purchased from Cell Applications, maintained in Fibroblast Medium (Knockout Dalbecco's Modified Eagle Medium (KO DMEM; Thermo Fisher), 10% fetal bovine serum (FBS; Atlanta Biologicals, Flowery Branch, GA), 1X NEAA, 1X L-glut, 0.1mM β -mercaptoethanol (Bio-Rad, Hercules, CA)), replated at 1×10^4 cells/cm², and cultured for up to 10 passages. iPS-derived teratoma-outgrowth stromal cells (iPS-F_{tera}) (Rand et al. 2018) were maintained in KO DMEM containing 10% FBS, 1mM NEAA, 1mM L-glut, and 1mM Antibiotic-Antimycotic (Thermo Fisher), replated at 1×10^4 cells/cm², and cultured for up to 15 passages. iPS-derived embryoid body-outgrowth stromal cells (iPS-F_{EB}) (Huebsch et al. 2016) were maintained in Fibroblast Medium, replated at 1×10^4 cells/cm², and cultured for up to 10 passages.

Table 3.1. Stromal cell source and donor information.

Cell Line	Company	Lot #	Donor Age	Donor Gender	Donor Ethnicity
Adult Human Cardiac Fibroblasts	Cell Applications	3067	50 years	Male	Caucasian
Adult Human Cardiac Fibroblasts	PromoCell	421Z006.1	48 years	Male	Caucasian
Fetal Human Cardiac Fibroblasts	Cell Applications	2584	18 week gestation	Male	African American
Human Dermal Fibroblasts	Cell Applications	1709	36 years	Female	Caucasian
Human Bone Marrow Mesenchymal Stromal Cells	RoosterBio	00009	43 years	Male	Caucasian
Human Bone Marrow Mesenchymal Stromal Cells	RoosterBio	00056	22 years	Male	Caucasian

3.2.2. Derivation of iPSC-derived fibroblasts

To derive iPS-derived teratoma-outgrowth stromal cells (iPS-F_{tera}) WTC11 hiPSCs were suspended in matrigel and injected into the muscle layer of mice. After 8 weeks, 2cm teratomas were harvested and digested in collagenase I (Sigma-Aldrich, St. Louis, MO). Cells were filtered and replated at 1×10^5 cells/cm². After the first passage, cells were cultured in 10 ng/mL FGF-2 (Stem Cell Technologies) in Knockout Dulbecco's Modified Eagle Medium containing 10% characterized Fetal Bovine Serum, 1mM non-essential amino acids, 1mM *L*-glutamine, and 1mM Antibiotic-Antimycotic (Thermo Fisher) and passaged three times to induce a rapid and complete differentiation to CD13⁺, Tra-1-60⁻ cells. iPS-F_{tera} were maintained in medium without FGF-2 and cultured up to 15 passages. iPS-derived embryoid body-outgrowth stromal cells (iPS-F_{EB}): On day 0, embryoid bodies (EBs) were formed from GCaMP WTC11 hiPSCs by seeding 3×10^6 cells into an ultra low adherent 10cm plate (Corning) in mTeSR medium supplemented with 10 μ M Rock inhibitor. 3 days later, half of the medium was changed to EB20 medium (Knockout Dalbecco's Modified Eagle Medium, 20% fetal bovine serum, 1X nonessential amino acids, 1X *L*-glutamine,

0.1mM β -mercaptoethanol). On day 5, medium was changed to fresh EB20. On day 8, EBs were transferred to a 0.1% Gelatin (Millipore, Burlington, MA) coated 10cm plate in fresh EB20 medium. Medium was changed on days 11 and 14. On day 15, outwardly migrating fibroblasts were selectively captured by incubating cells for 10 min in 0.25% trypsin, filtering through a 40- μ m mesh to remove EBs, and seeding the filtered cells onto a gelatin-coated 10cm plate in EB10 medium (Knockout Dalbecco's Modified Eagle Medium, 10% fetal bovine serum, 1X nonessential amino acids, 1X *L*-glutamine, 0.1mM β -mercaptoethanol). EB10 medium was refreshed on day 18; on day 21, the cells were passaged at a 1:3 split using 0.25% trypsin onto gelatin-coated 10cm plates in EB10 medium. On day 24, EB10 medium was refreshed and on day 27, cells were returned to EB20 medium and fed every 3 days thereafter.

Table 3.2. Antibody source information.

Antibody	Clone	Company	Catalog #	Dilution
Immunocytochemistry				
Vimentin	V9	DAKO	M0725	1:100
Alexa Fluor 647		Thermo Fisher	A31571	1:400
Phalloidin Alexa Fluor 488		Thermo Fisher	A12379	1:400
HCS Cell Mask Red		Thermo Fisher	H32712	1:5000
Hoechst		Thermo Fisher	62249	1:1000
Cardiac Troponin T		Abcam	ab45932	1:400
Wheat Germ Agglutinin		Thermo Fisher	W11263	1:500
Slow+Fast Troponin I		Abcam	ab47003	1:100
Cardiac Troponin I		Abcam	ab110132	1:100
Alexa Fluor 555		Thermo Fisher	A-31572	1:400
Alexa Fluor 488		Thermo Fisher	A-21202	1:400
Flow Cytometry				
CD90-FITC	DG3	Miltenyi Biotec	130-095-403	1:100
CD73-PerCP/Cy5.5	AD2	Biologend	344013	1:100
CD34-APC	AC136	Miltenyi Biotec	130-098-139	1:100
SSEA-4-PE	MC-813-70	Biologend	330405	1:100
CD45-PerCP/Cy5.5	2D1	Biologend	368503	1:100
CD205-Alexa Fluor 647	HD30	Biologend	342205	1:100
CD166-PE	3A6	Biologend	343903	1:100
Alexa Fluor 647 Mouse IgG1, κ isotype ctrl	MOPC-21	Biologend	400135	1:100

Antibody	Clone	Company	Catalog #	Dilution
PerCP/Cy5.5 Mouse IgG1, κ isotype Ctrl	MOPC-21	Biolegend	400149	1:100
PE Mouse IgG1, κ isotype ctrl		BD Biosciences	556027	1:50
FITC Mouse IgG1 isotype ctrl	X40	BD Biosciences	349041	1:50
APC Mouse IgG2a isotype ctrl	X39	BD Biosciences	340473	1:50

3.2.3. Flow cytometry

Stromal cells were fixed with 4% paraformaldehyde for 15-20 min at RT. Based on the standards issued by the International Society for Cellular Therapy for mesenchymal stromal markers, (Dominici et al. 2006) stromal cells were stained for CD166, CD90, CD73, CD45, and CD34 (Table 3.2) using Stain Buffer (FBS) (BD Biosciences). Samples were analyzed on a BD FACSCalibur DXP8 and the resulting data was analyzed using FlowJo software (v.10).

3.2.4. Immunocytochemistry

Stromal cells were fixed with 4% paraformaldehyde for 15-20 min at RT and stained with vimentin overnight at 4°C. Alexa Fluor 647, phalloidin 488, HCS Cell Mask Red, and Hoechst were added for 45 min at RT (Table 3.2 for antibody information and concentrations).

3.2.5. Image acquisition and morphometric assessment

A minimum of 150 stained cells was imaged for each stromal cell population on the Cellomics ArrayScan XTI (Thermo Fisher) and then analyzed with HCS Studio Cell Analysis Software using the Morphology Assay (v.6.0.3.4024) to obtain measurements of the following morphological features: cell length, cell width, cell area, fiber area, cell perimeter, nuclear area, fiber alignment 1, and fiber alignment 2. Fiber alignment 1 corresponds to the standard deviation of each fiber measurement with the axis of the image. Fiber alignment 2 is related to the anisotropy

of a cell that corresponds to the ratio of second moments of the principal axes. The Kolmogorov-Smirnov statistical test with Holm-Bonferroni multiple comparison correction was performed to compare empirical distributions of morphometric measurements between stromal cell populations. Statistical significance was determined at $p < 0.05$ for Holm-Bonferroni corrected p-values.

3.2.6. Principal component analysis

PCA was performed with a Python (v.3.6) script implementing the scikit-learn package (Pedregosa 2011) to analyze primary morphological feature measurements (cell length, cell width, cell perimeter, cell area, nuclear area, fiber area, fiber alignment 1, fiber alignment 2) of approximately 100-150 cells per stromal cell population obtained from the HCS Studio Cell Analysis Morphology Assay.

3.2.7. PhenoRipper

PhenoRipper software (v.1.20, www.phenoripper.org) (Rajaram et al. 2012) was used to compare stromal cell images in an unbiased fashion with minimal user input. Eight-bit tiff images acquired by Cellomics ArrayScan XTI ($n > 100$ for each stromal cell population) were analyzed with the following parameters specified within the software: threshold intensity: 16; block size: 10; # colors used: 10; # block types: 10; # superblock types: 30; training images: 50-100; use background images) to obtain a multidimensional scaling (MDS) plot and clustergram of top ranking superblocks found within the dataset.

3.2.8. RNA sequencing

Stromal cells were lysed with Trizol for RNA extraction with the Direct-zol RNA Miniprep kit (ZymoResearch, Irvine, CA). All groups were collected in duplicate or triplicate. RNA was quantified using the NanoDrop 2000c (Thermo Fisher). RNAseq libraries were created using the SMARTer Stranded Total RNA Sample Prep Kit (Takara Bio, Kusatsu, JP) and sequenced on the NextSeq 500 (Illumina, San Diego, CA) to a minimum depth of 25 million reads per sample. The sequences were aligned to hg19 using TopHat2 (Kim et al. 2013), reads were quantified using featureCounts (Liao et al. 2014), and differential expression analysis was determined using edgeR (Robinson et al. 2010, McCarthy et al. 2012). Hierarchical clustering was done using the HOPACH package in R (Van der Laan 2003). Raw data will be available at GEO (upload in progress).

3.2.9. Pluripotent stem cell culture

Human pluripotent stem cells (WTC11 cells modified with GCaMP6f reporter; generously donated by Dr. Bruce Conklin) (Huebsch et al. 2015, Ma 2018) were cultured on Matrigel-coated (80µg/mL; Corning, Corning, NY) plates in mTeSR medium (Stem Cell Technologies, Vancouver, CA). Cells were grown to 70% confluence, passaged using Accutase (Innovative Cell Technologies, San Diego, CA), and seeded in mTeSR medium with 10µM Rock inhibitor (Y27632, SelleckChem, Houston, TX) at a density of 1×10^4 cells/cm².

3.2.10. Cardiomyocyte differentiation

Differentiation of cardiomyocytes (CM) from human induced pluripotent stem cells (hiPSC) was achieved with a serum-free, chemically defined protocol on monolayer cultures (Lian et al. 2012, Lian et al. 2013). Briefly, GCaMP6f WTC11 hiPSC were seeded onto Matrigel-coated

dishes at 3×10^4 cells/cm² in mTeSR medium and grown to confluence for 3 days. On day 0 of differentiation, the cultures were fed with RPMI 1640 medium (Thermo Fisher, Waltham, MA) and B27 Supplement minus insulin (referred to as RPMI/B27- medium; Life Technologies, Grand Island, NY) supplemented with 12 μ M CHIR99021 (SelleckChem). The initial induction medium was completely removed after 24 h and exchanged with RPMI/B27- medium. On day 3 of differentiation, the medium was changed to RPMI/B27- medium supplemented with 5 μ M IWP2 (Tocris, Bristol, UK) for 48 h and then replaced with fresh RPMI/B27- on day 5. On day 7 of differentiation, medium was changed to RPMI 1640 medium with B27 Supplement plus insulin (referred to as RPMI/B27+ medium; Life Technologies) and refreshed every 3 days thereafter. Cells were replated on day 15 onto Matrigel-coated dishes in RPMI/B27+ medium (see Appendix A for detailed protocol). Purification of cardiomyocytes occurred on days 20-24 by feeding cells with Lactate purification medium (Tohyama et al. 2013) (no-glucose Dulbecco's Modified Eagle Medium (Thermo Fisher) with 1X Non Essential Amino Acids (NEAA; Corning), 1X Glutamax (L-glut; Life Technologies), and 4mM Lactate), refreshing the medium once on day 22. On day 24, the medium was refreshed with RPMI/B27+ and hPSC-CM were subsequently maintained with RPMI/B27+ medium completely exchanged every 3 days thereafter until harvest (D35 \pm 7).

3.2.11. Cardiac microtissue formation

Lactate purified cardiomyocytes (>85% cTnT+; Day 35 \pm 7) were mixed at a 3:1 ratio with adult cardiac fibroblasts, human dermal fibroblasts, mesenchymal stromal cells, or iPS-derived fibroblasts (teratoma-outgrowth stromal cells) before seeding ~2000 cells per inverted 400 μ m pyramidal agarose microwell (Hookway et al. 2016). Cells self-assembled over the course of 18-24 h and the resultant microtissues were then removed from the microwells and maintained in

rotary orbital suspension culture for 7 days in RPMI/B27+ medium at a density of ~2000 microtissues per 100mm Petri dish (Hookway et al. 2016). See Chapter 2 for detailed protocol.

3.2.12. Gene expression analysis

Stromal cells and cardiac microtissues were lysed with Trizol (Invitrogen, Carlsbad, CA) for RNA extraction with the RNeasy Mini Kit (Qiagen, Hilden, DE). All groups were collected in duplicate or triplicate. RNA was converted to cDNA following the iScript cDNA Synthesis Kit (Bio-Rad). Forward and reverse primers (Table 3.3) were designed with the NCBI Primer-BLAST. Preamplified cDNA samples and primers were mixed with Sso Fast EvaGreen Supermix (Bio-Rad), loaded onto a 96.96 Dynamic Array integrated fluidic circuit (Fluidigm, San Francisco, CA), and run on a BioMark HD system. Relative gene expression levels were normalized to reference gene 18s rRNA, and fold changes were calculated using the $\Delta\Delta C_t$ method (Livak and Schmittgen 2001) compared to expression in 3D microtissues composed of cardiomyocytes alone (CM). Results were plotted using Genesis software (Graz University of Technology; (Sturn et al. 2002)).

Table 3.3. Fluidigm primer sequences.

Gene Target	Forward Primer	Reverse Primer
RPS18	CTTCCACAGGAGGCCTACAC	CTTCGGCCCACACCCTTAAT
THY1	TGGATTAAGGATGAGGCCCG	TGGGGAGGTGCAGTCTGTAT
VIM	GGACCAGCTAACCAACGACA	AAGGTCAAGACGTGCCAGAG
DES	CAACAAGAACAACGACGCC	TCACTGGCAAATCGGTCCTC
GJA1	CAAGGGCGTTAAGGATCGGGTTA	TTGGTGAGGAGCAGCCATTGAAA
GJC1	CCCGTGCTACAATGGACCAA	TCTAGCAGGCGAGTCAGGAA
GJA5	GAGGAGGAAAAGAAGCAGAAGT	TCGTATCACACCGGAAATCAG
CDH2	GGACAGTTCCTGAGGGATCA	GGATTGCCTTCCATGTCTGT
NCAM1	GATGCGACCATCCACCTCAA	CCAGAGTCTTTTCTTCGCTGC
VCAM1	AATGCCTGGGAAGATGGTCG	GTCACCTTCCCATTTCAGTGGA
PDGFRA	GAAGGCGCAATCTGGACACT	AGTAATGGGCTCAAAAACCGC
CACNA1C	AGCACACCTCCTTCAGGAAC	ACTGGACTGGATGCCAAAGG

Gene Target	Forward Primer	Reverse Primer
ATP2A2	GGAGAACATCTGGCTCGTGG	CCAGTATTGCAGGTTCCAGGTA
KCNH2	TCATCCGCAAGTTTGAGGGC	GGAAGTCGCAGGTGCAGG
KCNJ12	AGGTTGAGGCACTATGGCAC	AGCCCGACTAGAAGAGAGCA
SCN5A	CTTCGGCCCACACCCTTAAT	CTTCGGCCCACACCCTTAAT
SLC8A1	ACAGGCCAACCTGTCTTCAG	CATTTCTGCAATGCGCCTCT
JPH2	ATACTGGAGCCAGGGCAAAC	TGAACTGGCCTTGGTACGTC
PLN	GATCACAGCTGCCAAGGCTA	TTTGACGTGCTTGTGAGGC
SLN	CAAGTGTTTGCCAGGGAAACG	TGGGTTGAAGGGATGTGTGG
ACTC1	TGTGCCAAGATGTGTGACGA	AGGGTCAGGATGCCTCTCTT
ACTN2	CTTCTACCACGCTTTTGCGG	AAAGCTCACTCGCTAGCCTC
TNNI1	AACGTGCTGTACAACCGCAT	ACCAGCTGCATCTCAACCAT
TNNI3	CCCTCACTGACCCTCCAAAC	CTGCAATTTTCTCGAGGGCGG
TNNT2	GAGAAGGAGCGGCAGAACC	CCTCTTCCCACTTTTCCGCT
MYBPC3	CTTTAGTGACAGAGCGGCCA	AATCTTGGGCTTGGGGCTAC
MYH6	ACCTGTCCAAGTCCGCAAG	CAAGAGTGAGGTTCCCGAGG
MYH7	CTTCGGCCCACACCCTTAAT	CTTCGGCCCACACCCTTAAT
GATA4	CTCAGAAGGCAGAGAGTGTGTCA	GGTTGATGCCGTTTCATCTTGTGGT
ISL1	TTGGCCTGTCCTGTAGCTGGTTTA	GTCAAACACAATCCCGAGACGCT
KDR	CAAGTGGCTAAGGGCATGGA	ATTTCAAAGGGAGGCGAGCA
LEF1	ATCACACCCGTCACACATCC	GGGTAGGGTTGCCTGAATCC
MEF2C	AGATGCTTGGACAGACCCGGTAAT	TGCAGGTTTGTGAGCATTCTTGGG
MESP1	TTCGAAGTGGTTCCTTGGA	GTCTAGCCCTATGGGTCCCT
NPPA	TAGAAGATGAGGTCGTGCC	GGGCAGATCGATCAGAGGAG
TBX5	CAGTCCCCCGGAACAACCTC	TTCTCCGGAGGAATGAGGGT
FABP2	GAAGCTTGCAGCTCATGACA	CCCCTGAGTTCAGTTCCGTC
PGC1A	TGCATGAGTGTGTGCTCTGT	GCACACTCGATGTCACTCCA
PGC1B	ACTATCTCGCTGACACGCAG	AGGAGGGCCTCATTCTCACT
PPARA	TCACCACAGTAGCTTGGAGC	TTCCAGAACTATCCTCGCCG

3.2.13. Calcium imaging analysis

WTC11 hiPSC with genetically encoded GCaMP6f calcium indicator were used to enable visualization of calcium transients in hPSC-CM. Day 7 aggregates were equilibrated in Tyrode's Solution (137mM NaCl, 2.7mM KCl, 1mM MgCl₂, 0.2mM Na₂HPO₄, 12mM NaHCO₃, 5.5mM D-glucose, 1.8mM CaCl₂; Sigma-Aldrich) in 35mm Petri dishes for 30 min at 37°C prior to measuring calcium transients. Samples were mounted on a Zeiss Axio Observer Z1 inverted

microscope equipped with an Orca Flash Hammamatsu camera. Electrodes were placed in the Petri dish and electrical field stimulation was applied at 1Hz (MyoPacer, IonOptix). Video acquisition of calcium flux was obtained using Zen Professional software (v.2.0.0.0) with 10ms exposure and 100fps. One circular 120-pixel region of interest was selected at the center of each aggregate and the mean fluorescent intensity values were plotted. Calcium fluorescent intensity profiles were further analyzed through a custom R-script to quantify the kinetics of each transient (i.e. amplitude, time, velocity, beat rate).

3.2.14. Histology and immunofluorescent staining

Microtissues were fixed for 1 hour in 10% neutral buffered formalin at room temperature. Microtissues were then embedded in HistoGel Specimen Processing Gel (ThermoFisher), paraffin processed, sectioned at 5 micron-thickness, and adhered to SuperFrost Plus microscope slides (ThermoFisher). Samples were deparaffinized with xylene, rehydrated by a series of graded ethanol steps, and washed in PBS. Slides were immersed in Citrate Buffer (Vector Laboratories, Burlingame, CA) at pH 6.0 in a 95°C water bath for 35 min for heat-induced epitope retrieval. Samples were then permeablized in 0.2% Triton X-100 (Sigma-Aldrich), blocked (1.5% normal donkey serum) for 1 hour at room temperature, probed with primary and secondary antibodies against cardiac troponin T, slow+fast troponin I, and cardiac troponin I, and counterstained with Hoechst and WGA (antibody information in Table 3.2). Coverslips were mounted with anti-fade mounting medium (ProlongGold, Life Technologies). All samples were imaged on a Zeiss Axio Observer Z1 inverted microscope equipped with an Orca Flash Hammamatsu camera.

3.2.15. Statistics

The mean +/- standard deviation was calculated from at least 10 biological replicates for all data unless otherwise noted. When comparing three or more groups, one-way analysis of variance (ANOVA) followed by Tukey's post hoc analysis was performed. For all comparisons, statistical significance was determined at $p < 0.05$. All statistical analysis was performed using GraphPad Prism 7.0 software.

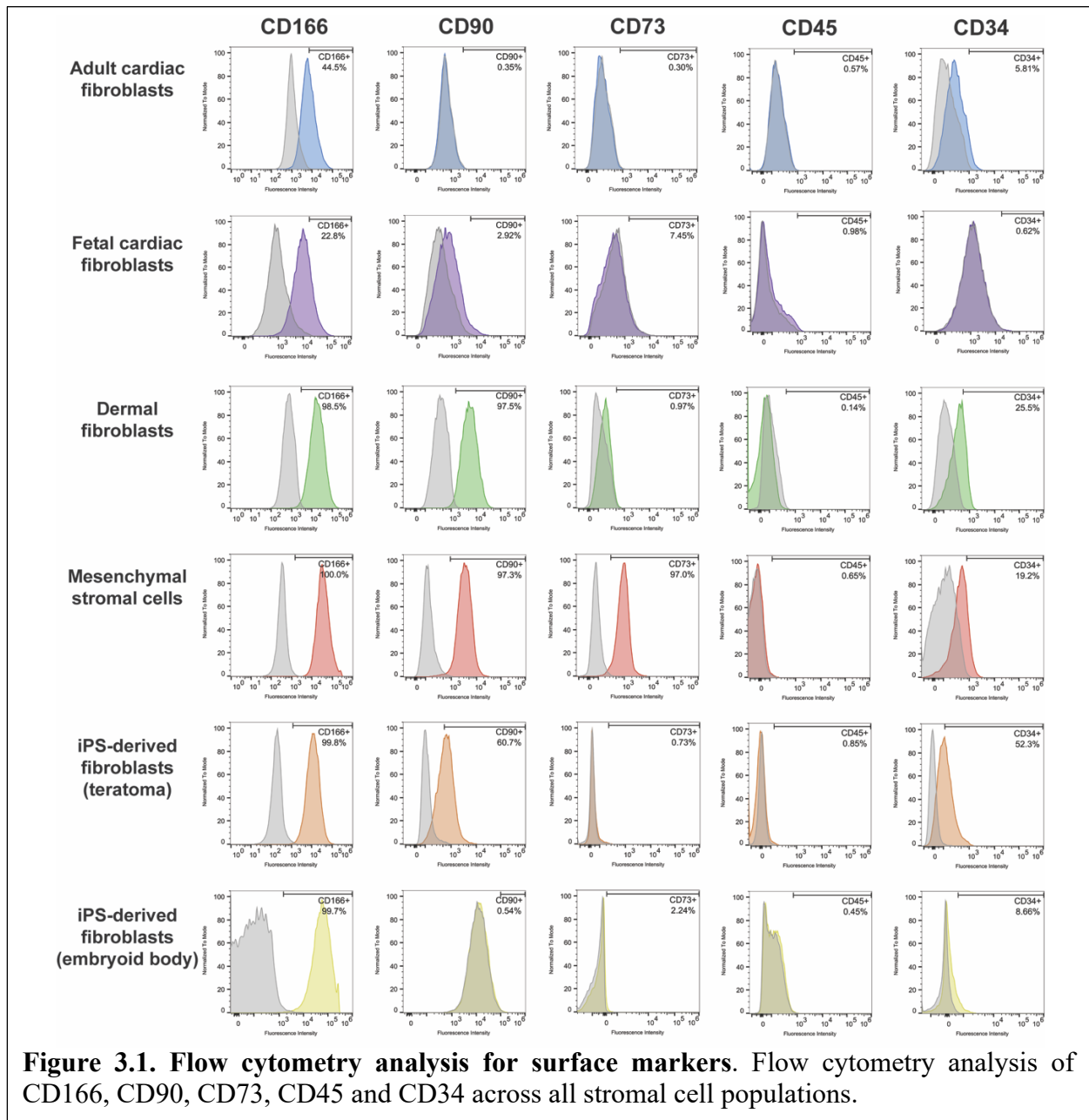
3.3. Results

3.3.1. Stromal populations have distinct expression and morphological profiles

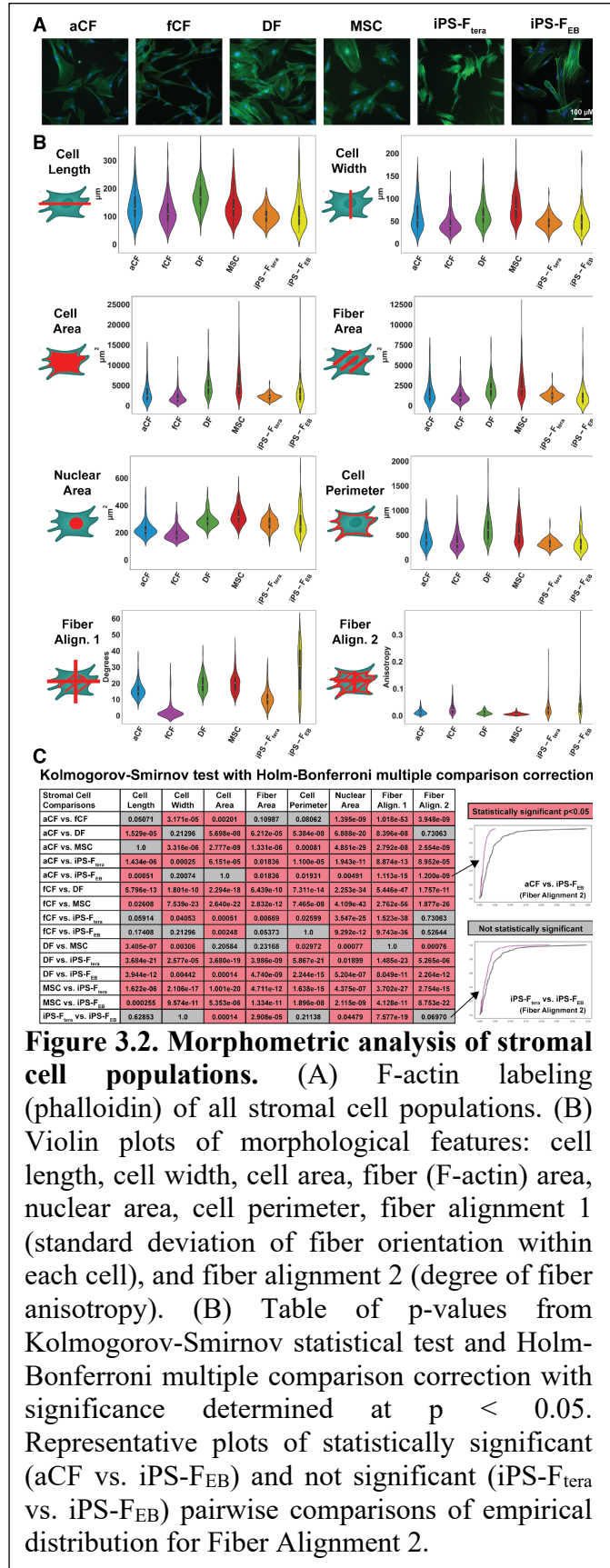
Phenotypic profiling of the stromal populations was performed to gain insight into the differences between fibroblast populations. In order to more completely reflect the breadth of stromal populations used in heterotypic co-culture studies across the field, a wide variety of stromal cell types (aCF, fCF, DF, MSC, iPS-F_{tera}, and iPS-F_{EB}) were examined by the following phenotypic analyses. A panel of common stromal surface markers was measured in individual cell types by flow cytometry to reveal expression levels across stromal populations. As expected, no cell types expressed CD45 and most cell types did not express CD34 at appreciable amounts except for iPS-F_{tera} (>50% of cells), MSC (~20%), and DF (~25%) (Figure 3.1, Table 3.4). All stromal populations contained many CD166⁺ cells, however fCF and aCF had lower moderate percent expression (~23% and ~45%, respectively) compared with DF, MSC, iPS-F_{tera}, and iPS-F_{EB}, which contained >98% CD166⁺ cells. MSC were the only cell population that expressed CD73 (~97%). CD90 expression was highly variable among the different cell populations with very little expression observed in adult and fetal cardiac fibroblasts (Table 3.4).

Table 3.4. Table of CD+ percentages as analyzed by flow cytometry.

	CD166	CD90	CD73	CD45	CD34
Adult cardiac fibroblasts	44.5%	0.4%	0.3%	0.6%	5.8%
Fetal cardiac fibroblasts	22.8%	2.9%	7.5%	1.0%	0.6%
Dermal fibroblasts	98.5%	1.0%	0.1%	25.5%	
Mesenchymal stromal cells	100.0%	97.3%	97.0%	0.7%	19.2%
iPS-derived fibroblasts (teratoma)	99.8%	60.7%	0.7%	0.9%	52.3%
iPS-derived fibroblasts (embryoid body)	99.7%	0.5%	2.2%	0.5%	8.7%



Dramatic differences among stromal cell morphometry were revealed via fluorescent labeling of F-actin with phalloidin (Figure 3.2A). MSC and DF were the largest cells that spread out the most (average area > 5,000 μm^2) in contrast to the iPS-F_{tera} and fCF that exhibited a small, compact morphology (average area < 2,500 μm^2 , Figure 3.2B). MSC were the most variable with regard to cell size and shape, as indicated by the wide distribution with each measured parameter (Figure 3.2B). Cultures of both aCF and fCF included many long, thin spindle-shaped cells whereas DF contained long, wide cells, giving rise to apparent differences in cell area across stromal type (Figure 3.2B). Automated imaging of each stromal cell type enabled high throughput analysis of population morphometry. Specific features of individual cells (length, width, perimeter, area, fiber area, nuclear area, and fiber alignment) extracted from the images were



compared between the different stromal populations (Figure 3.2B). iPS-F_{EB} displayed the widest distribution in length and area, indicating more morphological variability within this population. This variability reflects the iPS-F_{EB} differentiation itself, which was inconsistent and did not yield large quantities of stromal cells as easily as the iPS-F_{tera} differentiation did. DF and MSC exhibited the largest nuclear area ($>295 \mu\text{m}^2$), but the smallest nuclear area to cell area ratio given that they also had the largest average cell areas. MSC displayed the greatest cell area ($>6,200 \mu\text{m}^2$) and corresponding fiber area, although actin fibers were more unaligned compared to the other stromal populations (Figure 3.2B). The iPS-F_{EB} exhibited the highest actin fiber alignment despite having the lowest fiber area (Figure 3.2B).

While the individual morphometric parameters illustrate some differences between cell types, the correlated image-extracted measurements were subjected to principal component analysis (PCA) to reveal uncorrelated variables contributing to morphological differences (Figure 3.3). The overall variance in cell morphology was separated along two principal components on the PCA biplot based on their morphologic characteristics. PC1 captured 91% of the variance and was primarily correlated to differences in cell area (Figure 3.3), demonstrated by individual images of smaller cells on the left of the plot compared to the larger cells on the right of the plot. PC2 captured only 4% of the variance and was largely driven by fiber area. Cells did not completely separate by stromal type, but MSC, DF, and aCF appeared to cluster more closely together, perhaps reflecting a more similar morphology.

The PCA was run on a small number of known (i.e. biased) parameters that were pre-determined and measured from the images to quantify cell morphometrics. To contrast this approach, PhenoRipper was used to evaluate cell morphology in an unbiased fashion (Figure 3.4, Figure 3.5) (Rajaram et al. 2012). The individual cells were analyzed based on similarity of like

features within the images (Figure 3.4, examples of features are shown in images along the top of the heatmap). Clustering stromal cells based on like features indicated that primary isolated adult cells (DF, aCF, MSC) shared greater morphological similarity than the fetal or iPS-derived fibroblasts (fCF, iPS-F_{tera}, iPS-F_{EB}) (Figure 3.4B). Taken together, this phenotypic data suggests that cultured stromal cells adopt characteristic physical features that enable distinction based on morphometric analysis.

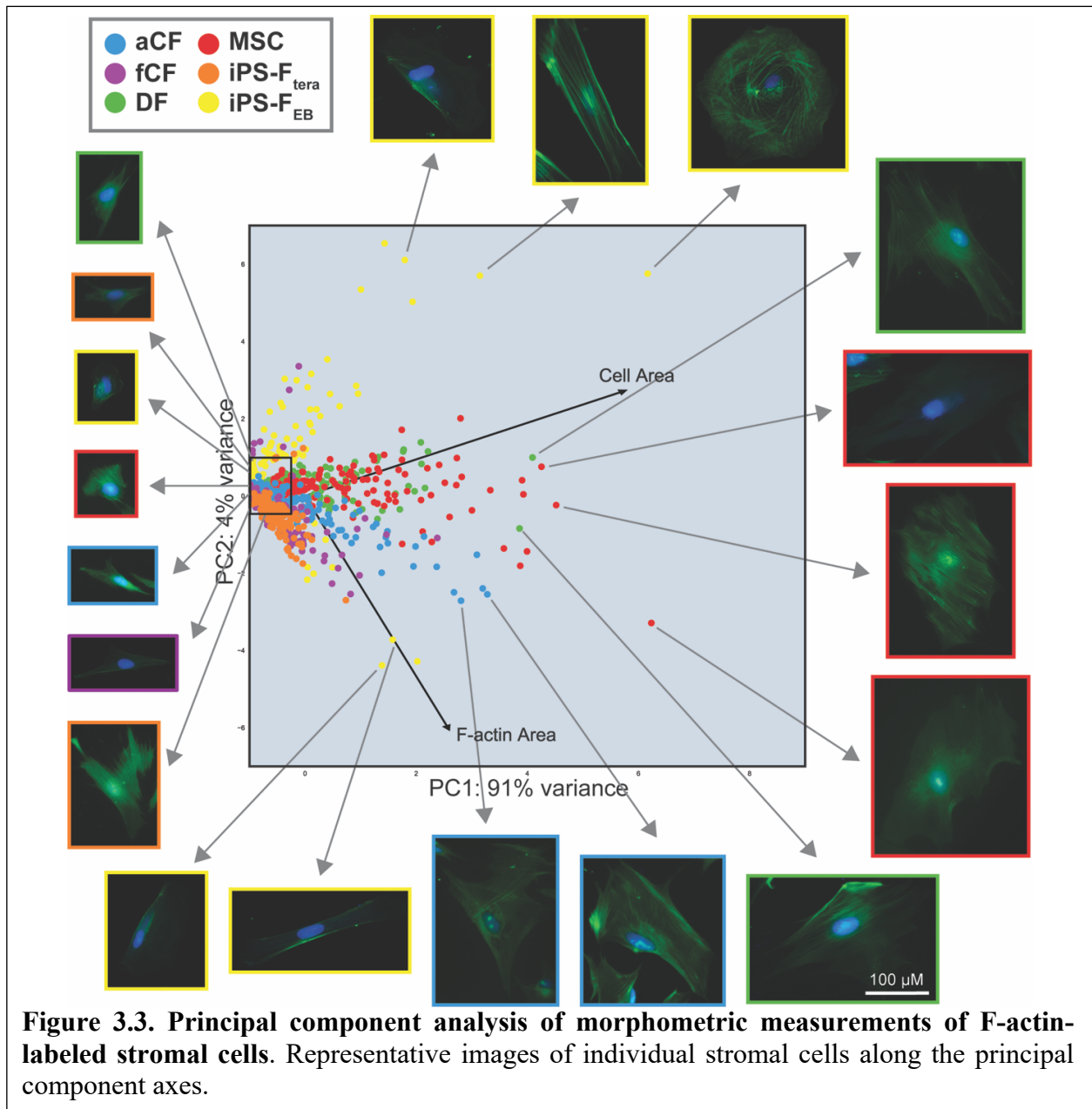
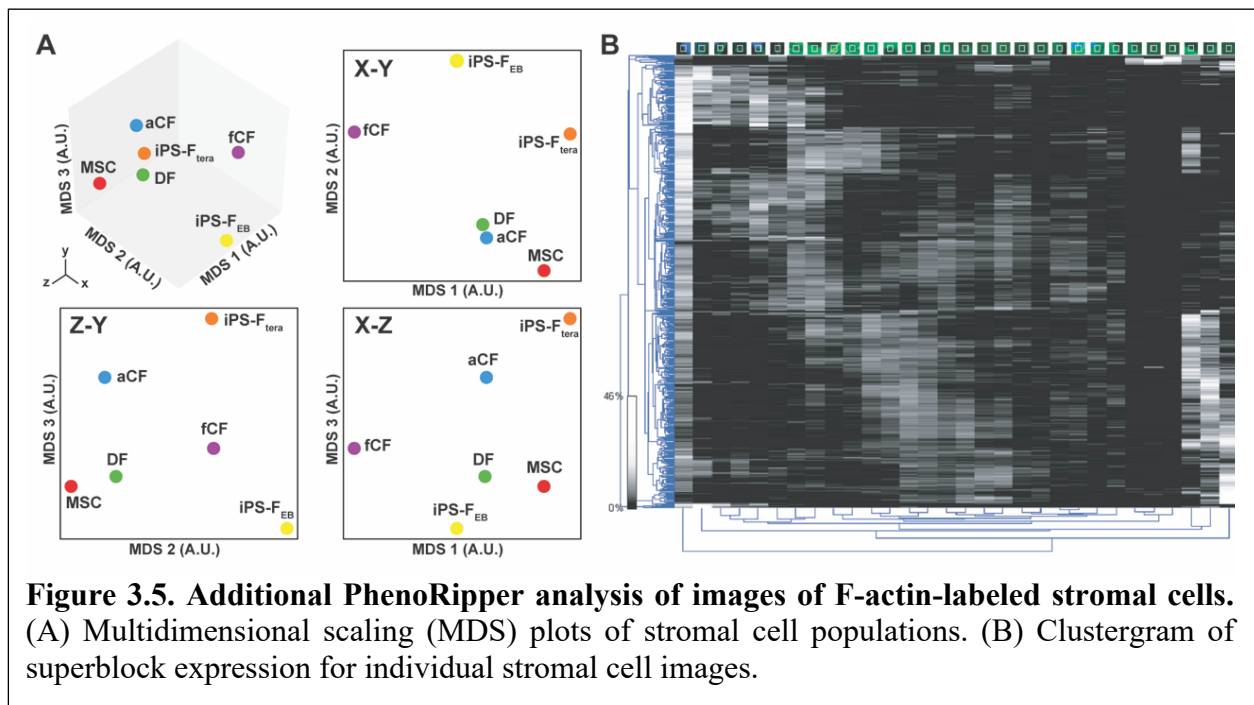
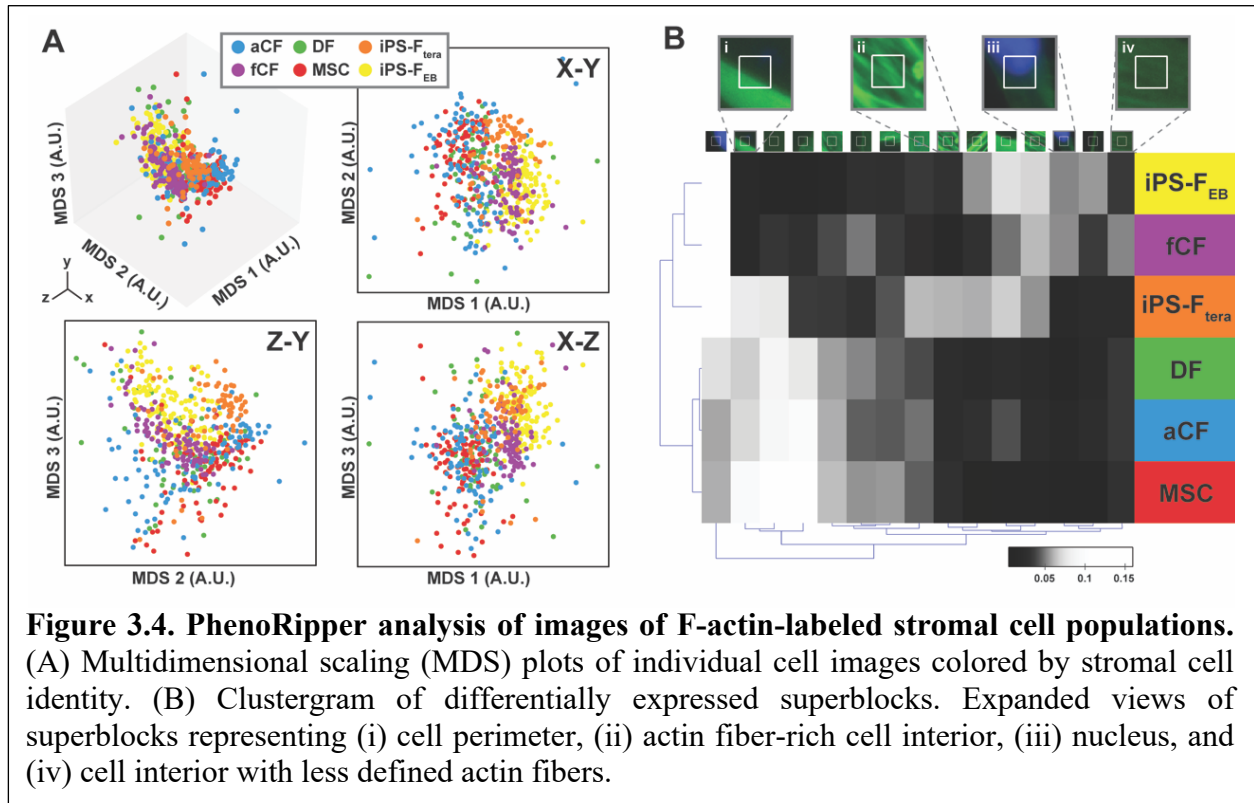
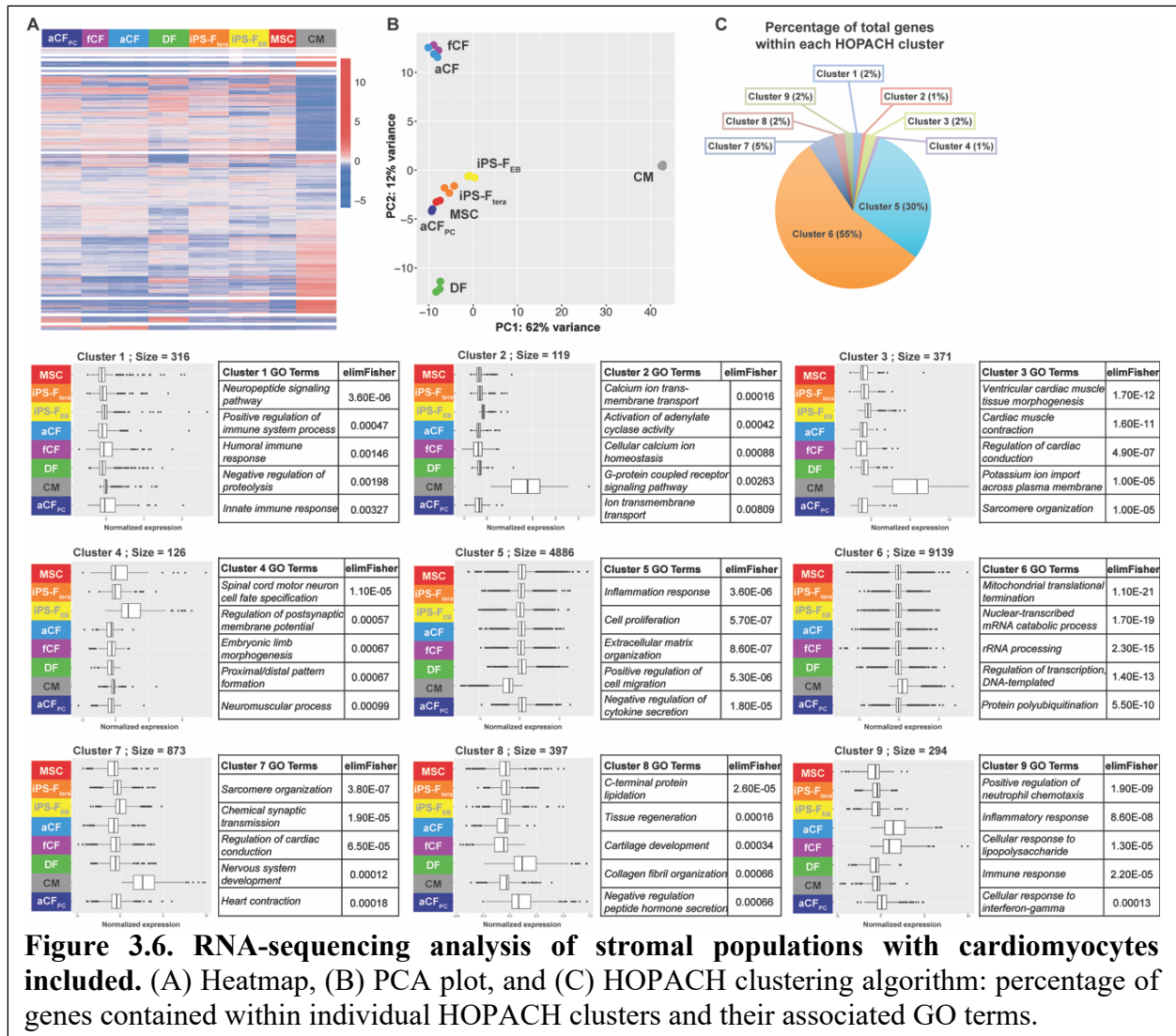


Figure 3.3. Principal component analysis of morphometric measurements of F-actin-labeled stromal cells. Representative images of individual stromal cells along the principal component axes.

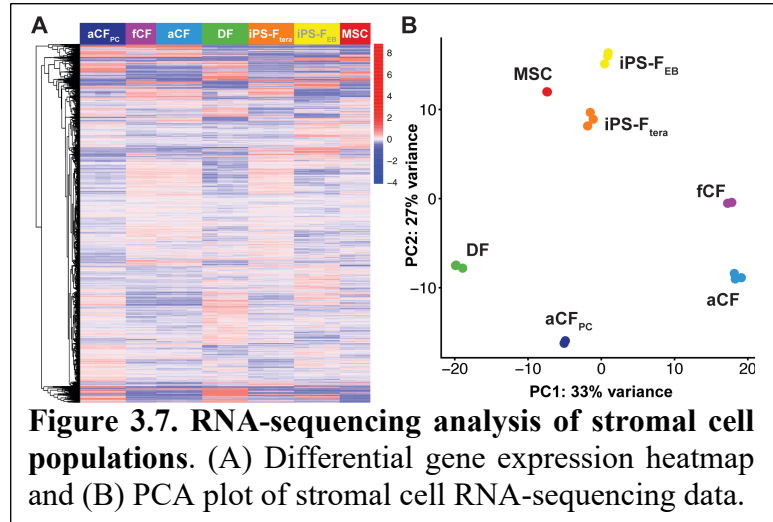


3.3.2. Stromal populations have distinct transcriptomic profiles

Transcriptional analysis was performed to characterize phenotypic differences between stromal cell populations. Not surprisingly, all of the stromal populations were more transcriptionally similar to each other than to hPSC-CM (Figure 3.6A,B). As illustrated in the PCA, the variance in cell phenotype was separated along two principal components based on their subtype. PC1 captured 62% of the variance and was based largely on the differences between cardiomyocytes and all stromal populations combined (Figure 3.6B). PC2 captured 12% of the variance and separated the stromal cells into 3 clusters based on their similarity with one another.



DF clustered individually, fCF and aCF clustered together, and MSC, iPS-F_{tera}, and iPS-F_{EB}, clustered together in the third group. To enable better separation of the individual stromal populations, the transcriptomic data was re-clustered without cardiomyocytes.



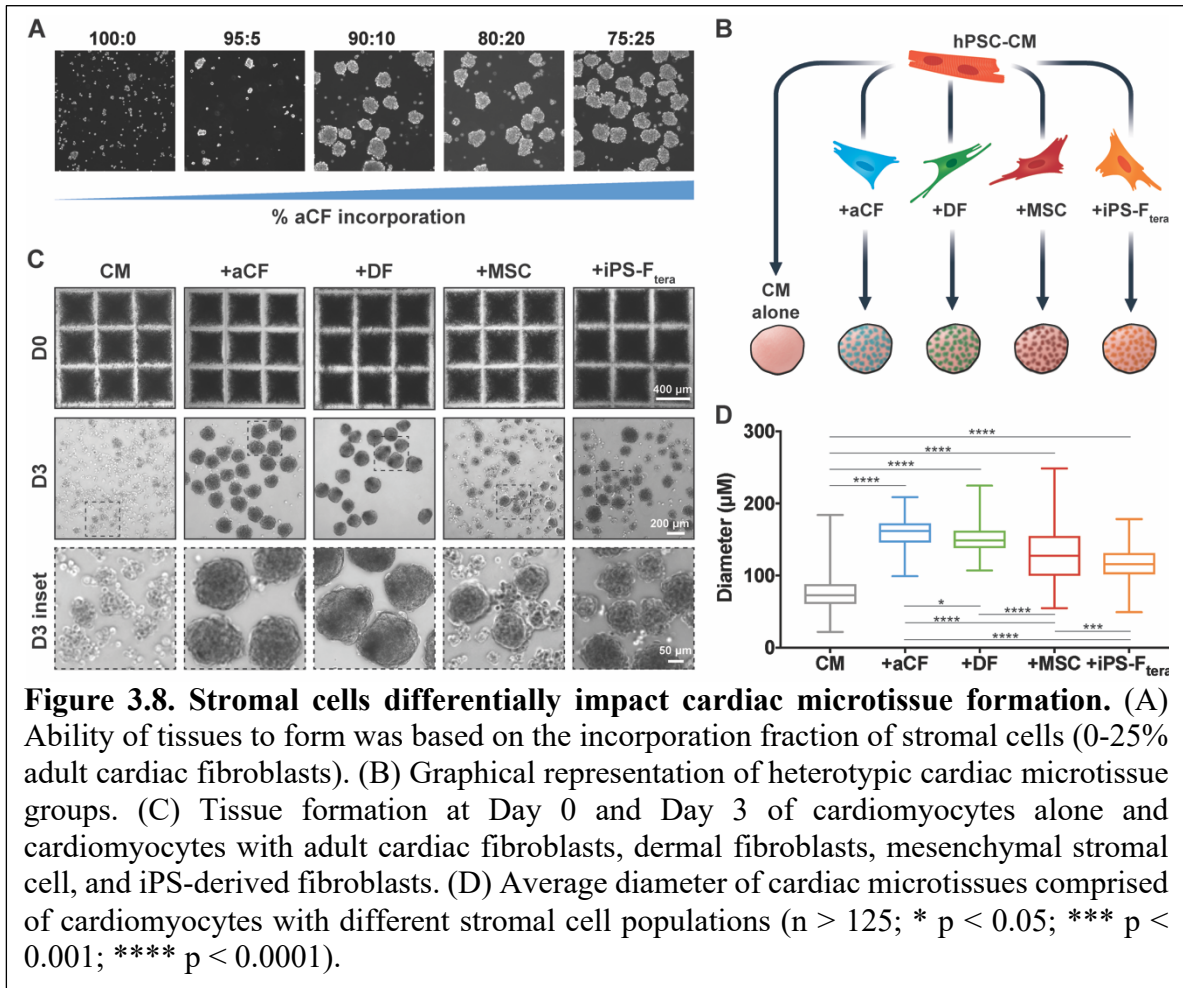
This re-clustering further highlighted the similarities between MSC, iPS-F_{tera}, and iPS-F_{EB} compared to the other stromal cell populations (Figure 3.6A,B), indicating a transcriptional difference in stromal cells isolated from progenitor or stem-cell based differentiations. Adult CF populations from different vendors (aCF which were used throughout these studies vs. aCF_{PC}) did not cluster together with the PCA analysis, indicating variability in fibroblasts even from the same tissue source, perhaps as a result of different isolation and culture methods.

Nine individual clusters of genes that shared similar expression patterns across the cell populations were identified using the Hierarchical Ordered Partitioning and Collapsing Hybrid (HOPACH) clustering algorithm on the RNAseq results (Van der Laan 2003). The separation of 5 clusters (2, 3, 5, 6, and 7) was driven entirely by the comparison of stromal cell to cardiomyocyte transcriptomes (Figure 3.6C). Several of the top GO terms associated with these clusters included cardiac developmental and regulatory pathways such as muscle contraction, conduction, and sarcomeric organization. However, the differences between the remaining HOPACH clusters (1, 4, 8, and 9) could be attributed to other specific stromal populations. For example, the differential genes in Cluster 4 were linked with MSC, iPS-F_{tera}, and iPS-F_{EB}, which contained several homeotic

genes (i.e. *HOXA9*, *HOXA13*, *HOXC10*, *HOXC11*, *HOXD10*) with associated GO terms involved in embryonic morphogenesis and pattern formation. In contrast, the differential genes in Cluster 8 were associated with DF and aCF_{PC}, which contained several extracellular matrix-related genes (ie. *HASI*, *ELN*, *COL22A1*, *VIT*, *ACAN*) and associated with GO terms involved in tissue regeneration and collagen organization (Figure 3.6C). The genes driving Clusters 1 and 9 were largely expressed in the cardiac fibroblast populations (aCF, fCF, aCF_{PC}) and associated with GO terms related to chemokine signaling, inflammatory response, and peptide signaling (Figure 3.6C). Taken together, these results demonstrate that stromal cells obtained from various sources are transcriptionally distinct from one another, but that some gene expression patterns may be conserved across primary isolated stromal cells (aCF, fCF, and DF) compared with progenitor or stem-cell derived stromal cells (MSC, iPS-F_{tera}, and iPS-F_{EB}).

3.3.3. Stromal cells enable variable cardiac microtissue formation

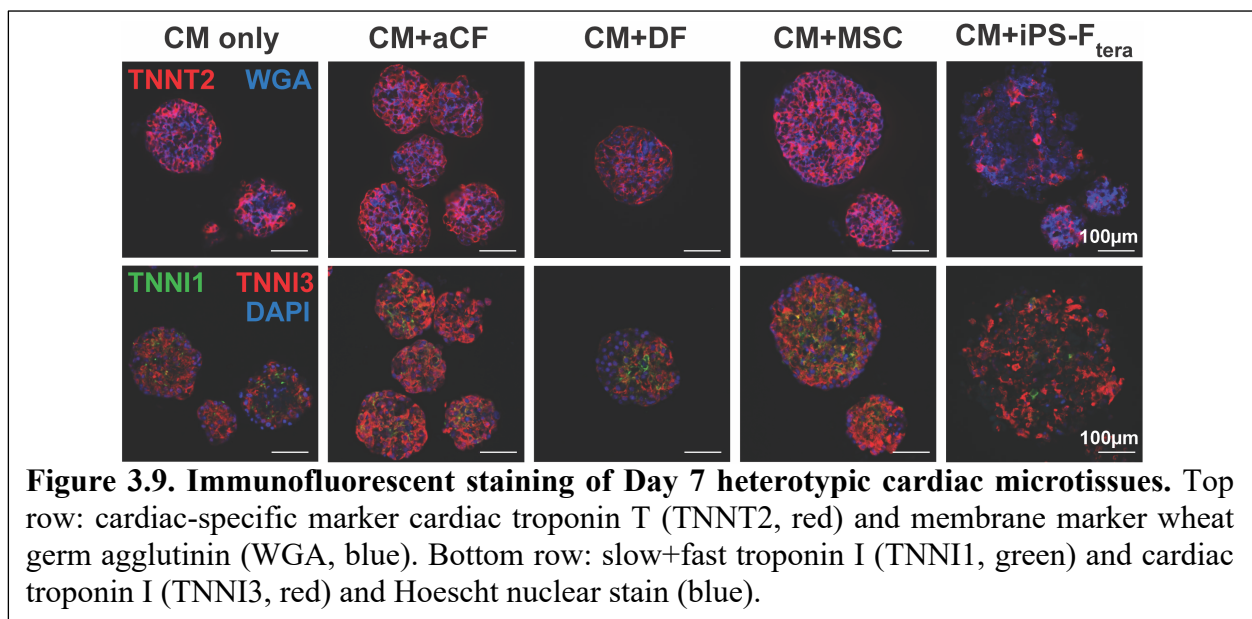
Given the observed variability in stromal phenotypes, we hypothesized each population would differentially impact cardiac microtissue formation, phenotype, and function. To determine the required stromal fraction for consistent cardiac microtissue formation, lactate-purified hPSC-CM were mixed with varying ratios of adult cardiac fibroblasts (0, 5, 10, 20, 25% fibroblasts). Aggregation with ratios below 10% aCF did not yield microtissues, only small clusters containing a few cells. Larger, more uniform aggregates were observed using greater than 10% stromal fraction. However, the most consistent, robust formation was observed with 25% stromal incorporation (Figure 3.8A). Thus, to ensure consistency across studies, lactate-purified hPSC-CM were combined with 25% stromal fraction for all subsequent experiments.



Since different stromal populations have been used in engineered cardiac tissues, microtissue aggregation potential was compared using cardiomyocytes mixed with the most commonly used stromal types: aCF, DF, MSC, and iPS-F_{tera} (Figure 3.8B). The resulting microtissues were highly variable in size across groups. Microtissues composed of only cardiomyocytes did not form well with many small clusters of only a few cells, similar to that observed in the cell ratio study. Microtissues generated with mesenchymal stromal cells or iPS-derived fibroblasts also contained small clusters of cells in addition to larger, non-uniform aggregates leading to highly heterogeneous size distributions based on measured aggregate diameter (+MSC: ~55-250µm; +iPS-F_{tera}: ~50-180µm) (Figure 3.8C,D). The variability in size of aggregates led to an overall decrease in the total number of cardiac microtissues observed in groups

with CM alone, MSC, or iPS-F_{tera} compared to groups with aCF or DF. The inclusion of adult cardiac fibroblasts and dermal fibroblasts led to formation of large, uniform aggregates with consistent size (~180µm in diameter) (Figure 3.8C,D). This data suggests that some stromal populations (MSC and iPS-F_{tera}) do not support uniform formation of microtissues, whereas other stromal populations (aCF and DF) readily support consistent generation of cardiac tissues.

To determine structural uniformity between different heterotypic mixes, cardiac troponin T (TNNT2) distribution was analyzed across fixed, 7 day old microtissues (Figure 3.9). Even distribution of cardiomyocytes (TNNT2) was observed in all aggregates. Stromal cells (WGA) appeared to be evenly distributed within individual aggregates, outnumbered by TNNT2⁺ cells in all groups except microtissues with iPS-F_{tera}. Differences in expression of cardiac troponin I isoforms were observed between groups. Microtissues formed with aCF and MSC contained the most robust TNNI3 staining throughout whereas TNNI1 and TNNI3 were more diffuse in microtissues without stromal cells or with DF or iPS-F_{tera} (Figure 3.9). These data reflect the similarity in microtissue composition between groups and suggests that different stromal interactions may lead to CM phenotypic changes (TNNI1 vs. TNNI3 expression).



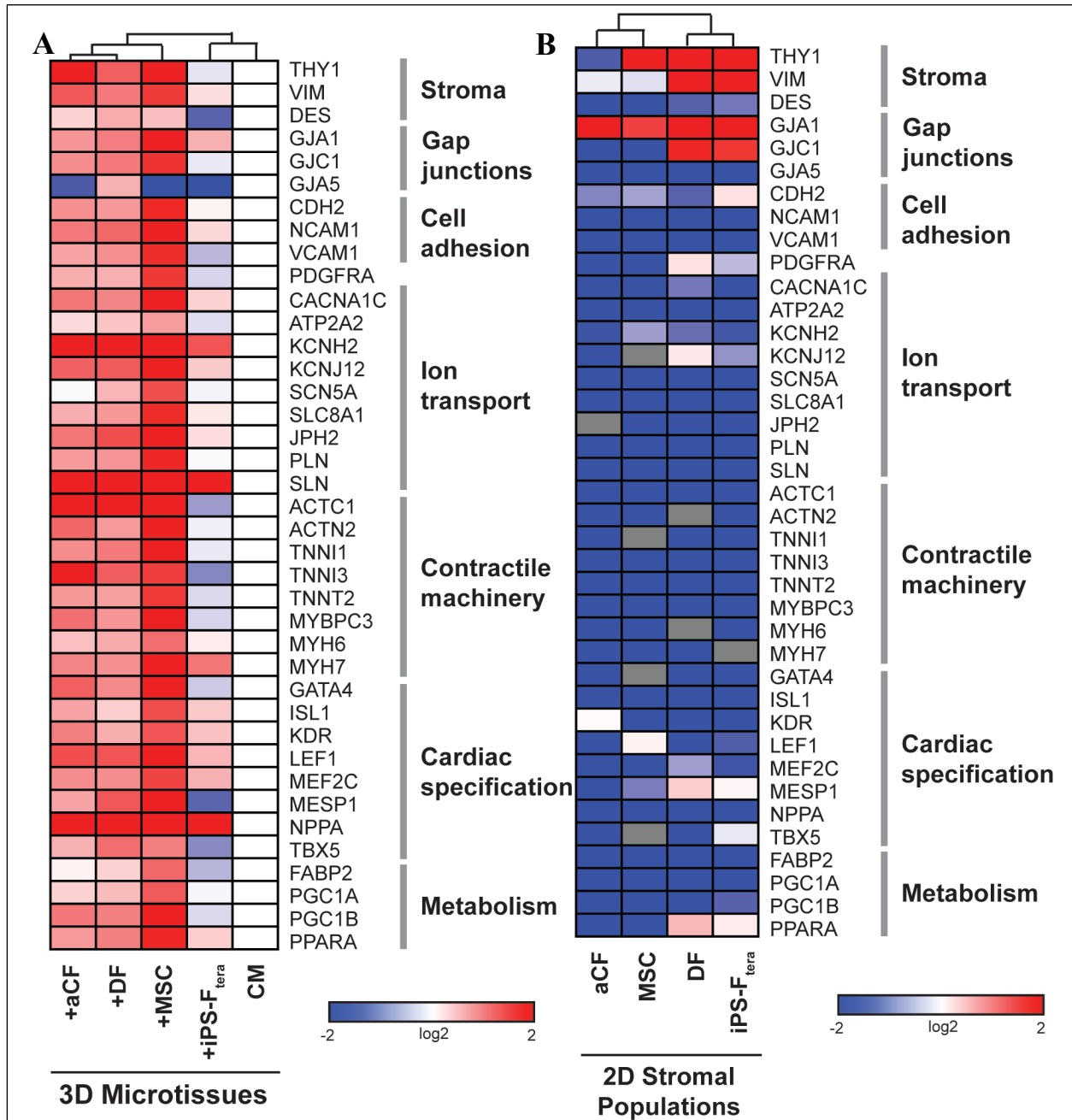


Figure 3.10. Gene expression analysis of 3D heterotypic cardiac microtissues and 2D stromal cell populations. (A) Cardiac- and stromal-specific gene expression of Day 7 heterotypic microtissues compared to Day 7 homotypic microtissues comprised of only cardiomyocytes. (B) Cardiac- and stromal-specific gene expression of 2D stromal cell populations compared to homotypic microtissues comprised of only cardiomyocytes.

3.3.4. Stromal cell inclusion yields phenotypic variation among cardiac microtissues

In addition to differences in aggregation potential resulting from heterotypic interactions, CM phenotype was compared across 7 day old microtissues to analyze changes in cardiac gene expression as a result of culture with various stromal populations (Figure 3.10A). A panel of primarily cardiac-specific gene markers was assessed for the cardiac microtissues and normalized to microtissues comprised entirely from cardiomyocytes. The same panel of markers was characterized on individual stromal cell populations and, as expected, cardiac-related genes were not expressed in the stromal cells (Figure 3.10B). Gene expression profiles of cardiac microtissues comprised of only CM or with iPS-F_{tera} were clearly distinguished from the other stromal cell populations via hierarchical clustering of the gene expression profiles (Figure 3.10A). Commonly expressed stroma-related genes (i.e. *THY1*, *VIM*, *GJAI*, *GJCI*) were abundant, albeit differentially expressed, by the different stromal cell populations. The stark contrast in gene expression profiles between the heterotypic cardiac microtissues and their respective individual stromal populations allowed for direct comparison of the specific influence of stromal cell type on cardiomyocyte phenotype within the microtissues.

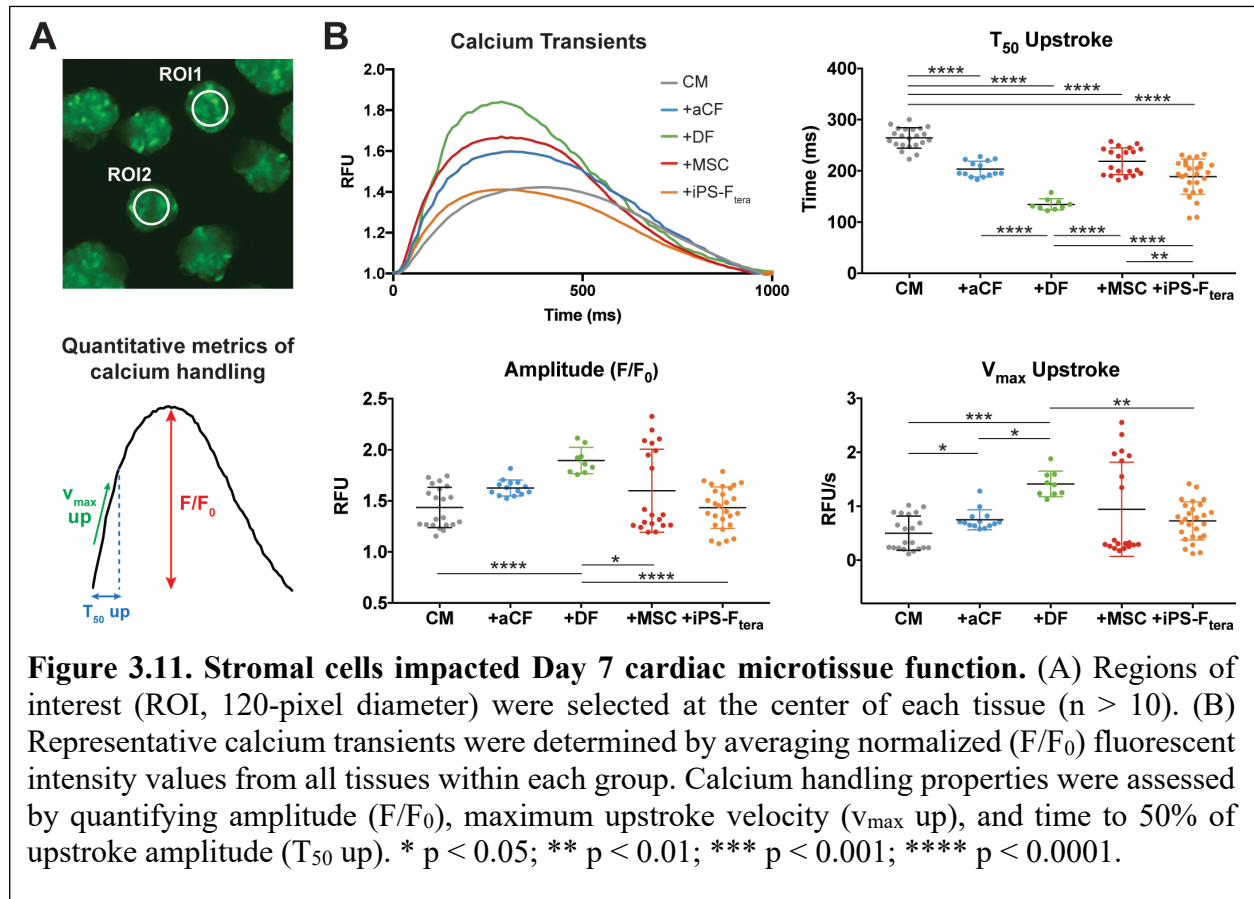
Increased expression of genes mediating ion exchange (*SLN*, *KCNH2*) was observed in all microtissues containing stromal cells compared to microtissues consisting of only CM (Figure 3.10A). Several genes involved in cardiomyocyte development (*TBX5*, *MESP1*, *MEF2C*, *GATA4*, *ISL1*, *LEF1*), contractility (*MYH6*, *MYH7*, *MYL7*, *TNNT2*, *TNNI1*, *TNNI3*), and metabolism (*PGC1B*, *PPARA*) were expressed at higher levels in the microtissues cultured with MSC, aCF, and DF compared to those containing iPS-F_{tera}. Microtissues containing MSC expressed higher levels of most genes, including regulators of metabolism (*FABP2*, *PGC1A*) and sodium ion channels (*SCN5A*, *SLC8A1*) compared to microtissues with aCF or DF. Interestingly, a subset of

genes related to early cardiac development (*TBX5*, *MESP1*) were expressed at higher levels in microtissues containing DF compared to aCF, whereas some genes related to myocyte contractility (*ACTN2*, *MYBPC3*) were expressed at higher levels in microtissues containing aCF compared to DF. Overall, microtissues containing iPS-F_{tera} expressed lower levels of most cardiac-related genes, suggesting that iPS-F_{tera} cells may not support cardiac phenotype as well as the stromal cell populations sourced from primary tissues. Together, this data demonstrates that cardiomyocyte phenotype is altered by heterotypic interactions and that culture with primary derived stromal cells (aCF, DF, MSC) promotes a more robust cardiac phenotype compared to culture without exogenous fibroblasts or with iPS-derived fibroblasts.

3.3.5. Stromal cell modulation of cardiac microtissue calcium handling

Calcium transients of individual aggregates were optically monitored 7 days after tissue formation to evaluate the influence of various stromal populations on cardiac tissue calcium handling properties (Figure 3.11A). All of the heterotypic microtissues exhibited a decreased T_{50} upstroke compared to homotypic microtissues formed only with CM, demonstrating improved kinetics of calcium influx with the inclusion of stromal cells. The amplitude of calcium transients was greatest for microtissues containing DF and the V_{max} upstroke was significantly higher in microtissues containing aCF or DF compared to CM alone microtissues (Figure 3.11B). The calcium handling properties of microtissues containing CM alone, +MSC, or +iPS-F_{tera} exhibited greater variability with increased standard deviations for each measurement, reflecting inconsistent responses between microtissues within these groups. These results demonstrate that calcium handling properties of engineered microtissues are modulated by heterotypic interactions with different stromal cell populations and that microtissues comprised of CM with aCF or DF yield

the most consistent microtissues with accelerated functional maturation with respect to their calcium handling properties.



3.4. Discussion

The observed phenotypic differences between fibroblastic populations instigated assessment of the structural and functional benefits of heterotypic microtissues. The International Society for Cellular Therapy along with researchers working with MSC have come to consensus on a typical panel of marker expression expected within the cell population (Dominici et al. 2006): $CD166^+$, $CD90^+$, $CD73^+$, $CD34^-$, and $CD45^-$. However, stromal cells in general are broadly defined as adherent cells that secrete extracellular matrix and are usually characterized by a spindle-shaped morphology. Morphometric profiling of the different stromal populations examined in this study

revealed significant variability in cell shape, size, and actin fiber organization, indicating that qualitative assessment of cell appearance is insufficient to describe fibroblast phenotype. Furthermore, flow cytometry data demonstrated variable surface marker expression across stromal populations. CD90 is generally thought to be an identifying marker of fibroblasts, yet reports of CD90 expression in cardiac fibroblasts is variable, from high expression levels (Hudon-David et al. 2007, Jonsson et al. 2016) to mixed expression (Furtado et al. 2014), and in this study, a distinct lack of CD90 expression in both the fetal and adult cardiac fibroblast populations. The reported variability could be due to *in vivo* vs. *in vitro* phenotype of cardiac fibroblasts and changes that arise during *in vitro* culture (Cho et al. 2018). For example, FGF-2 specifically decreases CD90 expression in MSC populations (Hagmann et al. 2013), indicating that specific culture conditions can lead to changes in surface marker expression. Altogether, this data demonstrates that singular metrics are insufficient to characterize stromal cells and predict their suitability for use in engineered tissues.

In recent years, there has been an increase in studies using pluripotent stem cell-derived cardiomyocytes as *in vitro* models of cardiac behavior given the advancement of differentiation protocols, which yield more robust cardiomyocyte populations. Several studies have shown that engineered 3D cardiac tissues generated from hPSC-CM serve as better predictive models of cardiac physiology and drug response than 2D monolayers (Nguyen et al. 2014, Huebsch et al. 2016, Kerscher et al. 2016, Vuorenmaa et al. 2017, Correia et al. 2018). Within the context of 3D engineered tissues, strong evidence has been presented for the inclusion of a non-myocyte fraction to form stable cardiac tissues (Thavandiran et al. 2013, Huebsch et al. 2016, Giacomelli et al. 2017). However, the requisite ratio of stromal cells and the effects of different stromal cell populations on multicellular cardiac tissue function have not been fully explored. Consistent with

previous reports (Kensah et al. 2013, Thavandiran et al. 2013, Ariyasinghe et al. 2017, Mills et al. 2017, Ronaldson-Bouchard et al. 2018), the data presented here demonstrates the need for a minimum 10-25% stromal fraction to ensure robust tissue formation and stability. The variability in stromal fraction observed across studies can be explained in part by the variety of stromal cell types used in different engineered constructs, as well as inconsistencies with CM differentiation efficiencies from batch-to-batch and derivation protocols between labs (Laco et al. 2018). In this study, microtissues generated from CM alone resulted in inconsistent tissue formation despite following the same differentiation and purification protocols, highlighting the variability in pure hPSC-CM. This study aimed to systematically compare the impacts of multiple commonly used stromal populations on 3D engineered cardiac tissue to determine if specific sources of stromal cells influenced cardiac tissue formation and function differentially.

To date, cardiac tissues have been generated using cardiomyocytes alone (Balistreri et al. 2017, Kofron et al. 2017, Correia et al. 2018, Kim et al. 2018), or by mixing with cardiac fibroblasts (Ravenscroft et al. 2016), dermal fibroblasts (Noguchi et al. 2016, Ravenscroft et al. 2016, Vuorenmaa et al. 2017, Ronaldson-Bouchard et al. 2018), mesenchymal stromal cells (Stevens et al. 2009, Emmert et al. 2013), and, more recently, pluripotent stem cell-derived fibroblasts (Huebsch et al. 2016, Masumoto et al. 2016, Mills et al. 2017, Nakane et al. 2017). In a subset of these studies, endothelial cells (EC) have also been combined with cardiomyocytes and stromal cells to generate complex tricellular cardiac tissues (Caspi et al. 2007, Burridge et al. 2014, Giacomelli et al. 2017, Archer et al. 2018). However, as a result of cell type and source variability, the functional consequences of stromal inclusion have remained elusive. Cardiac tissues comprised of CM+CF+EC exhibited appropriate contractile responses to inotropic chemical agents compared to microtissues comprised of CM+DF+EC that did not respond to these drugs, suggesting that

inclusion of DF may not support proper pharmacological response of cardiac tissues (Ravenscroft et al. 2016). However, these results are confounded by the fact that the specific influences of the fibroblasts on the cardiomyocytes cannot be dissected apart from the cardiomyocyte-endothelial cell interactions. Therefore, in the study described here, only one non-myocyte population was paired with cardiomyocytes to study heterotypic impacts in a more controlled manner. In contrast to the reports above, DF in this two-population system supported cardiac microtissue formation, cardiac gene expression, and calcium handling similar to or better than CF. Moreover, a recent report of engineered cardiac tissues comprised of CM+DF under electrical stimulation demonstrated the greatest extent of CM phenotypic and functional maturation seen to date (Ronaldson-Bouchard et al. 2018), suggesting that DF are able to support cardiac function. It is important to note that the use of primary human cells is accompanied by inherent limitations in availability and donor-matching. The CF and DF in this study came from donors of different ages and sexes, making it challenging to dissect the exact mechanism as to why DF showed greater improvements in calcium handling compared to CF. One other limitation to this study is the *in vitro* passage artifact associated with primary cells. While restrictions on passage use (<10 passages) were implemented in this study, primary stromal cells expanded in culture may exhibit varying degrees of phenotypic drift leading to further observed differences in performance.

It is also highly possible to imagine that individual stromal cells contribute to cardiac microenvironments in different ways. MSC in co-culture models have been reported to deliver paracrine signals to cardiomyocytes (Mureli et al. 2013). In the present study, a global increase in cardiac gene expression was observed in co-culture of CM+MSC; however, functional benefits of MSC were variable, mirroring the inconsistent ability of MSC to form robust cardiac tissues. This variability in MSC microtissue function may be a direct result of the variability in formation given

that previous reports have demonstrated a link between microtissue size and resulting functional consequences, (Tan et al. 2017) highlighting the importance of robust microtissue formation for consistent functional outcomes. The variable impact on cardiac microtissue calcium handling properties imparted by MSC was consistent with reports of MSC exerting little effect on cardiac contractile function in other engineered systems (Burridge et al. 2014). Also consistent with previous reports that suggest MSC exert paracrine effects on tissue regulation and organization (Takebe et al. 2015, Richards et al. 2017), we observed improved cardiac gene expression with the presence of MSC, suggesting that MSC may contribute to phenotypic changes in CM but have limited functional consequences on engineered cardiac tissues. This highlights the idea that stromal populations may serve different functions within the context of microtissues and that there is not a single stromal cell type that will out-perform others in all aspects.

As the field moves toward engineering heterotypic tissues derived entirely from iPS sources to enable isogenic modeling, how to best define iPS-derived stromal cells remains a major question. There are several reports of hPSC-derived MSC-like cells (Barberi et al. 2005, Boyd et al. 2009) and fibroblastic cells using 2D directed approaches (Shamis et al. 2012), 3D embryoid body-based approaches (Itoh et al. 2013, Huebsch et al. 2016), and *in vivo*-based derivation methods (Chan et al. 2018). However, differences between these hPSC-derived stromal populations' morphology, characteristic phenotypic marker expression, and ability to support formation and function of engineered tissues remain unclear. In this study we compared iPS-F using two different derivation methods from the same isogenic iPS line as the cardiomyocytes: an *in vivo*-based derivation capturing teratoma outgrowth cells (iPS-F_{tera}) (Rand et al. 2018) and an *in vitro*-based derivation using an embryoid body outgrowth method (iPS-F_{EB}) (Huebsch et al. 2016). The resulting cells exhibited different morphologies with the iPS-F_{tera} adopting a small and

spindly shape whereas the iPS-F_{EB} were large and flat. The iPS-derived fibroblasts also had distinct surface marker expression with ~60% of iPS-F_{tera} expressing CD90 compared to no expression in the iPS-F_{EB} and iPS-F_{tera} did not support cardiac tissue formation, gene expression, or functional properties. Despite their morphological differences, transcriptomic analysis of the iPS-F_{tera} and iPS-F_{EB} suggested that both stem cell-derived stromal populations were more closely related to each other than to either the CF or DF populations, reflecting that the iPS-F cells may represent a more immature stromal population. Image analysis software, PhenoRipper, classified the two iPS-derived fibroblast populations as more similar to each other and to fetal CF than any of the primary-derived adult populations, suggesting that the iPS-derived cells may be morphologically more similar to an early “immature” developmental stromal cell. The concept of cell maturation has been a focus of iPS-derived parenchymal populations, but its relevance to supporting stromal cells has largely been overlooked. A recent study comparing the transcriptome of fetal vs. adult cardiac fibroblasts revealed distinct signatures between fCF and aCF with genes related to muscle development and function as well as immune cell trafficking upregulated in aCF, further highlighting the phenotypic changes that occur throughout stromal maturation (Jonsson et al. 2016). The distinctions observed in our study between early developmental stromal populations and adult tissue-derived fibroblasts indicates the need to further develop fibroblast differentiation protocols to yield homogeneous, mature populations of stromal cells that consistently support all aspects of cardiac tissue development and function.

In conclusion, this study provides a direct comparison of individual stromal populations through quantitative phenotypic and transcriptomic approaches, revealing distinct differences between primary adult fibroblasts and iPS-derived stromal cells. These phenotypic differences were also demonstrated through the inability of iPS-derived stromal cells to support consistent

cardiac microtissue formation and function. With the current shift toward engineering complex heterotypic tissues from isogenic sources, ongoing development of robust directed fibroblast differentiation protocols from iPS sources should remain a focus of research. Recent reports of iPS-derived cardiac fibroblasts have been described (Bao et al. 2016, Bao et al. 2017), but the ability of these cells to contribute to cardiac function remains unknown. Given the observed benefits of adult tissue-derived fibroblasts in contributing to improved cardiac microtissue function seen in this study, identifying methods to “mature” iPS-derived fibroblasts toward an adult-like phenotype may provide the key to improved function of isogenic tissues.

3.5. *Conclusions*

In conclusion, this first study of engineered cardiac tissue heterogeneity was conceived in response to the wide array of stromal cells that are utilized across the field. We saw that not all stromal cells are created equal (whereas historically stromal cells were largely uncharacterized and used interchangeably) and we found that, of the stromal cells we tested, there was not one clear winner that best supported both cardiac microtissue phenotype and function. Therefore, this study demonstrated that the identity of the stromal fraction needs to be taken into account when comparing different engineered cardiac tissue constructs. Since the primary cardiac fibroblasts supported calcium handling properties well, did not have disadvantageous effects on cardiac phenotype, and were derived from a relevant tissue source, we decided to move forward with using primary human cardiac fibroblasts as our stromal cell source for future studies. At the time of this study, however, cardiac-specific stem cell-derived stromal cells were not yet described, leaving a gap for the study of age-matched, isogenic heterotypic cardiac microtissues.

3.6. *Bibliography*

- Archer, C. R., et al. (2018). "Characterization and Validation of a Human 3D Cardiac Microtissue for the Assessment of Changes in Cardiac Pathology." Sci Rep **8**(1): 10160.
- Ariyasinghe, N. R., et al. (2017). "Engineering micromyocardium to delineate cellular and extracellular regulation of myocardial tissue contractility." Integr Biol (Camb) **9**(9): 730-741.
- Balistreri, M., et al. (2017). "Effect of Glucose on 3D Cardiac Microtissues Derived from Human Induced Pluripotent Stem Cells." Pediatr Cardiol **38**(8): 1575-1582.
- Bang, C., et al. (2014). "Cardiac fibroblast-derived microRNA passenger strand-enriched exosomes mediate cardiomyocyte hypertrophy." J Clin Invest **124**(5): 2136-2146.
- Bao, X., et al. (2016). "Long-term self-renewing human epicardial cells generated from pluripotent stem cells under defined xeno-free conditions." Nat Biomed Eng **1**.
- Bao, X., et al. (2017). "Directed differentiation and long-term maintenance of epicardial cells derived from human pluripotent stem cells under fully defined conditions." Nat Protoc **12**(9): 1890-1900.
- Barberi, T., et al. (2005). "Derivation of multipotent mesenchymal precursors from human embryonic stem cells." PLoS Med **2**(6): e161.
- Boyd, N. L., et al. (2009). "Human embryonic stem cell-derived mesoderm-like epithelium transitions to mesenchymal progenitor cells." Tissue Eng Part A **15**(8): 1897-1907.
- Burrige, P. W., et al. (2014). "Multi-cellular interactions sustain long-term contractility of human pluripotent stem cell-derived cardiomyocytes." Am J Transl Res **6**(6): 724-735.
- Camelliti, P., et al. (2005). "Structural and functional characterisation of cardiac fibroblasts." Cardiovasc Res **65**(1): 40-51.

- Camelliti, P., et al. (2006). "Structural and functional coupling of cardiac myocytes and fibroblasts." Adv Cardiol **42**: 132-149.
- Cartledge, J. E., et al. (2015). "Functional crosstalk between cardiac fibroblasts and adult cardiomyocytes by soluble mediators." Cardiovasc Res **105**(3): 260-270.
- Caspi, O., et al. (2007). "Tissue engineering of vascularized cardiac muscle from human embryonic stem cells." Circ Res **100**(2): 263-272.
- Chan, S. S., et al. (2018). "Skeletal Muscle Stem Cells from PSC-Derived Teratomas Have Functional Regenerative Capacity." Cell Stem Cell **23**(1): 74-85 e76.
- Cho, N., et al. (2018). "Featured Article: TGF-beta1 dominates extracellular matrix rigidity for inducing differentiation of human cardiac fibroblasts to myofibroblasts." Exp Biol Med (Maywood) **243**(7): 601-612.
- Correia, C., et al. (2018). "3D aggregate culture improves metabolic maturation of human pluripotent stem cell derived cardiomyocytes." Biotechnol Bioeng **115**(3): 630-644.
- Dominici, M., et al. (2006). "Minimal criteria for defining multipotent mesenchymal stromal cells. The International Society for Cellular Therapy position statement." Cytotherapy **8**(4): 315-317.
- Emmert, M. Y., et al. (2013). "Human stem cell-based three-dimensional microtissues for advanced cardiac cell therapies." Biomaterials **34**(27): 6339-6354.
- Furtado, M. B., et al. (2014). "Cardiogenic genes expressed in cardiac fibroblasts contribute to heart development and repair." Circ Res **114**(9): 1422-1434.
- Gaudesius, G., et al. (2003). "Coupling of cardiac electrical activity over extended distances by fibroblasts of cardiac origin." Circ Res **93**(5): 421-428.

- Giacomelli, E., et al. (2017). "Three-dimensional cardiac microtissues composed of cardiomyocytes and endothelial cells co-differentiated from human pluripotent stem cells." Development **144**(6): 1008-1017.
- Hagmann, S., et al. (2013). "FGF-2 addition during expansion of human bone marrow-derived stromal cells alters MSC surface marker distribution and chondrogenic differentiation potential." Cell Prolif **46**(4): 396-407.
- Hookway, T. A., et al. (2016). "Aggregate formation and suspension culture of human pluripotent stem cells and differentiated progeny." Methods **101**: 11-20.
- Hudon-David, F., et al. (2007). "Thy-1 expression by cardiac fibroblasts: lack of association with myofibroblast contractile markers." J Mol Cell Cardiol **42**(5): 991-1000.
- Huebsch, N., et al. (2016). "Miniaturized iPSC-Cell-Derived Cardiac Muscles for Physiologically Relevant Drug Response Analyses." Sci Rep **6**: 24726.
- Huebsch, N., et al. (2015). "Automated Video-Based Analysis of Contractility and Calcium Flux in Human-Induced Pluripotent Stem Cell-Derived Cardiomyocytes Cultured over Different Spatial Scales." Tissue Eng Part C Methods **21**(5): 467-479.
- Itoh, M., et al. (2013). "Generation of 3D skin equivalents fully reconstituted from human induced pluripotent stem cells (iPSCs)." PLoS One **8**(10): e77673.
- Jonsson, M. K. B., et al. (2016). "A Transcriptomic and Epigenomic Comparison of Fetal and Adult Human Cardiac Fibroblasts Reveals Novel Key Transcription Factors in Adult Cardiac Fibroblasts." JACC Basic Transl Sci **1**(7): 590-602.
- Kensah, G., et al. (2013). "Murine and human pluripotent stem cell-derived cardiac bodies form contractile myocardial tissue in vitro." Eur Heart J **34**(15): 1134-1146.

- Kerscher, P., et al. (2016). "Direct hydrogel encapsulation of pluripotent stem cells enables ontomimetic differentiation and growth of engineered human heart tissues." Biomaterials **83**: 383-395.
- Kim, D., et al. (2013). "TopHat2: accurate alignment of transcriptomes in the presence of insertions, deletions and gene fusions." Genome Biol **14**(4): R36.
- Kim, T. Y., et al. (2018). "Directed fusion of cardiac spheroids into larger heterocellular microtissues enables investigation of cardiac action potential propagation via cardiac fibroblasts." PLoS One **13**(5): e0196714.
- Kofron, C. M., et al. (2017). "Gq-activated fibroblasts induce cardiomyocyte action potential prolongation and automaticity in a three-dimensional microtissue environment." Am J Physiol Heart Circ Physiol **313**(4): H810-H827.
- Laco, F., et al. (2018). "Unraveling the Inconsistencies of Cardiac Differentiation Efficiency Induced by the GSK3beta Inhibitor CHIR99021 in Human Pluripotent Stem Cells." Stem Cell Reports **10**(6): 1851-1866.
- Lian, X., et al. (2012). "Robust cardiomyocyte differentiation from human pluripotent stem cells via temporal modulation of canonical Wnt signaling." Proc Natl Acad Sci U S A **109**(27): E1848-1857.
- Lian, X., et al. (2013). "Directed cardiomyocyte differentiation from human pluripotent stem cells by modulating Wnt/beta-catenin signaling under fully defined conditions." Nat Protoc **8**(1): 162-175.
- Liao, Y., et al. (2014). "featureCounts: an efficient general purpose program for assigning sequence reads to genomic features." Bioinformatics **30**(7): 923-930.

Livak, K. J. and T. D. Schmittgen (2001). "Analysis of relative gene expression data using real-time quantitative PCR and the 2(-Delta Delta C(T)) Method." Methods **25**(4): 402-408.

Lyu, L., et al. (2015). "A critical role of cardiac fibroblast-derived exosomes in activating renin angiotensin system in cardiomyocytes." J Mol Cell Cardiol **89**(Pt B): 268-279.

Ma, Z. H., N.; Koo, S.; Mandegar, M.A.; Siemons, B.; Boggess, S; Conklin, B.R.; Grigoropoulos, C.P.; Healy, K.E (2018). "Contractile deficits in engineered cardiac microtissues as a result of MYBPC3 deficiency and mechanical overload." Nature Biomedical Engineering.

Masumoto, H., et al. (2016). "The myocardial regenerative potential of three-dimensional engineered cardiac tissues composed of multiple human iPS cell-derived cardiovascular cell lineages." Sci Rep **6**: 29933.

McCarthy, D. J., et al. (2012). "Differential expression analysis of multifactor RNA-Seq experiments with respect to biological variation." Nucleic Acids Res **40**(10): 4288-4297.

Mills, R. J., et al. (2017). "Functional screening in human cardiac organoids reveals a metabolic mechanism for cardiomyocyte cell cycle arrest." Proc Natl Acad Sci U S A **114**(40): E8372-E8381.

Mureli, S., et al. (2013). "Mesenchymal stem cells improve cardiac conduction by upregulation of connexin 43 through paracrine signaling." Am J Physiol Heart Circ Physiol **304**(4): H600-609.

Nakane, T., et al. (2017). "Impact of Cell Composition and Geometry on Human Induced Pluripotent Stem Cells-Derived Engineered Cardiac Tissue." Sci Rep **7**: 45641.

Nguyen, D. C., et al. (2014). "Microscale generation of cardiospheres promotes robust enrichment of cardiomyocytes derived from human pluripotent stem cells." Stem Cell Reports **3**(2): 260-268.

- Noguchi, R., et al. (2016). "Development of a three-dimensional pre-vascularized scaffold-free contractile cardiac patch for treating heart disease." J Heart Lung Transplant **35**(1): 137-145.
- Nunes, S. S., et al. (2013). "Biowire: a platform for maturation of human pluripotent stem cell-derived cardiomyocytes." Nat Methods **10**(8): 781-787.
- Pedregosa, F. V., G.; Gramfort, A.; Michel, V.; Thirion, B.; Grisel, O.; Blondel, M.; Prettenhofer, P.; Weiss, R.; Dubourg, V.; Vanderplas, J.; Passos, A.; Cournapeau, D; Brucher, M; Perrot, M; Duchesnay, E. (2011). "Scikit-learn: Machine Learning in Python." Journal of Machine Learning Research **12**: 2825–2830.
- Rajaram, S., et al. (2012). "PhenoRipper: software for rapidly profiling microscopy images." Nat Methods **9**(7): 635-637.
- Rand, T. A., et al. (2018). "MYC Releases Early Reprogrammed Human Cells from Proliferation Pause via Retinoblastoma Protein Inhibition." Cell Rep **23**(2): 361-375.
- Ravenscroft, S. M., et al. (2016). "Cardiac Non-myocyte Cells Show Enhanced Pharmacological Function Suggestive of Contractile Maturity in Stem Cell Derived Cardiomyocyte Microtissues." Toxicol Sci **152**(1): 99-112.
- Richards, D. J., et al. (2017). "Inspiration from heart development: Biomimetic development of functional human cardiac organoids." Biomaterials **142**: 112-123.
- Robinson, M. D., et al. (2010). "edgeR: a Bioconductor package for differential expression analysis of digital gene expression data." Bioinformatics **26**(1): 139-140.
- Ronaldson-Bouchard, K., et al. (2018). "Advanced maturation of human cardiac tissue grown from pluripotent stem cells." Nature **556**(7700): 239-243.

- Rother, J., et al. (2015). "Crosstalk of cardiomyocytes and fibroblasts in co-cultures." Open Biol **5**(6): 150038.
- Shamis, Y., et al. (2012). "iPSC-derived fibroblasts demonstrate augmented production and assembly of extracellular matrix proteins." In Vitro Cell Dev Biol Anim **48**(2): 112-122.
- Souders, C. A., et al. (2009). "Cardiac fibroblast: the renaissance cell." Circ Res **105**(12): 1164-1176.
- Stevens, K. R., et al. (2009). "Physiological function and transplantation of scaffold-free and vascularized human cardiac muscle tissue." Proc Natl Acad Sci U S A **106**(39): 16568-16573.
- Sturn, A., et al. (2002). "Genesis: cluster analysis of microarray data." Bioinformatics **18**(1): 207-208.
- Takebe, T., et al. (2015). "Vascularized and Complex Organ Buds from Diverse Tissues via Mesenchymal Cell-Driven Condensation." Cell Stem Cell **16**(5): 556-565.
- Tan, Y., et al. (2017). "Cell number per spheroid and electrical conductivity of nanowires influence the function of silicon nanowired human cardiac spheroids." Acta Biomater **51**: 495-504.
- Thavandiran, N., et al. (2013). "Design and formulation of functional pluripotent stem cell-derived cardiac microtissues." Proc Natl Acad Sci U S A **110**(49): E4698-4707.
- Tohyama, S., et al. (2013). "Distinct metabolic flow enables large-scale purification of mouse and human pluripotent stem cell-derived cardiomyocytes." Cell Stem Cell **12**(1): 127-137.
- Tomoda, Y., et al. (2001). "Cardiac fibroblasts are major production and target cells of adrenomedullin in the heart in vitro." Cardiovasc Res **49**(4): 721-730.
- Tulloch, N. L., et al. (2011). "Growth of engineered human myocardium with mechanical loading and vascular coculture." Circ Res **109**(1): 47-59.

- Van der Laan, M. P. K. (2003). "Hybrid clustering of gene expression data with visualization and the bootstrap." Journal of Statistical Planning and Inference **117**: 275-303.
- Vuorenmaa, H., et al. (2017). "Maturation of human pluripotent stem cell derived cardiomyocytes is improved in cardiovascular construct." Cytotechnology **69**(5): 785-800.
- Zeng, Q. C., et al. (2013). "Cardiac fibroblast-derived extracellular matrix produced in vitro stimulates growth and metabolism of cultured ventricular cells." Int Heart J **54**(1): 40-44.
- Zhang, P., et al. (2012). "Cross talk between cardiac myocytes and fibroblasts: from multiscale investigative approaches to mechanisms and functional consequences." Am J Physiol Heart Circ Physiol **303**(12): H1385-1396.
- Zhou, P. and W. T. Pu (2016). "Recounting Cardiac Cellular Composition." Circ Res **118**(3): 368-370.

CHAPTER 4

BI-DIRECTIONAL IMPACTS OF HETEROTYPIC INTERACTIONS IN ENGINEERED 3D HUMAN CARDIAC MICROTISSUES REVEALED BY SINGLE- CELL RNA-SEQUENCING AND FUNCTIONAL ANALYSIS

4.1. Introduction

Technological advancements have enabled the design of increasingly complex engineered tissue constructs, which better mimic native tissue cellularity. Therefore, dissecting the bi-directional interactions between distinct cell types in 3D is necessary to understand how heterotypic interactions at the single-cell level impact tissue-level properties. We systematically interrogated the interactions between cardiomyocytes (CMs) and cardiac non-myocytes in 3D self-assembled tissue constructs in an effort to determine the phenotypic and functional contributions of cardiac fibroblasts (CFs) and endothelial cells (ECs) to cardiac tissue properties. One week after tissue formation, cardiac microtissues containing CFs exhibited improved calcium handling function compared to microtissues comprised of CMs alone or CMs mixed with ECs, and CMs cultured with CFs exhibited distinct transcriptional profiles, with increased expression of cytoskeletal and ECM-associated genes. However, one month after tissue formation, functional and phenotypic differences between heterotypic tissues were mitigated, indicating diminishing impacts of non-myocytes on CM phenotype and function over time. The combination of single-cell RNA-sequencing and calcium imaging enabled the determination of reciprocal transcriptomic changes accompanying tissue-level functional properties in engineered heterotypic cardiac microtissues.

4.2. *Materials and Methods*

4.2.1. Pluripotent stem cell culture

WTC11 human induced pluripotent stem cells (hiPSCs) modified with a genetically-encoded calcium indicator GCaMP6f (Huebsch et al. 2015, Mandegar et al. 2016) (generously donated by Dr. Bruce Conklin) were cultured in mTeSR medium (Stem Cell Technologies, Vancouver, CA) on plates coated with 80µg/mL Matrigel (Corning, Corning, NY). Cells were seeded at 1×10^4 cells/cm² in mTeSR medium, supplemented with 10µM Rock inhibitor (Y27632, SelleckChem, Houston, TX) for the first 24h, and passaged using Accutase (Innovative Cell Technologies, San Diego, CA) every 3 days at ~70% confluence.

4.2.2. Cardiomyocyte differentiation

Cardiomyocytes (CM) were differentiated from WTC11 GCaMP6f hiPSCs following a chemically-defined, serum-free protocol (Lian et al. 2012, Lian et al. 2013). Cells were seeded onto Matrigel-coated 12-well tissue culture plates at 3×10^4 cells/cm² in mTeSR medium with 10µM Rock inhibitor. Once the cells reached 100% confluence, 12µM CHIR99021 (SelleckChem) was added into RPMI 1640 medium (Thermo Fisher, Waltham, MA) supplemented with B27 minus insulin (denoted as RPMI/B27-; Life Technologies, Grand Island, NY) (differentiation day 0). CHIR was removed exactly 24h later by replacing medium with fresh RPMI/B27-. On day 3, 5µM IWP2 (Tocris, Bristol, UK) in RPMI/B27- was added and then removed 48h later by refreshing the medium. The cells were fed with fresh RPMI/B27- on day 5. On day 7, medium was switched to RPMI 1640 medium supplemented with B27 with insulin (RPMI/B27+; Life Technologies) and fed every 3 days thereafter. On day 15, cells were re-plated onto Matrigel-coated dishes at 1×10^5 cells/cm² in RPMI/B27+ with 10µM Rock inhibitor (see Appendix A for

detailed protocol). Purification of cardiomyocytes occurred by feeding cultures with Lactate purification medium (Tohyama et al. 2013) (no-glucose Dulbecco's Modified Eagle Medium (Thermo Fisher) with 1X Non Essential Amino Acids (NEAA; Corning), 1X Glutamax (*L*-glut; Life Technologies), and 4mM Lactate) on days 20 and 22. On day 24, medium was exchanged to RPMI/B27+ and fed every three days thereafter until harvest (day 35 ± 7).

4.2.3. Endothelial cell differentiation

Differentiation of endothelial cells from hiPSCs was achieved by modifying a previously described protocol (Zhang et al. 2017). Briefly, on day 0, WTC11 hiPSCs were seeded onto Matrigel-coated dishes in E8 medium (Thermo Fisher) supplemented with 5ng/mL BMP4 (Stem Cell Technologies), 25ng/mL Activin A (Stem Cell Technologies), and 1μM CHIR99021, with daily media changes. On day 2, cells were cultured in E6 medium (Thermo Fisher) supplemented with 100ng/mL bFGF (Stem Cell Technologies), 50ng/mL VEGF-A (Stem Cell Technologies), 50ng/mL BMP4, and 5μM SB431542 (Stem Cell Technologies), with daily media changes. On day 4, cells were split onto a fibronectin (Sigma-Aldrich, St. Louis, MO) coated plate and maintained in EGM medium (Lonza, Basel, SUI). The efficiency of the differentiation was assessed on day 8 with flow cytometry using CD31 and CD144 antibodies, and was typically >95% CD31+/CD144+.

4.2.4. Fibroblast cell culture

Human fetal (18wk gestation, male, lot #2584) and adult (50 y.o., male, lot #3067) cardiac fibroblasts (Cell Applications, San Diego, CA) were cultured according to manufacturer

recommendations. Briefly, cells were seeded and passaged at a density of 1×10^4 cells/cm², and fed with Cardiac Fibroblast Medium (Cell Applications) every 2-3 days, for up to 10 passages.

4.2.5. Cardiac microtissue formation

Lactate-purified cardiomyocytes (day 35 ± 7), fetal cardiac fibroblasts, adult cardiac fibroblasts, and endothelial cells were dissociated with 0.25% Trypsin for 5-10 min and then mixed together at a 3:1 ratio of CM to non-myocytes. Cell mixtures in RPMI/B27+ with 10 μ M Rock inhibitor were seeded into 400 μ m inverted pyramidal agarose microwells at a density of 2000 cells/well and allowed to self-assemble overnight (Hookway et al. 2016). After 18-24h, the self-assembled cardiac microtissues were removed from the wells and maintained in rotary suspension culture at a density of 2000 tissues per 10cm Petri dish for 7 or 30 days. See Chapter 2 for detailed protocol.

4.2.6. Histology and immunofluorescence staining

Samples were fixed in 10% Neutral Buffered Formalin (VWR, Radnor, PA) for 1h at room temperature and embedded in HistoGel Specimen Processing Gel (Thermo Fisher) prior to paraffin processing. Five micron sections were cut and adhered to positively charged glass slides. Slides were deparaffinized with xylene and re-hydrated through a series of decreasing ethanol concentrations (100%, 100%, 95%, 80%, 70%). For immunofluorescence staining, epitope retrieval was performed by submersing slides in Citrate Buffer pH 6.0 (Vector Laboratories, Burlingame, CA) in a 95°C water bath for 35min. Slides were cooled at RT for 20 min and washed with PBS. Samples were permeabilized in 0.2% Triton X-100 (Sigma-Aldrich) for 5min, blocked in 1.5% normal donkey serum (Jackson ImmunoResearch, West Grove, PA) for 1h, and probed

with primary and secondary antibodies against cardiac troponin T, slow+fast troponin I, and cardiac troponin I, and counterstained with Hoechst and WGA (antibody information in Table 4.1). Coverslips were mounted with anti-fade mounting medium (ProlongGold, Life Technologies) and samples were imaged on a Zeiss Axio Observer Z1 inverted microscope equipped with a Hamamatsu ORCA-Flash 4.0 camera.

Table 4.1. Antibody and in situ hybridization probe source information.

Immunocytochemistry				
Antibody	Company	Catalog #	Dilution	
Cardiac Troponin T	Abcam	ab45932	1:400	
Wheat Germ Agglutinin	Thermo Fisher	W11263	1:500	
Slow+Fast Troponin I	Abcam	ab47003	1:100	
Cardiac Troponin I	Abcam	ab110132	1:100	
Alexa Fluor 555	Thermo Fisher	A-31572	1:400	
Alexa Fluor 488	Thermo Fisher	A-21202	1:400	
Hoechst	Thermo Fisher	62249	1:10000	
RNAscope in situ hybridization (Advanced Cell Diagnostics)				
Gene	Species	Target Region	Amplification Channel	Catalog #
<i>PDLIM3</i>	Hs	254-1190 of NM_014476.5	C3	533411
<i>RGS5</i>	Hs	339-1572 of NM_003617.3	C3	533421
<i>COL3A1</i>	Hs	3550-5057 of NM_000090.3	C1	549431
<i>IGF2</i>	Hs	339-1572 of NM_003617.3	C2	594361

4.2.7. Calcium imaging analysis

Calcium transients of cardiac microtissues were visible due to the genetically-encoded calcium indicator GCaMP6f in the hiPSC-CMs. Microtissues at day 7 or day 30 were incubated in Tyrode's solution (137mM NaCl, 2.7mM KCl, 1mM MgCl₂, 0.2mM Na₂HPO₄, 12mM NaHCO₃,

5.5mM D-glucose, 1.8mM CaCl₂) in a 35mm Petri dish for 30min at 37°C prior to imaging. Samples were mounted on a Zeiss Axio Observer Z1 inverted microscope with a Hamamatsu ORCA-Flash 4.0 camera. Electrodes were placed in the Petri dish to apply electrical field stimulation at 1Hz as well as a stimulation regimen of increasing frequencies (0.5Hz, 1Hz, 2Hz, 4Hz) (MyoPacer, IonOptix). Calcium transient videos were acquired with Zen Professional software (v.2.0.0.0) at 10ms exposure and 100 frames per second. Circular regions of interest (ROI; 75-pixel diameter) were selected at the center of each microtissue and the mean fluorescent intensity values were plotted against time. Metrics of calcium transient kinetics, such as amplitude, stroke velocities, and beat rate, were analyzed using a custom python script (Silva et al. 2020). Source code is available at <https://github.com/david-a-joy/multilineage-organoid>.

4.2.8. Statistics

The mean +/- standard deviation was calculated from at least 9 biological replicates for all data unless otherwise noted. When comparing three or more groups, one-way analysis of variance (ANOVA) followed by Tukey's post hoc analysis was performed. For all comparisons, statistical significance was determined at $p < 0.05$. All statistical analysis was performed using GraphPad Prism 7.0 software.

4.2.9. Single-cell RNA-sequencing sample preparation and sequencing

At the time of cardiac tissue formation (day 0), a subset of dissociated heterotypic cell mixtures was retained for sequencing. After 7 or 30 days of microtissues culture, cells were dissociated with 0.25% Trypsin for 45 minutes and (~8000 cells/group) were prepared for analysis through droplet encapsulation by the Chromium Controller and library preparation with the

Chromium Single Cell 3' v2 Library and Gel Bead Kit (10x Genomics, San Francisco, CA). cDNA was sheared using a Covaris S2 sonicator and 12 PCR cycles were run during cDNA amplification. Libraries were sequenced on a HiSeq 4000 (Illumina, San Diego, CA). Sequences were demultiplexed and aligned to human reference genome grch38 using the default settings of 10x Genomics *CellRanger* v2.0.2. After *CellRanger* filtering, there were ~700 million valid reads, 88.6% of which were mapped to a unique UMI.

4.2.10. Single-cell RNA-sequencing zinbwave reduction

The raw counts for genes from all cells across culture conditions and time points were loaded with Seurat v2 (Butler et al. 2018, Stuart et al. 2019). The cells were filtered using the number of detected genes between the bottom 1% and top 99% across all cells, and percent mitochondrial genes within the top 99% across all cells. Genes were filtered out of further analyses if they did not have at least 5 counts in at least 5 cells. The zinbwave function (with parameter $K=2$) in the R bioconductor package zinbwave was used to generate a 2-dimensional (2D) representation of the gene expression profiles for each of the cells after adjusting for the number of detected genes per cell (Huber et al. 2015, Risso et al. 2018). The zinbwave function (with parameter $K=0$ and adjusting for the number of genes detected per cell) was used to generate weights per gene-cell combination that were used in the gene expression association analyses with edgeR (Robinson et al. 2010, McCarthy et al. 2012). The 2D zinbwave reduction of all of the cells was visualized as a umap (McInnes et al. 2018). The resulting zinbwave reduction was loaded as a Seurat v2 object using SetDimReduction function. Clustering of cells was performed using the FindClusters function in Seurat v2 using parameter resolution=0.6. Cells in clusters expressing *TNNT2*, *TNNI1*, and *ACTC1* were chosen for the CM-specific analyses, cells in clusters expressing

POSTN, *THY1*, and *FNI* were chosen for the CF-specific analyses, and cells in clusters expressing *PECAMI*, *KDR*, and *FLT1* were chosen for the EC specific-analyses. The raw counts from the resulting cells of an identified cell type (CM, CF, or EC) were used to generate the 2D representation of the gene expression profiles as before, using the zinbwave function. The resulting zinbwave reductions were loaded as a Seurat v3 object using the `as.Seurat` function. Clustering of each cell type was performed using the `FindClusters` function in Seurat v3 using parameter `resolution=0.4`. Genes whose expression was associated with culture condition and/or time were determined using edgeR. Weights associated with gene-cell combinations that were estimated from running the zinbwave functions were used as weights in the edgeR-specific DGE object. The design matrix used for the all-cell analyses (pre-cell type subsetting) for each gene's expression was: $Y \sim nGene + Clusters + Culture + Time + Clusters:Culture + Culture:Time + Clusters:Time$. The design matrix for the cell-type specific analysis was: $Y \sim nGene + Clusters + Time + Clusters:Time$. Associated genes were determined by the significance ($FDR < 0.05$) of the composite null hypothesis involving terms containing culture conditions and/or time. Normalized expression for all genes meeting the significance threshold over all cells was obtained from the `computeDevianceResiduals` function in zinbwave.

4.2.11. Single-cell RNA-sequencing HOPACH analysis

The normalized gene expression data were used to cluster genes across all of the cells using Hierarchical Ordered Partitioning and Collapsing Hybrid (HOPACH) analysis (van der Laan and Pollard 2003). HOPACH determined the optimal number of gene clusters that best described the given data as well as the identity of the genes belonging to each HOPACH cluster. The normalized expression data was visualized as a heatmap using the `pheatmap` package (Kolde 2012). Gene

clusters were also visualized as box plots of expression of medoid (representative) genes from each HOPACH cluster, based on groups of cells belonging to a particular combination of culture condition, time-point and cell-cluster membership. GO analysis and WikiPathways analysis were performed on the HOPACH cluster gene lists using the Cluster Profiler R package (Yu et al. 2012).

4.2.12. In situ hybridization

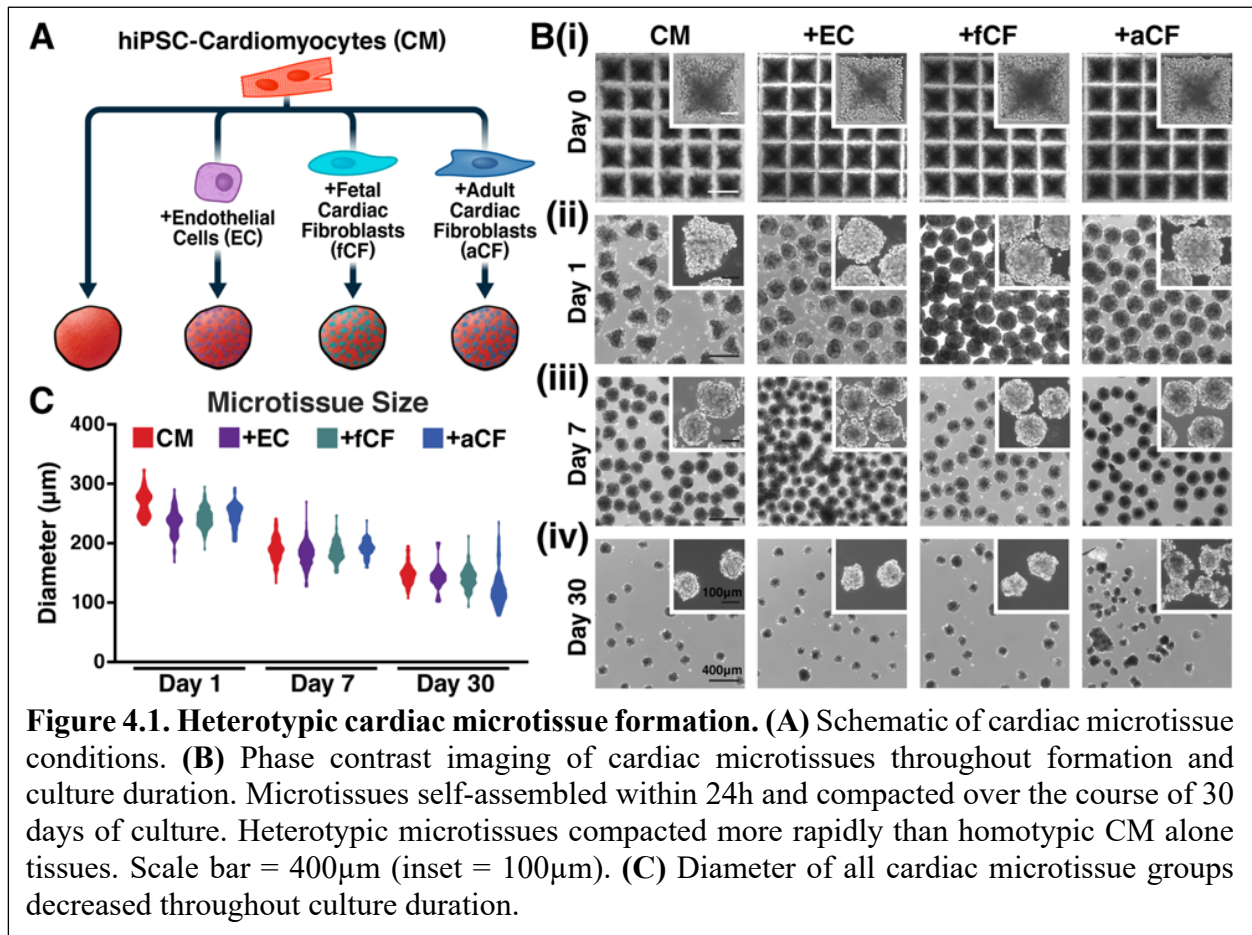
RNAScope for *PDLIM3*, *RGS5*, *COL3A1*, and *IGF2* (probe information in Table 4.1) was performed on sections of formalin-fixed paraffin-embedded samples (see “histology and immunofluorescence staining”) using the RNAScope Multiplex Fluorescent Reagent Kit v2 (Advanced Cell Diagnostics, Newark, CA) and following the protocol outlined in User Manual 323100-USM. Sections were imaged on a Zeiss Axio Observer Z1 inverted microscope equipped with a Hamamatsu ORCA-Flash 4.0 camera.

4.3. Results

4.3.1. Non-myocytes enable rapid microtissue compaction

To explore the effects of non-myocytes on cardiac microtissue formation and function, we compared homotypic microtissues formed from CMs alone to heterotypic cardiac microtissues formed from CMs+endothelial cells (CM+EC), CMs+fetal cardiac fibroblasts (CM+fCF), and CMs+adult cardiac fibroblasts (CM+aCF) (Figure 4.1A). These cardiac cells self-assembled (Hookway et al. 2016) into 3D microtissues within 24h after seeding into inverted pyramidal microwells (Figure 4.1Bi); however, all heterotypic microtissues compacted to form spheroids more rapidly than homotypic tissues (Figure 4.1Bii,C). After 7 days of culture, CM alone microtissues were of similar size to heterotypic microtissues (Figure 4.1Biii) and all groups

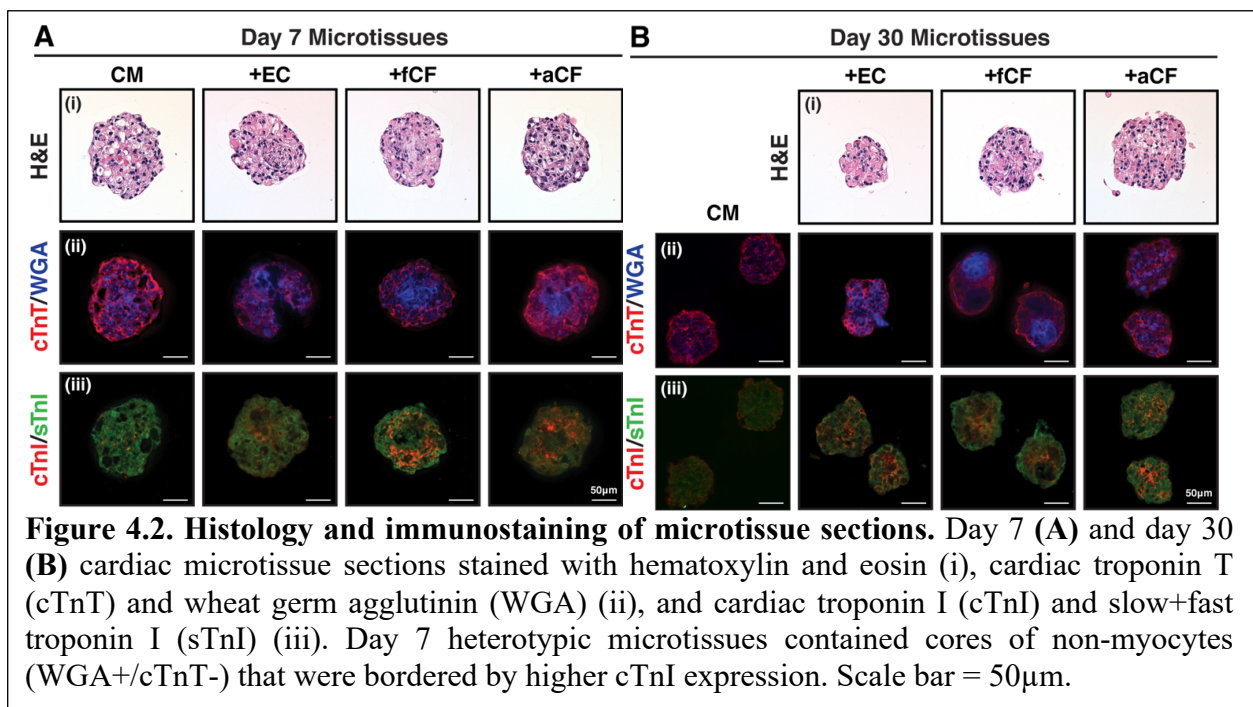
continued to decrease in tissue diameter (Figure 4.1C), but the heterotypic microtissue groups displayed a dark core at the center that was absent in the CM alone microtissues (Figure 4.1Biii). After 30 days of culture, all microtissue groups had decreased in size (Figure 4.1C), but there were no major differences in microtissue size or morphology between conditions (Figure 4.1Biv).



4.3.2. Non-myocytes form a core within heterotypic cardiac microtissues

Hematoxylin and eosin staining of the microtissues revealed relatively uniform, high cell densities, regardless of heterotypic pairings (Figure 4.2Ai, 4.2Bi). Therefore, to characterize the multicellular organization of heterotypic cell populations, we stained the microtissues for specific phenotypic markers. At day 7, most of the heterotypic microtissues contained a core of non-myocytes, based upon the absence of cardiac troponin T (cTnT) expression in regions that were

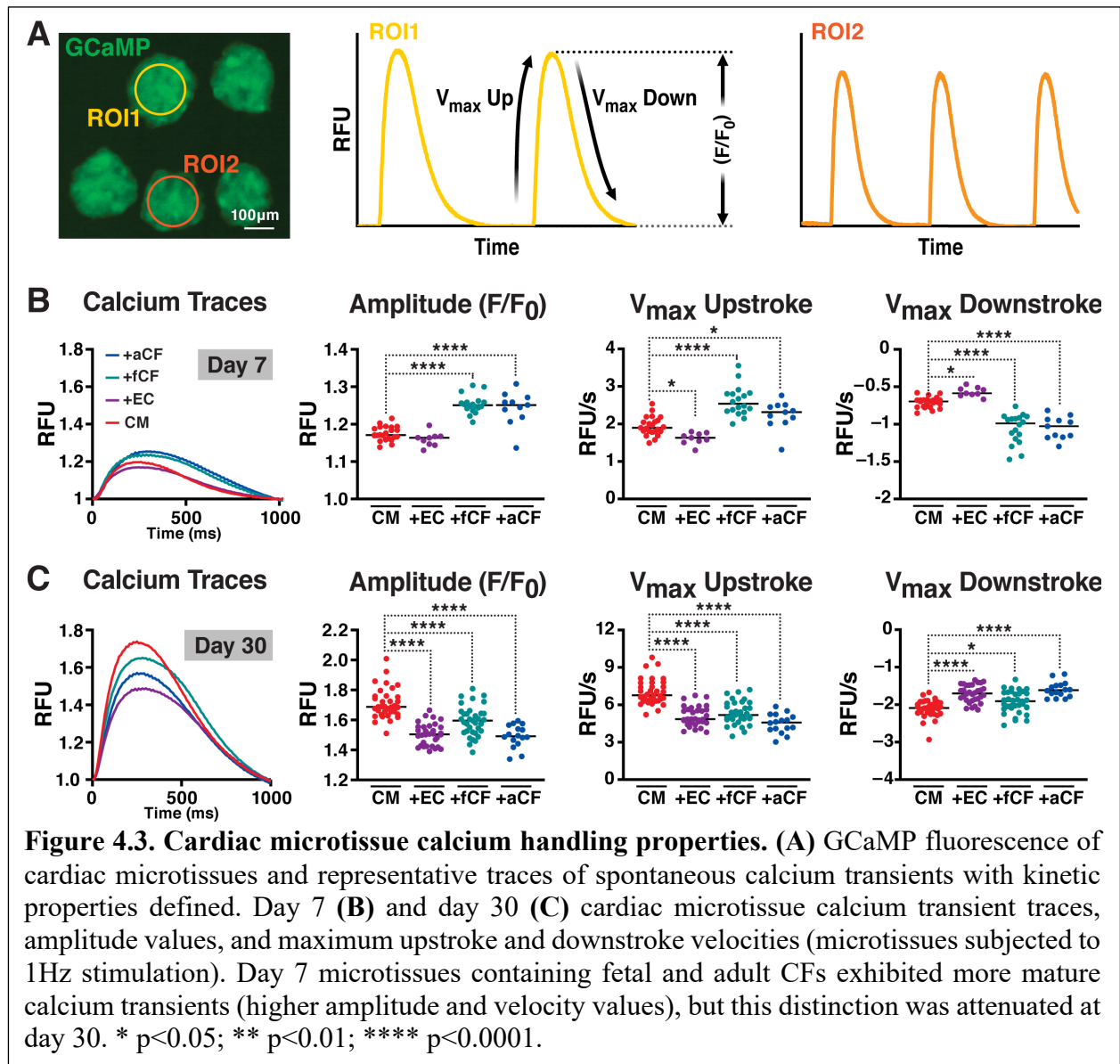
positive for wheat germ agglutinin (WGA; Figure 4.2Aii), which correlated to the dark centers observed in the phase contrast images (Figure 4.1Biii). After 30 days of culture, non-myocyte cores were only evident in a subset of the heterotypic microtissues, primarily those containing fetal CFs (Figure 4.2Bii). To determine whether culture with non-myocytes impacted the phenotypic maturation of the CMs, we stained for various isoforms of troponin I. Seven days post tissue formation, expression of cardiac troponin I (cTnI) expression—a marker of CM maturity compared to slow/fast skeletal troponin I (sTnI)—was more abundant in microtissues containing CFs and localized adjacent to the non-myocyte cores (Figure 4.2Aiii). However, after 30 days, there were less apparent differences in cTnI expression between experimental groups (Figure 4.2Biii).



4.3.3. Cardiac fibroblasts accelerate calcium handling properties of cardiac microtissues

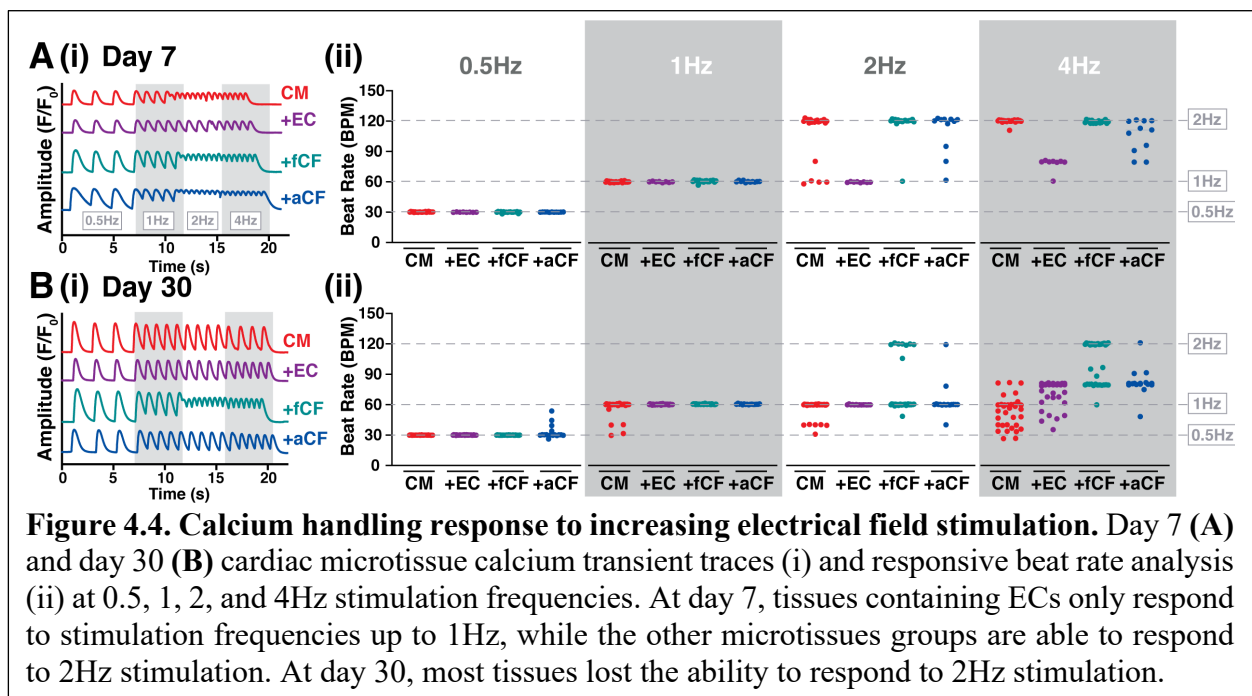
In order to assess the effect of heterotypic culture on microtissue function, we performed calcium imaging. Individual microtissues in each condition exhibited independent spontaneous beating, indicating that they functioned as autonomous tissue constructs (Figure 4.3A). Seven days

after tissue formation, cardiac microtissues containing CFs (both fetal and adult) exhibited improved calcium handling profiles, characterized by increased amplitude (F/F_0), and higher maximum upstroke and downstroke velocities than homotypic or CM+EC microtissues (Figure 4.3B). Microtissues cultured for 30 days exhibited higher amplitudes and faster stroke velocities than their day 7 counterparts (Figure 4.3C), demonstrating that culture duration improved calcium handling properties regardless of starting conditions. However, no distinction in transient profiles of the microtissues containing CFs compared to those with CMs alone or ECs was evident after

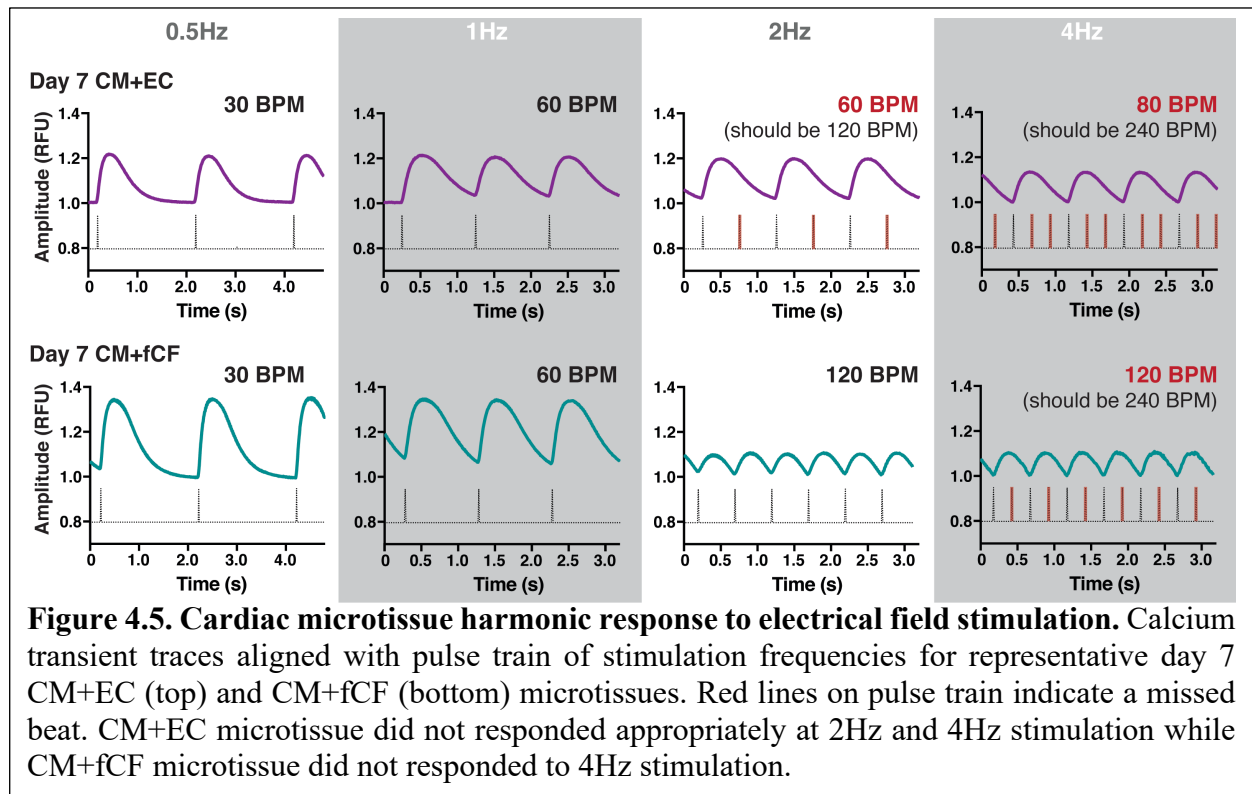


30 days, and instead, the CM alone microtissues exhibited calcium transients with the greatest amplitude and fastest stroke velocities.

To further assess calcium handling properties, we subjected day 7 and day 30 cardiac microtissues to a series of increasing electrical field stimulation frequencies, at 0.5Hz, 1Hz, 2Hz, and 4Hz (Figure 4.4Ai,Bi). At day 7, all microtissue groups were able to keep pace with 0.5Hz and 1Hz stimulation (Figure 4.4Aii). At 2Hz, all groups except CM+EC were able to keep pace with the stimulation, but all tissue groups failed to respond appropriately above 2Hz stimulation. Aligning the calcium transient traces to the input stimulation pulses revealed that the microtissues that failed to respond appropriately to the stimulation frequency instead responded at a lower, but harmonic beat rate (Figure 4.5). At day 30, despite the improved calcium transient profiles (Figure 4.3C), the microtissues did not respond as robustly to the higher stimulation frequencies as their day 7 counterparts (Figure 4.4Bii). Most CM alone tissues (85.7%) and 100% of heterotypic microtissues were able to pace at 1Hz stimulation, yet only 20.6% of CM+fCF microtissues and 6.3% of CM+aCF tissues were able to respond to 2Hz stimulation. The lower harmonic response



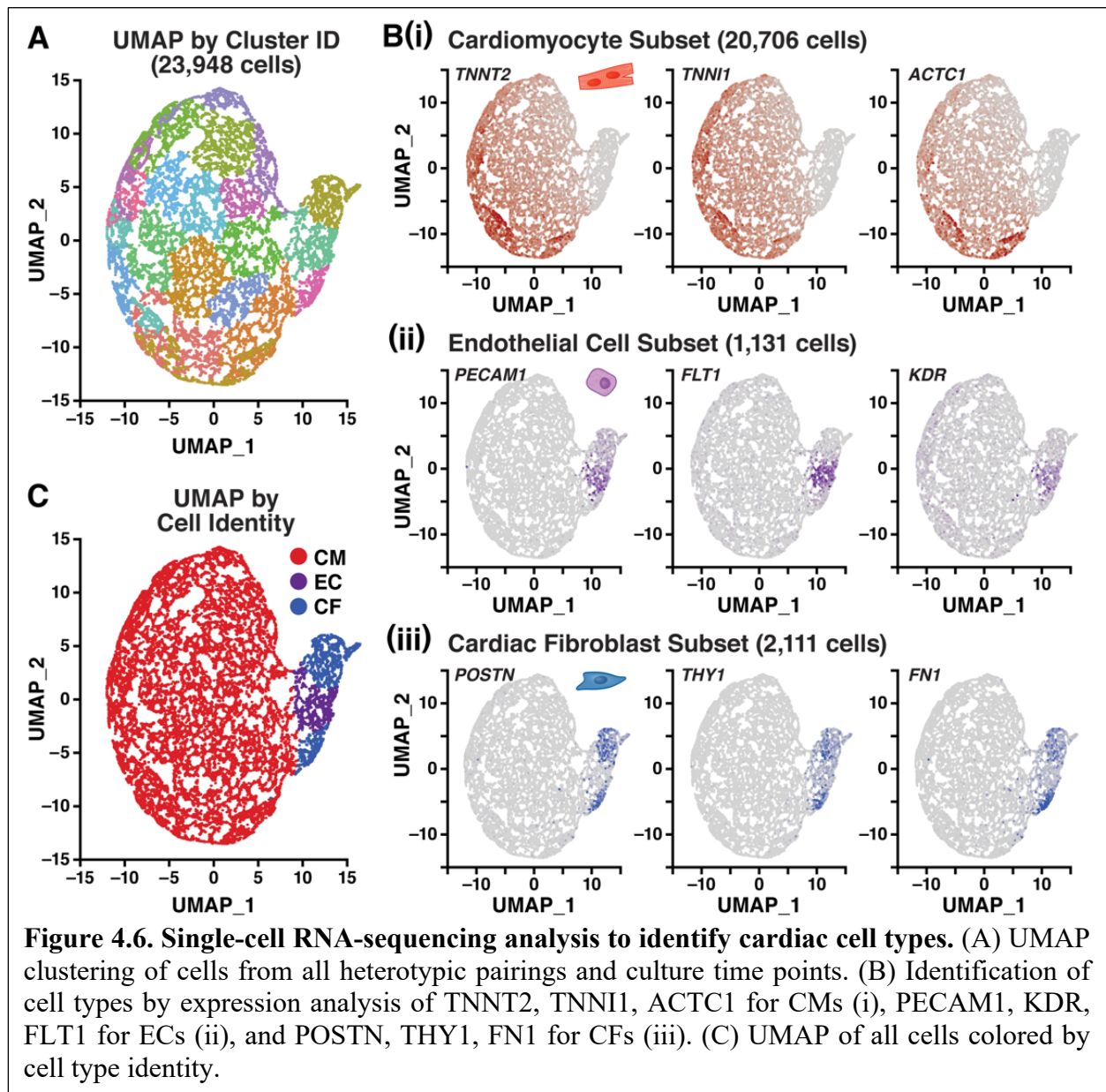
of these microtissues indicates that their calcium handling machinery could not take up and release calcium stores in time for higher pulse stimulation frequencies.



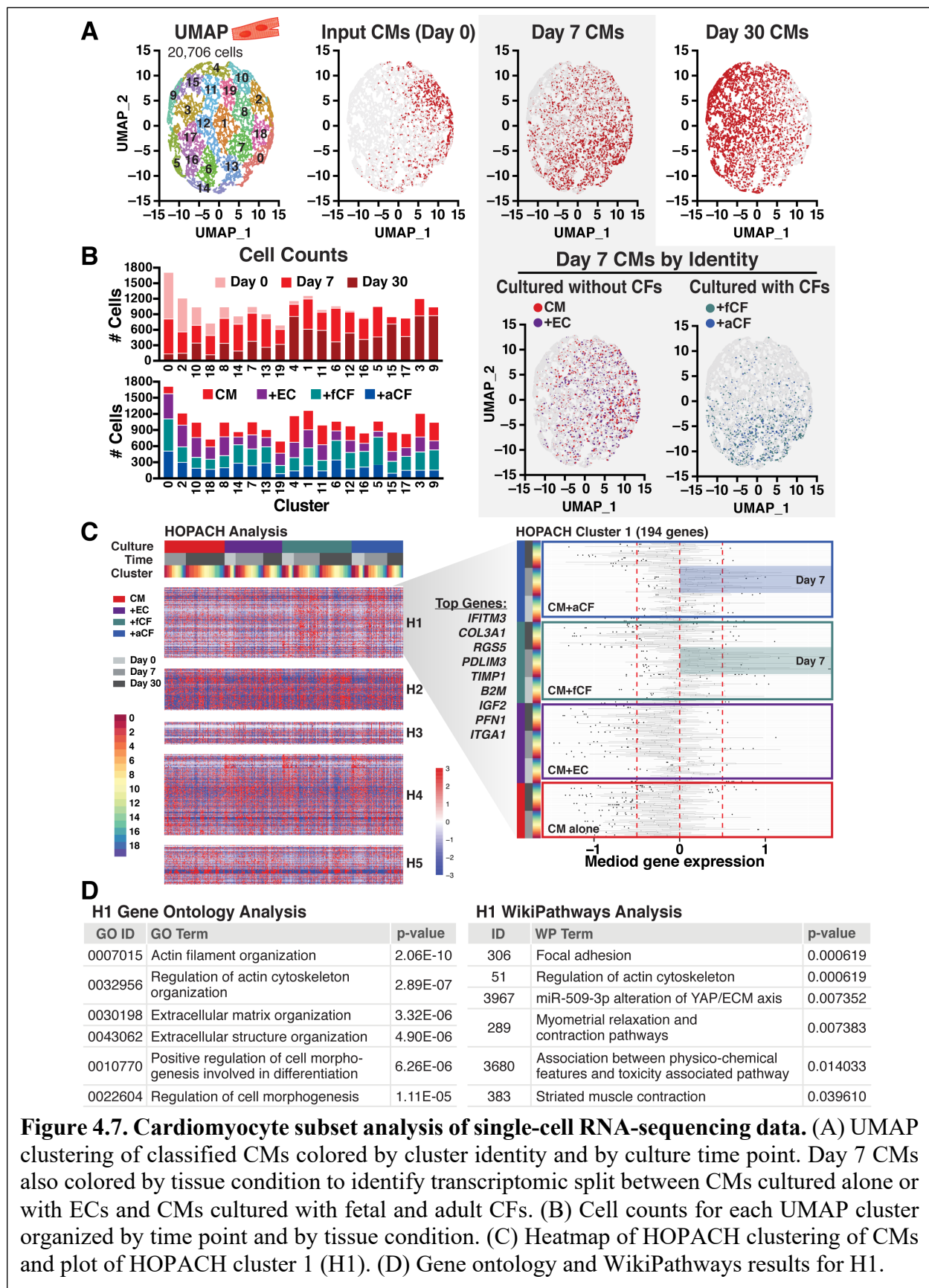
4.3.4. Cardiomyocyte phenotype changes as a result of cardiac fibroblast co-culture

In order to determine the phenotypic influences of heterotypic interactions, we performed single-cell RNA-sequencing on cells from each culture condition and each time point (input day 0, day 7, and day 30; Figure 4.6A). Since flow cytometry methods are notoriously difficult to accurately sort cardiac cells due to lack of differential surface markers, we “sorted” cells using transcriptomic identification methods. A single cluster was identified as ECs based on expression of PECAM1, FLT, and KDR (4.7% cells total; Figure 4.6Bii,C) and two clusters were classified as CFs based on elevated expression of POSTN, FN1, and THY1 (8.8% cells total; Figure 4.6Biii,C). The remaining clusters were characterized as CMs based on expression of TNNT2,

TNNI1, and ACTC1 (86.5% cells total; Figure 4.6Bi,C). A total of 18 clusters were assigned as CMs, suggesting that several different CM phenotypes existed in the pooled population of cells.



To interrogate these phenotypes, we performed secondary analysis by subsetting the cells classified as CMs, ECs, or CFs and separately re-clustering and analyzing differential gene expression within the different cell identities. Cells classified as CMs were subset and re-normalized using zinbwave reduction, resulting in 20 clusters that were separated largely along

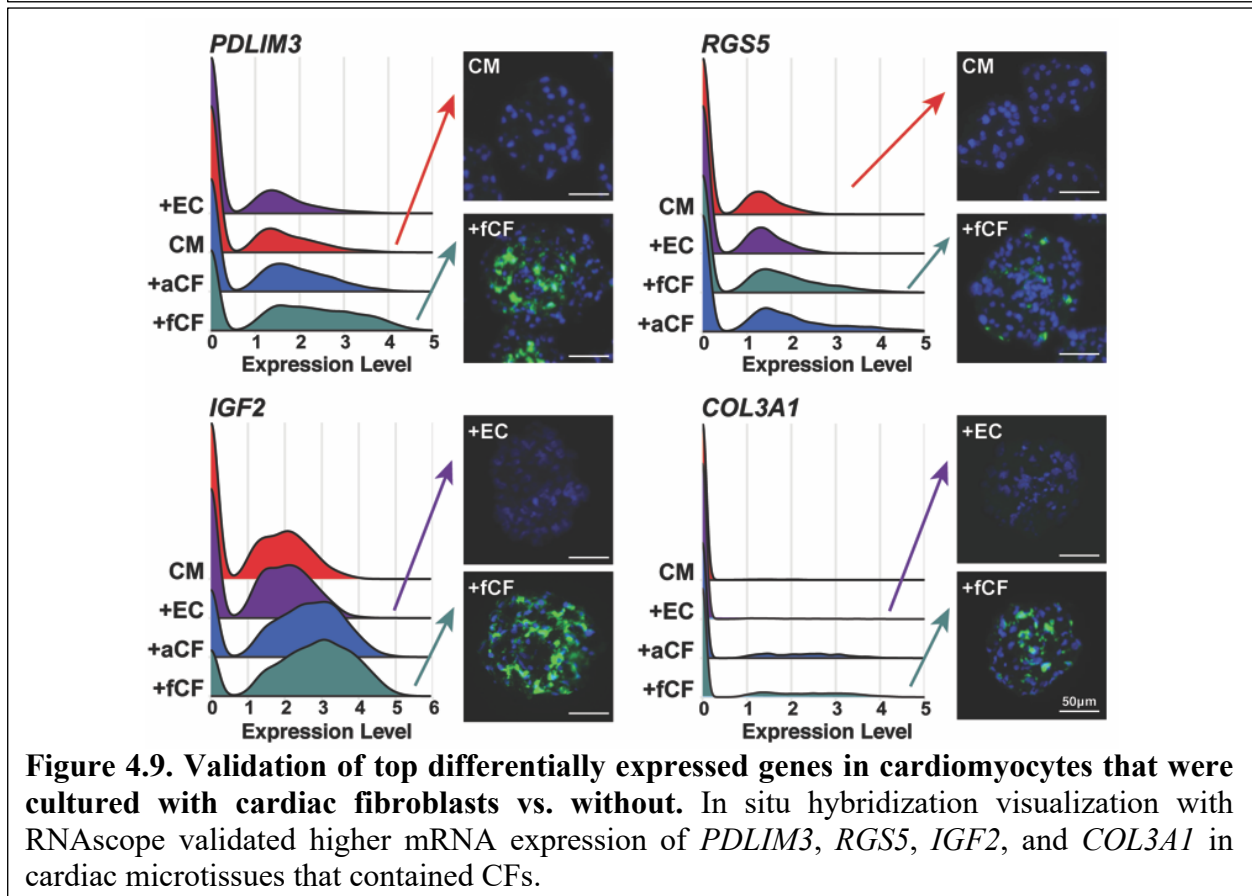
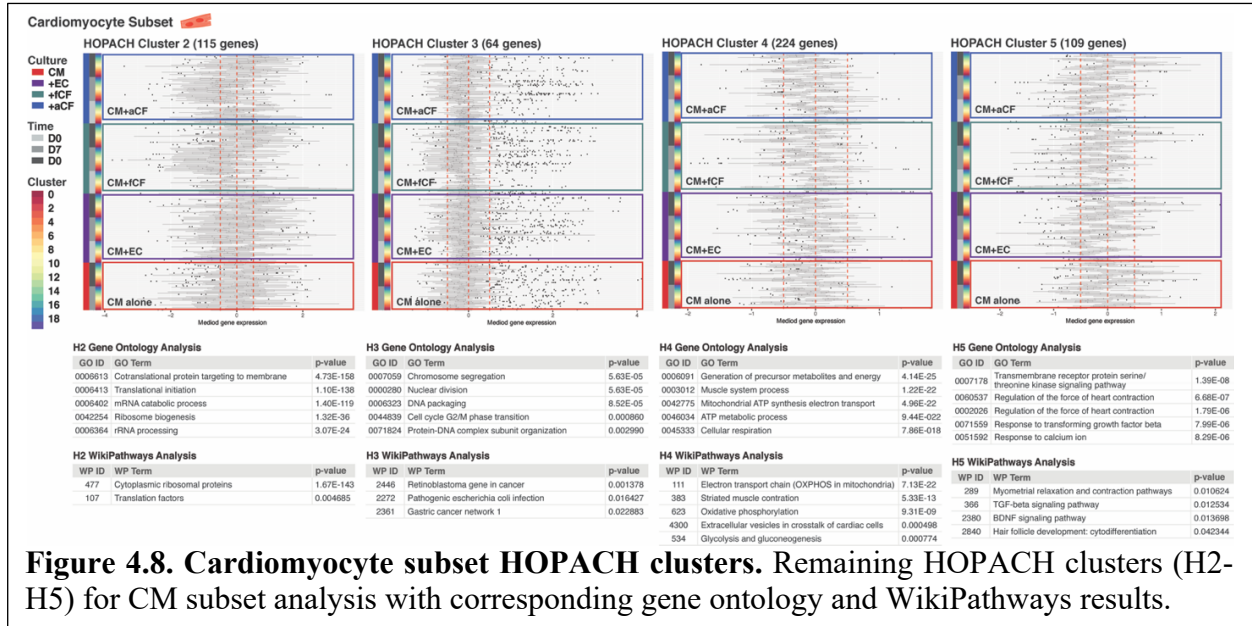


the axis of culture time (Figure 4.7A). Day 0 CMs represented ~15% of the analyzed CMs and clustered together regardless of initial heterotypic mixing, confirming a homogeneous input population. By day 7, however, CMs mixed with either fetal or adult CFs (4,182 CMs) were largely separated from CMs that were mixed with ECs or from homotypic cultures (4,233 CMs), highlighting a shift in CM phenotype as a result of CF co-culture for 7 days (Figure 4.7B). Yet, after 30 days of culture, CMs from all microtissue conditions (~44% of total CMs) clustered together regardless of heterotypic pairing, indicating a return to a more homogeneous CM phenotype after prolonged 3D culture.

We next employed Hierarchical Ordered Partitioning and Collapsing Hybrid (HOPACH) clustering to derive unbiased cell type-specific gene lists (H1_{CM}-H5_{CM}), followed by gene ontology (GO) and WikiPathways analysis. HOPACH identified the specific groups of CMs that contributed to the differential expression in each gene list, regardless of UMAP cluster, time point, or heterotypic pairing (Figure 4.7C, Figure 4.8). For instance, H1_{CM} mirrored the UMAP clustering split of CMs that were cultured with CFs versus without. H1_{CM} contained 194 genes which were upregulated in CMs from day 7 +fCF and +aCF co-cultures, including *IFITM3*, *COL3A1*, *RGS5*, *PDLIM3*, *TIMP1*, *IGF2*, and *SPARC* (Figure 4.7C). These genes corresponded to ECM organization, cytoskeletal organization, and cell morphogenesis GO terms, as well as cytoskeletal, ECM, and physical contraction WikiPathways results (Figure 4.7D), indicating that the presence of CFs may lead to a CM phenotype that is more capable of remodeling its local environment. We confirmed upregulation of several of the top differentially-expressed genes between day 7 CMs cultured with CFs vs. without (*PDLIM3*, *RGS5*, *IGF2*, and *COL3A1*) by RNAscope (Figure 4.9).

Other HOPACH clusters contained genes related to ribosomal processing (H2_{CM}), cell cycle (H3_{CM}), and mitochondria (H5_{CM}) (Figure 4.8). H5_{CM} contained genes with increased

expression in day 30 CMs from UMAP clusters 4, 9, and 15 (increased expression in all microtissue groups), with GO terms that were largely relevant to cardiac function and development (Figure 4.8), reflecting increased culture differentiation or maturation profiles.



4.3.5. Non-myocyte phenotypic changes as a result of heterotypic co-culture

During initial cell identification after sequencing, 1,131 cells were identified as ECs based on a panel of markers (Figure 4.6B). However, only about 67% of these originated from an EC-containing microtissue group; the remainder came from CM+CF microtissues (Figure 4.10A,B). The majority of cells identified as ECs were from the initial (day 0) time point (~94%). However, HOPACH analysis and GO assessment identified several gene clusters (H1_{EC}-H9_{EC}) that changed expression patterns at day 7 and 30 as a result of heterotypic culture (Figure 4.11). H1_{EC} contained 63 genes, such as *EDNI*, that were expressed at higher levels in input (day 0) ECs than in ECs post-3D-heterotypic culture (Figure 4.10C). H1_{EC} was enriched with genes annotated by GO terms related to neutrophil activation, muscle contraction, intracellular transport, and metabolic processes, as well as proteasomal- and glycolysis-related WikiPathways terms (Figure 4.10D). H3_{EC}, on the other hand, contained genes that were upregulated in day 7 and day 30 ECs, including *KDR*, *IL32*, and *HYAL2* (Figure 4.10C). The relevant GO terms were related to endothelial development and migration as well as ECM organization and cell junction assembly, and WikiPathways results included cardiac calcium regulation and contraction pathways, indicating that heterotypic culture alters CM-EC interactions related to cardiac function (Figure 4.10D). The other HOPACH clusters listed differential gene expression in cells that did not come from the CM+EC microtissues, and therefore were not included in this secondary analysis (Figure 4.11).

A total of 2,111 CFs were identified across all culture conditions and time points (Figure 4.6B), with only a small fraction of CFs (~6%) coming from the CM+EC and CM alone tissue groups, likely attributable to the stromal/fibroblastic cells derived from hiPSC-CM and hiPSC-EC differentiations. Of the identified CFs that came from the +CF microtissue groups, 73% were a result of the input cells (aCF and fCF at day 0), ~24% came from day 7 tissues, and only ~3% were

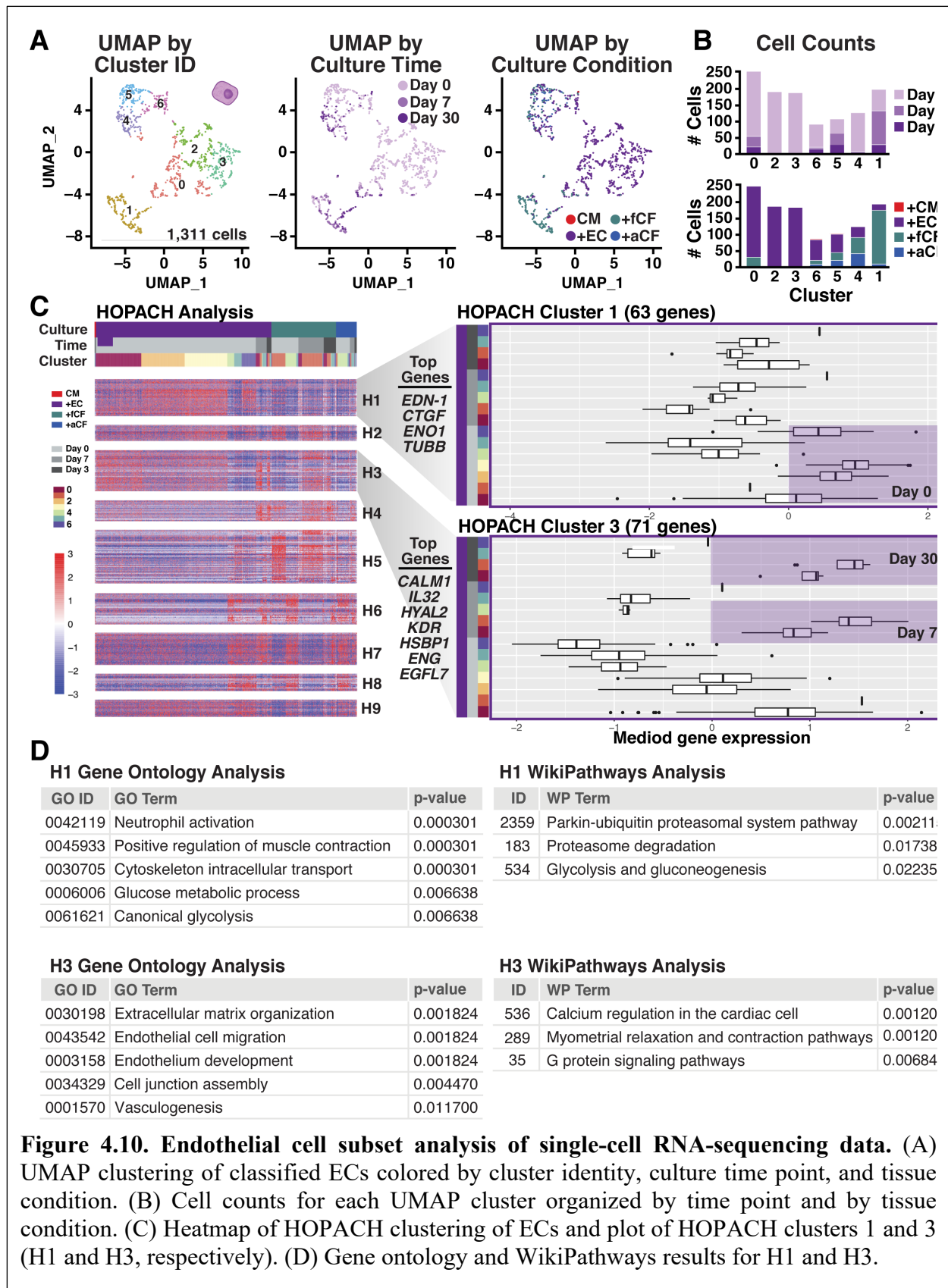
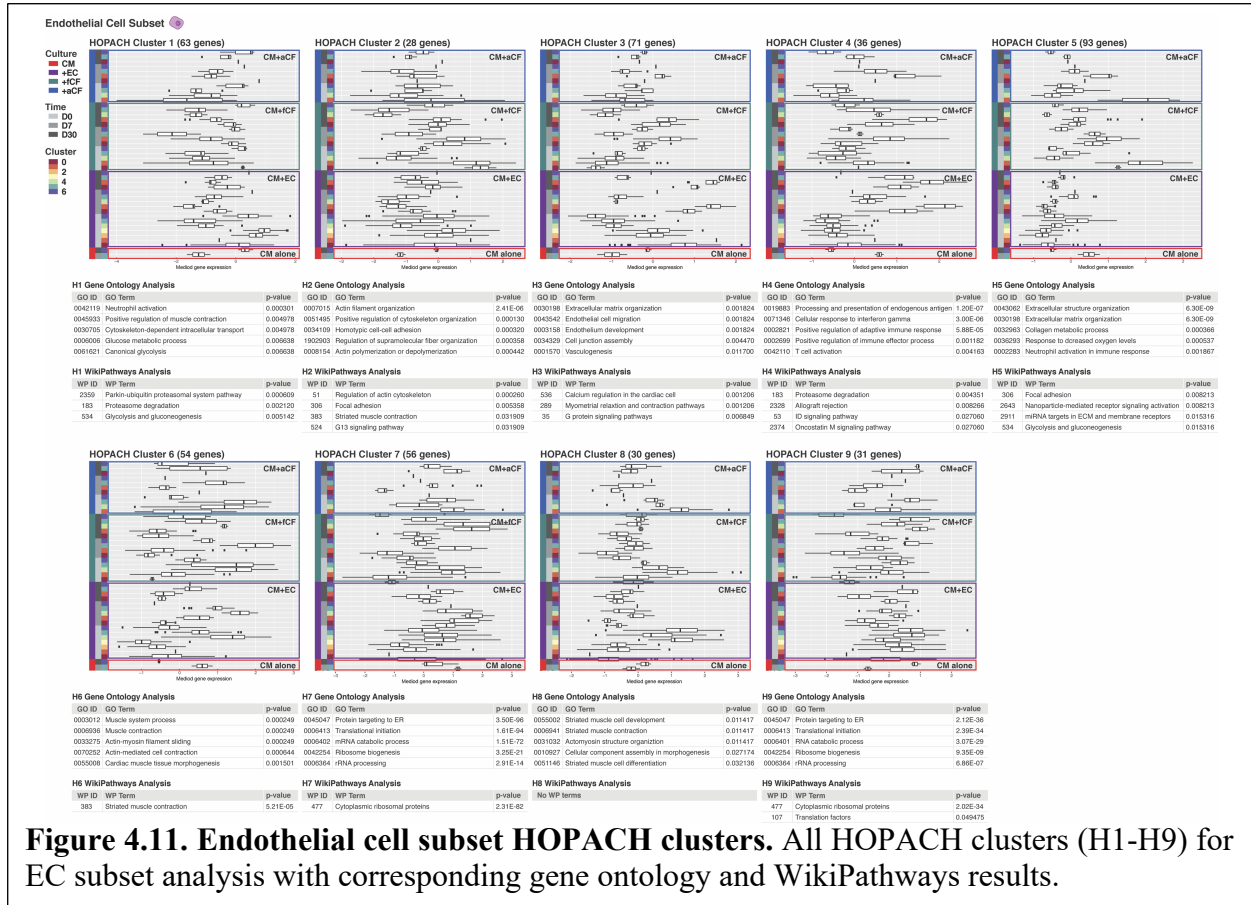
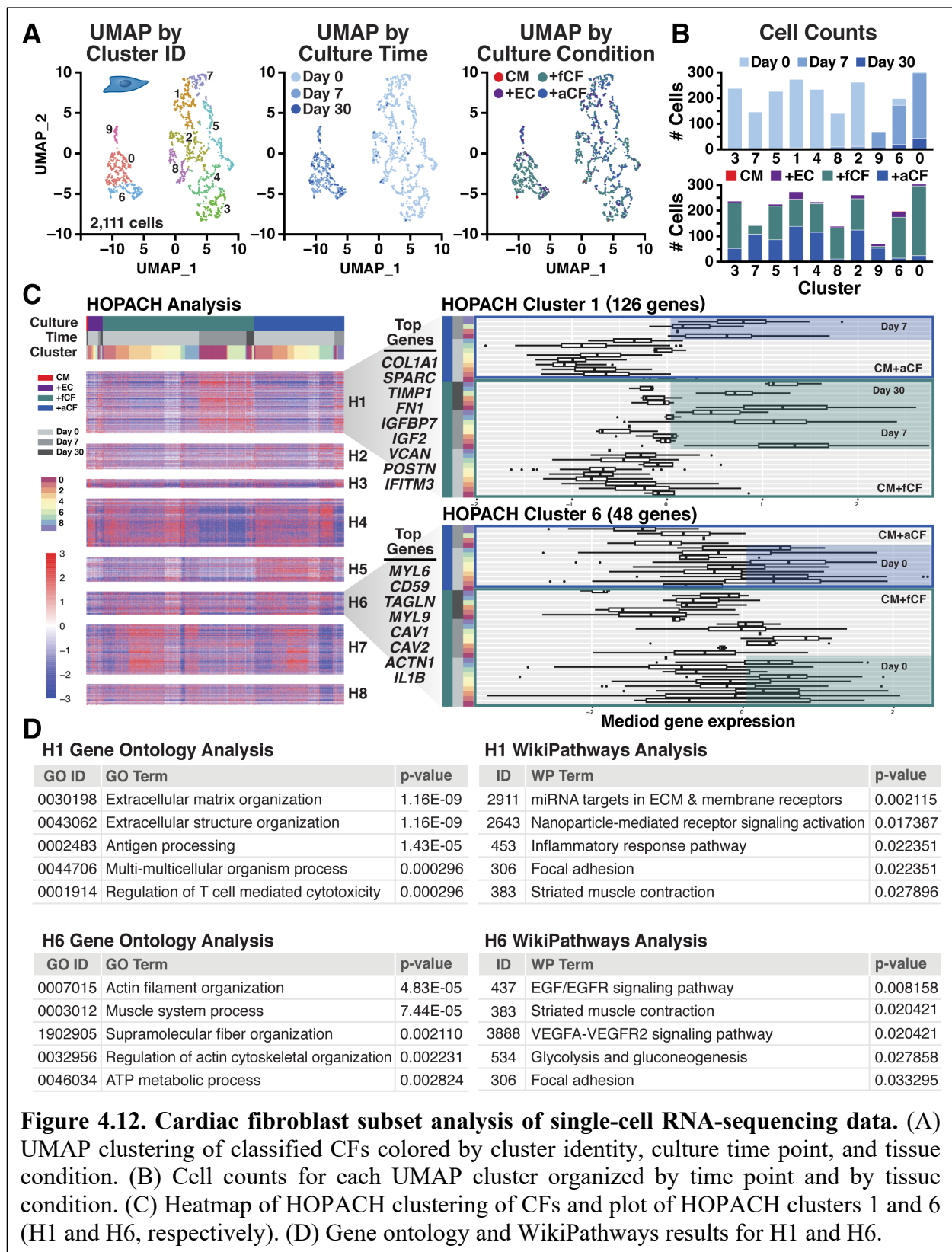


Figure 4.10. Endothelial cell subset analysis of single-cell RNA-sequencing data. (A) UMAP clustering of classified ECs colored by cluster identity, culture time point, and tissue condition. (B) Cell counts for each UMAP cluster organized by time point and by tissue condition. (C) Heatmap of HOPACH clustering of ECs and plot of HOPACH clusters 1 and 3 (H1 and H3, respectively). (D) Gene ontology and WikiPathways results for H1 and H3.

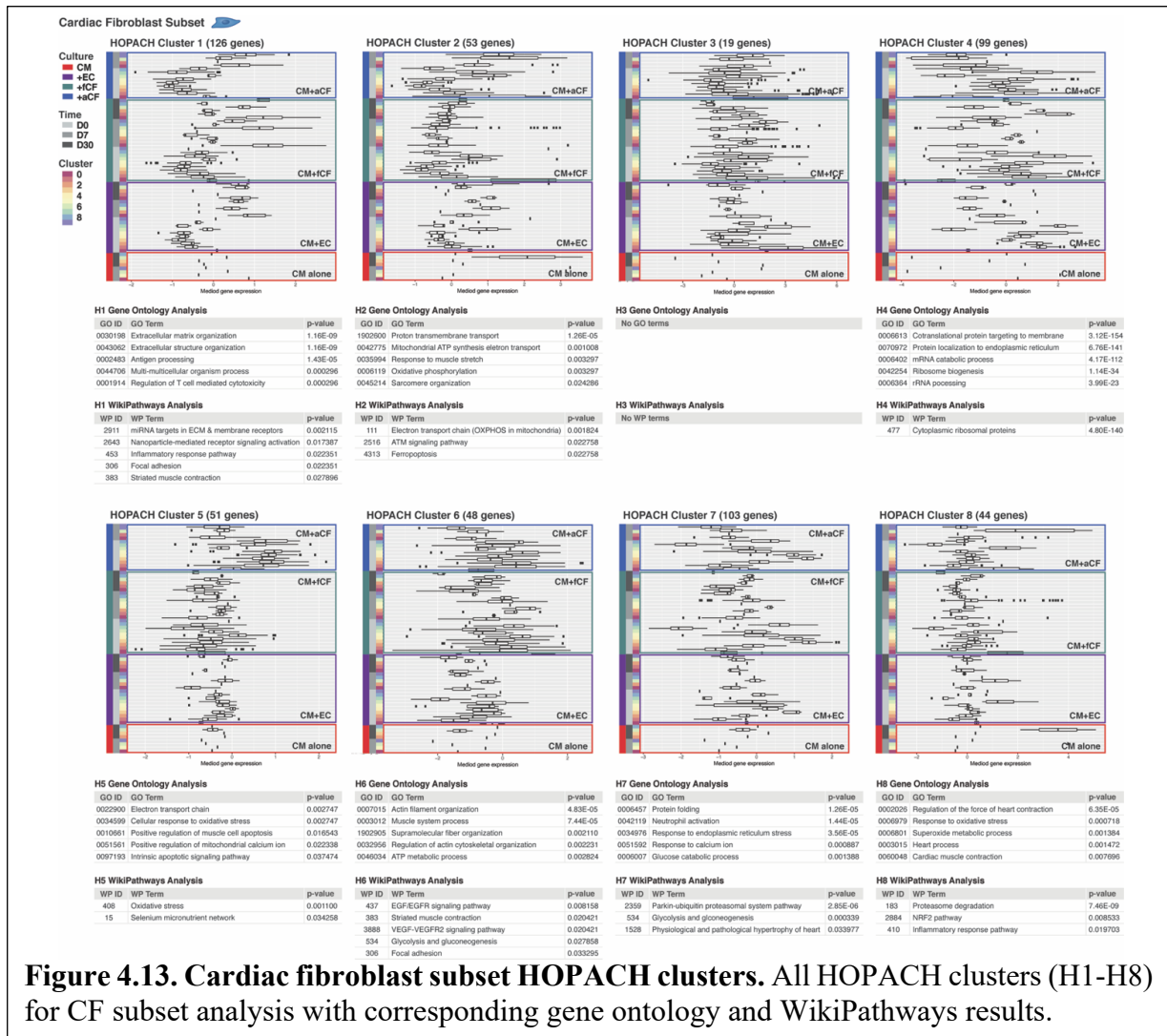
identified after the full 30 days of culture (Figure 4.12A,B). Since immunostaining demonstrated the presence of non-myocytes in day 7 and 30 CM+CF microtissues (Figure 4.2A), the sharp decline in the numbers of CFs identified after 3D heterotypic co-culture is likely due to loss of the cells during microtissue dissociation rather than cell death or differentiation.



Cluster analysis revealed 10 individual subsets of fibroblasts, with CF expression patterns after 7 and 30 days of microtissue culture (UMAP clusters 0, 6, and 9) clearly distinct from the starting CF populations (Figure 4.12A). HOPACH analysis identified 8 clusters of genes (H1_{CF}-H8_{CF}) that drove phenotypic differences in CFs as a result of time in culture (day 0, day 7, day 30) and developmental stage (fCF vs. aCF). H1_{CF} contained 126 genes that were highly expressed in fCFs and aCFs after 3D heterotypic culture (days 7 and 30), while H6_{CF} contained 48 genes that were upregulated in input (day 0) CFs (Figure 4.12C). The H1_{CF} genes (*COL1A1*, *SPARC*, *TIMP1*,



FNI) are related to extracellular matrix organization and antigen processing, while *H6_{CF}* genes (*MYL6*, *TAGLN*, *MYL9*) are related to cytoskeletal organization and muscle contraction (Figure 4.12D). Differences between CFs at distinct developmental stages were reflected in *H5_{CF}*, which contained 51 genes (including *TPM1*, *MYL12A*, and *IL1B*) that were expressed at higher levels in day 0 adult CFs than day 0 fetal CFs, with GO terms related to muscle contraction and actin organization (Figure 4.13). The remaining HOPACH clusters listed differentially expressed genes that were not specific to CFs (Figure 4.13). In summary, this data reveals that 3D cardiomyocyte co-culture induces a less contractile fibroblast phenotype and promotes the fibroblasts' ability to remodel their extracellular environment.



4.4. Discussion

This study interrogated the heterotypic influences of paired cardiac populations on cellular phenotype and function within 3D engineered cardiac tissues. Due to the single cell-based nature of the analyses, we were able to dissect bi-directional phenotypic changes in each specific cellular sub-type and evaluate them in the context of tissue level functional performance. While it is well established that non-myocytes are required to promote stable tissue formation (Thavandiran et al. 2013, Hookway et al. 2016, Huebsch et al. 2016, Iseoka et al. 2018, Hookway et al. 2019), previous studies have described variable effects of different stromal or non-myocyte populations on cardiac function with limited details reported on phenotypic shifts in the co-cultured cells (Hookway et al. 2019, Giacomelli et al. 2020, Thavandiran et al. 2020). Therefore, we aimed to determine how age-specific CFs and ECs differentially affect cardiac tissue organization and calcium handling dynamics, resulting in transcriptional changes in the different heterotypic populations of cells.

hiPSC-CMs lack a fully mature phenotype, and transcriptional progression throughout differentiation renders them most comparable to early-/mid-gestation fetal CMs (DeLaughter et al. 2016, Dunn and Palecek 2018, Karbassi et al. 2020). Several key environmental parameters have been implicated in promoting the developmental phenotype of hiPSC-CMs, such as three-dimensional culture (Nunes et al. 2013, Nguyen et al. 2014, Ronaldson-Bouchard et al. 2018, Beauchamp et al. 2020), biochemical cues (Correia et al. 2017, Parikh et al. 2017, Yang et al. 2019), electromechanical stimulation (Chan et al. 2013, Nunes et al. 2013, Mihic et al. 2014, Ruan et al. 2015, Eng et al. 2016, Ronaldson-Bouchard et al. 2018), and extended culture duration (Kamakura et al. 2013, Lundy et al. 2013, Piccini et al. 2015). Consistent with previous studies, the cardiac microtissues examined here exhibited overall improvements in calcium handling properties (amplitude, maximum upstroke and downstroke velocities) with prolonged (30 day)

culture in the engineered 3D platform. However, despite more mature calcium transient profiles, the day 30 microtissues could not respond to the higher stimulation frequencies, potentially indicating that since the microtissues were able to take up more calcium (increased amplitude) they might not have been able to release it in time, and therefore were still in a refractory phase when the faster stimulation pulses were fired. Overall, the functional changes at day 30 occurred in all microtissues regardless of the heterotypic pairing, highlighting culture duration aids in modest CM maturation.

In contrast, short-term co-culture (first 7 days) with CFs promoted more rapid phenotypic maturation of CMs, in terms of both microtissue calcium handling dynamics and CM gene expression. Our finding that co-culture with ECs did not improve cardiac microtissue function is consistent with previous reports showing that while CMs may be transcriptionally or structurally impacted by EC co-culture, functional parameters are not improved (Giacomelli et al. 2017, Dunn et al. 2019). However, a recent study demonstrated that ECs can improve stem cell-derived cardiac microtissue function when they are incorporated with a stromal population (i.e. CM+CF+EC microtissues), indicating a potential additive effect of heterotypic tri-culture on tissue function (Giacomelli et al. 2020).

After 7 days of culture, cytoskeletal (*RGS5*, *PDLIM3*) as well as ECM-associated (*COL3A1*, *IGF2*, *SPARC*, *TIMPI*) genes were more highly expressed in CMs cultured with CFs than in CMs cultured alone or with ECs. Notably, both *RGS5* and *PDLIM3* are implicated in cardiac homeostasis and calcium handling. *RGS5*, a regulator of G protein signaling that is expressed in multiple cardiac cell types throughout development, protects CMs from apoptosis, inflammation, and fibrotic remodeling (Li et al. 2010, Wang et al. 2016). Moreover, a mouse model of *RGS5* deficiency exhibits prolonged cardiac repolarization and increased action potential

duration (Qin et al. 2012), indicating a role for *RGS5* in cardiac electrophysiology. *PDLIM3* (PDZ and LIM Domain 3), also known as actin-associated LIM protein or ALP, works in concert with muscle LIM protein (MLP), by co-localizing to the intercalated disks and interacting with alpha actinin (Henderson et al. 2003), contributing to cardiac muscle organization and maintenance. Absence or dysfunction of ALP and MLP are associated with heart disease (Pashmforoush et al. 2001, Zhou et al. 2001), and MLP-deficient hPSC-CMs display impaired calcium handling and progressively mimic hypertrophic cardiomyopathy (Li et al. 2019). Therefore, the roles of *RGS5* and *PDLIM3* in cytoskeletal structure and cardiac function are consistent with our finding that increased expression of those genes in CMs paired with CFs correlated with improved calcium handling properties.

Throughout heart development and in response to injury, CFs are considered the primary cell type responsible for ECM synthesis and remodeling (Souders et al. 2009, Furtado et al. 2016). Consistent with this paradigm, we observed increased expression of several genes related to ECM-production (*COL1A1*, *FNI*, *VCAN*, *POSTN*) and ECM-remodeling (*TIMP1*) in CFs from microtissues. Notably, however, CMs co-cultured with CFs also exhibited increased expression of ECM-related genes (e.g. *COL3A1* and *TIMP1*), suggesting that CMs may also actively modulate their extracellular microenvironment in the presence of CFs.

Endothelial cells were also impacted by 3D heterotypic co-culture, though the effects were harder to dissect due to low numbers of cells in the day 7 and day 30 sequencing analysis as well as the identified cells that came from CF microtissues, which could be due to the impure nature of primary CF isolations or a result of the bioinformatic cell “sorting” pipeline. Cell classification was based on expression of cell-specific genes, but the lack of definitive non-myocytes markers makes the bioinformatic pipeline vulnerable to the same potential flaws of physical cell sorting,

where there is not enough stark contrast between the non-myocytes to accurately distinguish ECs and CFs. HOPACH analysis of the EC subset identified clusters of genes that aligned with tissue culture time points: H1_{EC} was driven by input (day 0) ECs (98% from +EC tissues) and corresponded to metabolic-related GO and Wikipathways terms, while H3_{EC} and H4_{EC} were driven by day 7 and day 30 ECs (~22% from +EC tissues, 78% from +CF tissues), and were associated with endothelial development and cardiac calcium regulation (H3_{EC}) and immune response (H4_{EC}) terms. It is difficult to interpret these data due to the relatively large presence of ECs in the +fCF and +aCF microtissues, but the genes that informed the cardiac calcium regulation WikiPathways terms in H3_{EC} included Connexin 37 (*GJA4*) and Calmodulin 1 (*CALM1*), both of which are known regulators of ion transport. Gap junction GJA4 is most commonly found between endothelial cells, and both CALM1 and GJA4 interact with endothelial nitric oxide synthase (eNOS), which synthesizes the nitric oxide that ECs secrete for CM homeostasis and contractility (Greif et al. 2004, Pfenniger et al. 2010, Colliva et al. 2019). Therefore, the presence of these genes may indicate that 3D heterotypic culture with CMs promotes paracrine signaling in ECs.

In the context of this study, there were few discernable differences in the performance or phenotype of microtissues comprised of CMs with either fetal or adult CFs, indicating that the temporal stage of a specific non-myocyte population does not impact phenotypic and functional differences as much as the type of non-myocyte. We observed a set of genes expressed in input adult CFs that were not expressed in input fetal CFs, but after mixing with CMs in microtissue culture, these differences largely disappeared and the CFs were more phenotypically similar to one another. CM+fCF microtissues maintained a core of fibroblasts throughout the 30 days of culture and were able to maintain 2Hz electrical pacing at day 30, whereas the non-myocyte cores within CM+aCF tissues became more diffuse by day 30 and the microtissues were not able to sustain

pacing >1Hz. This may indicate that the persistent presence of a non-myocyte core is key to improved pacing response. Furthermore, in day 7 microtissues, the expression of cTnI was elevated at the borders of the fCF and aCF cores, indicating that CMs juxtaposed with CFs may mature faster. The expression of increased by day 30 in all conditions, consistent with the paradigm that culture duration increases maturation, and with the finding that day 30 tissues had improved calcium handling compared to their day 7 counterparts. The ability of CFs to act as electrical insulators or provide impulse propagation and excitability to their neighbors remains debated in the field, though a recent study demonstrated that Connexin 43 gap junctions between CMs and CFs are necessary for microtissue function and maturation (Giacomelli et al. 2020). Advanced spatial transcriptomic and 3D imaging technologies (Turaga et al. 2020) will provide further insight into the influence of multicellular spatial organization on beat rate, pacing responses, and intratissue heterogeneity.

Previous characterization of cardiac microtissue heterogeneity using light sheet microscopy determined that the initial seeding ratio of 3:1 CMs:CFs is maintained after 7 days of microtissue culture (Turaga et al. 2020), which suggests that the lower numbers of ECs and CFs identified at day 7 in the single-cell RNA-seq analysis may be due to a technical artifact. Low recovery of non-myocytes could result from dissociation removing cells in radial manner, such that the central core of CFs are last and hardest to dissociate. However, the number of identified non-myocytes was even further diminished in day 30 heterotypic cultures, indicating that this experimental system favors CMs. This further decline may be related to the use of hiPSC-CM maintenance medium, and therefore media optimization may be required to support non-myocyte survival and/or function long term (Giacomelli et al. 2020). Morphologically, we observed that the frequency of non-myocyte cores decreased by day 30, and functionally, day 30 heterotypic

microtissues displayed less mature calcium handling properties than the homotypic microtissues. Therefore, it remains unclear whether the positive contribution of CFs was a transient phenomenon, or if the progressive loss of non-myocytes with long-term culture adversely affected microtissue function.

Increasing complexity of microtissues by incorporation of multiple cardiac cell types, modified tissue geometries, and the addition of biophysical or electromechanical cues will advance understanding of the complex multisystem crosstalk in these systems. This study demonstrates how single-cell phenotypic analysis can yield a deeper understanding of how heterotypic interactions affect individual cell phenotypes and their collective contribution to tissue-level structural and functional properties. The ability to merge single-cell metrics with multicellular tissue behaviors is paramount to developing advanced systems capable of modeling human development and disease *ex vivo*.

4.5. Conclusions

This study achieved a comprehensive characterization of the interactions between and cardiomyocytes and cardiac tissue-specific non-myocytes in a 3D microtissue model. It further cemented the concept that identity of the non-myocyte is important to cardiac tissue phenotype and function, as early calcium handling analysis demonstrated that cardiac fibroblasts and not endothelial cells improved tissue function and altered cardiomyocyte phenotype. Furthermore, this study was unique in that it combined advanced assessments of single-cell transcriptomics and microtissue calcium handling properties in order to link single-cell measures of phenotype to bulk tissue-level measures of function. This combination of technologies therefore allowed us to dissect interesting reciprocal interactions between multiple cell types, which, while demonstrated

here in cardiac microtissues, can be extended to assess heterotypic tissues of many varieties. A caveat of this study was that hiPSC-derived cardiomyocytes and endothelial cells were utilized, but cardiac fibroblasts (both fetal and adult) were isolated from primary human tissue. During the course of these experiments, protocols to derived cardiac-specific fibroblasts were described, enabling the generation of completely isogenic cardiac microtissue constructs in future studies.

4.6. *Bibliography*

- Beauchamp, P., et al. (2020). "3D Co-culture of hiPSC-Derived Cardiomyocytes With Cardiac Fibroblasts Improves Tissue-Like Features of Cardiac Spheroids." Front Mol Biosci **7**: 14.
- Butler, A., et al. (2018). "Integrating single-cell transcriptomic data across different conditions, technologies, and species." Nat Biotechnol **36**(5): 411-420.
- Chan, Y. C., et al. (2013). "Electrical stimulation promotes maturation of cardiomyocytes derived from human embryonic stem cells." J Cardiovasc Transl Res **6**(6): 989-999.
- Colliva, A., et al. (2019). "Endothelial cell-cardiomyocyte crosstalk in heart development and disease." J Physiol.
- Correia, C., et al. (2017). "Distinct carbon sources affect structural and functional maturation of cardiomyocytes derived from human pluripotent stem cells." Sci Rep **7**(1): 8590.
- DeLaughter, D. M., et al. (2016). "Single-Cell Resolution of Temporal Gene Expression during Heart Development." Dev Cell **39**(4): 480-490.
- Dunn, K. K. and S. P. Palecek (2018). "Engineering Scalable Manufacturing of High-Quality Stem Cell-Derived Cardiomyocytes for Cardiac Tissue Repair." Front Med (Lausanne) **5**: 110.
- Dunn, K. K., et al. (2019). "Coculture of Endothelial Cells with Human Pluripotent Stem Cell-Derived Cardiac Progenitors Reveals a Differentiation Stage-Specific Enhancement of Cardiomyocyte Maturation." Biotechnol J **14**(8): e1800725.
- Eng, G., et al. (2016). "Autonomous beating rate adaptation in human stem cell-derived cardiomyocytes." Nat Commun **7**: 10312.

- Furtado, M. B., et al. (2016). "View from the heart: cardiac fibroblasts in development, scarring and regeneration." Development **143**(3): 387-397.
- Giacomelli, E., et al. (2017). "Three-dimensional cardiac microtissues composed of cardiomyocytes and endothelial cells co-differentiated from human pluripotent stem cells." Development **144**(6): 1008-1017.
- Giacomelli, E., et al. (2020). "Human-iPSC-Derived Cardiac Stromal Cells Enhance Maturation in 3D Cardiac Microtissues and Reveal Non-cardiomyocyte Contributions to Heart Disease." Cell Stem Cell.
- Greif, D. M., et al. (2004). "Calmodulin phosphorylation and modulation of endothelial nitric oxide synthase catalysis." Proc Natl Acad Sci U S A **101**(5): 1165-1170.
- Henderson, J. R., et al. (2003). "ALP and MLP distribution during myofibrillogenesis in cultured cardiomyocytes." Cell Motil Cytoskeleton **54**(3): 254-265.
- Hookway, T. A., et al. (2016). "Aggregate formation and suspension culture of human pluripotent stem cells and differentiated progeny." Methods **101**: 11-20.
- Hookway, T. A., et al. (2019). "Phenotypic Variation Between Stromal Cells Differentially Impacts Engineered Cardiac Tissue Function." Tissue Eng Part A **25**(9-10): 773-785.
- Huber, W., et al. (2015). "Orchestrating high-throughput genomic analysis with Bioconductor." Nat Methods **12**(2): 115-121.
- Huebsch, N., et al. (2016). "Miniaturized iPS-Cell-Derived Cardiac Muscles for Physiologically Relevant Drug Response Analyses." Sci Rep **6**: 24726.
- Huebsch, N., et al. (2015). "Automated Video-Based Analysis of Contractility and Calcium Flux in Human-Induced Pluripotent Stem Cell-Derived Cardiomyocytes Cultured over Different Spatial Scales." Tissue Eng Part C Methods **21**(5): 467-479.

- Iseoka, H., et al. (2018). "Pivotal Role of Non-cardiomyocytes in Electromechanical and Therapeutic Potential of Induced Pluripotent Stem Cell-Derived Engineered Cardiac Tissue." Tissue Eng Part A **24**(3-4): 287-300.
- Kamakura, T., et al. (2013). "Ultrastructural maturation of human-induced pluripotent stem cell-derived cardiomyocytes in a long-term culture." Circ J **77**(5): 1307-1314.
- Karbassi, E., et al. (2020). "Cardiomyocyte maturation: advances in knowledge and implications for regenerative medicine." Nat Rev Cardiol **17**(6): 341-359.
- Kolde, R. (2012). "Pheatmap: pretty heatmaps." R package version **1**(2).
- Li, H., et al. (2010). "Regulator of G protein signaling 5 protects against cardiac hypertrophy and fibrosis during biomechanical stress of pressure overload." Proc Natl Acad Sci U S A **107**(31): 13818-13823.
- Li, X., et al. (2019). "MLP-deficient human pluripotent stem cell derived cardiomyocytes develop hypertrophic cardiomyopathy and heart failure phenotypes due to abnormal calcium handling." Cell Death & Disease **10**(8): 610.
- Lian, X., et al. (2012). "Robust cardiomyocyte differentiation from human pluripotent stem cells via temporal modulation of canonical Wnt signaling." Proc Natl Acad Sci U S A **109**(27): E1848-1857.
- Lian, X., et al. (2013). "Directed cardiomyocyte differentiation from human pluripotent stem cells by modulating Wnt/beta-catenin signaling under fully defined conditions." Nat Protoc **8**(1): 162-175.
- Lundy, S. D., et al. (2013). "Structural and functional maturation of cardiomyocytes derived from human pluripotent stem cells." Stem Cells Dev **22**(14): 1991-2002.

- Mandegar, M. A., et al. (2016). "CRISPR Interference Efficiently Induces Specific and Reversible Gene Silencing in Human iPSCs." Cell Stem Cell **18**(4): 541-553.
- McCarthy, D. J., et al. (2012). "Differential expression analysis of multifactor RNA-Seq experiments with respect to biological variation." Nucleic Acids Res **40**(10): 4288-4297.
- McInnes, L., et al. (2018). "UMAP: Uniform Manifold Approximation and Projection for Dimension Reduction." arXiv e-prints.
- Mihic, A., et al. (2014). "The effect of cyclic stretch on maturation and 3D tissue formation of human embryonic stem cell-derived cardiomyocytes." Biomaterials **35**(9): 2798-2808.
- Nguyen, D. C., et al. (2014). "Microscale generation of cardiospheres promotes robust enrichment of cardiomyocytes derived from human pluripotent stem cells." Stem Cell Reports **3**(2): 260-268.
- Nunes, S. S., et al. (2013). "Biowire: a platform for maturation of human pluripotent stem cell-derived cardiomyocytes." Nat Methods **10**(8): 781-787.
- Parikh, S. S., et al. (2017). "Thyroid and Glucocorticoid Hormones Promote Functional T-Tubule Development in Human-Induced Pluripotent Stem Cell-Derived Cardiomyocytes." Circ Res **121**(12): 1323-1330.
- Pashmforoush, M., et al. (2001). "Adult mice deficient in actinin-associated LIM-domain protein reveal a developmental pathway for right ventricular cardiomyopathy." Nat Med **7**(5): 591-597.
- Pfenniger, A., et al. (2010). "Gap junction protein Cx37 interacts with endothelial nitric oxide synthase in endothelial cells." Arterioscler Thromb Vasc Biol **30**(4): 827-834.

- Piccini, I., et al. (2015). "Human pluripotent stem cell-derived cardiomyocytes: Genome-wide expression profiling of long-term in vitro maturation in comparison to human heart tissue." Genom Data **4**: 69-72.
- Qin, M., et al. (2012). "Absence of Rgs5 prolongs cardiac repolarization and predisposes to ventricular tachyarrhythmia in mice." J Mol Cell Cardiol **53**(6): 880-890.
- Risso, D., et al. (2018). "A general and flexible method for signal extraction from single-cell RNA-seq data." Nat Commun **9**(1): 284.
- Robinson, M. D., et al. (2010). "edgeR: a Bioconductor package for differential expression analysis of digital gene expression data." Bioinformatics **26**(1): 139-140.
- Ronaldson-Bouchard, K., et al. (2018). "Advanced maturation of human cardiac tissue grown from pluripotent stem cells." Nature **556**(7700): 239-243.
- Ruan, J. L., et al. (2015). "Mechanical Stress Promotes Maturation of Human Myocardium From Pluripotent Stem Cell-Derived Progenitors." Stem Cells **33**(7): 2148-2157.
- Silva, A. C., et al. (2020). "Developmental co-emergence of cardiac and gut tissues modeled by human iPSC-derived organoids." bioRxiv: 2020.2004.2030.071472.
- Souders, C. A., et al. (2009). "Cardiac fibroblast: the renaissance cell." Circ Res **105**(12): 1164-1176.
- Stuart, T., et al. (2019). "Comprehensive Integration of Single-Cell Data." Cell **177**(7): 1888-1902 e1821.
- Thavandiran, N., et al. (2013). "Design and formulation of functional pluripotent stem cell-derived cardiac microtissues." Proc Natl Acad Sci U S A **110**(49): E4698-4707.
- Thavandiran, N., et al. (2020). "Functional arrays of human pluripotent stem cell-derived cardiac microtissues." Sci Rep **10**(1): 6919.

- Tohyama, S., et al. (2013). "Distinct metabolic flow enables large-scale purification of mouse and human pluripotent stem cell-derived cardiomyocytes." Cell Stem Cell **12**(1): 127-137.
- Turaga, D., et al. (2020). "Single cell determination of cardiac microtissue structure and function using light sheet microscopy." Tissue Eng Part C Methods.
- van der Laan, M. J. and K. S. Pollard (2003). "A new algorithm for hybrid clustering of gene expression data with visualization and the bootstrap." Journal of Statistical Planning and Inference **117**(2): 275-303.
- Wang, Z., et al. (2016). "Regulator of G-protein signaling 5 protects cardiomyocytes against apoptosis during in vitro cardiac ischemia-reperfusion in mice by inhibiting both JNK1/2 and P38 signaling pathways." Biochem Biophys Res Commun **473**(2): 551-557.
- Yang, X., et al. (2019). "Fatty Acids Enhance the Maturation of Cardiomyocytes Derived from Human Pluripotent Stem Cells." Stem Cell Reports **13**(4): 657-668.
- Yu, G., et al. (2012). "clusterProfiler: an R package for comparing biological themes among gene clusters." OMICS **16**(5): 284-287.
- Zhang, J., et al. (2017). "Functional characterization of human pluripotent stem cell-derived arterial endothelial cells." Proc Natl Acad Sci U S A **114**(30): E6072-E6078.
- Zhou, Q., et al. (2001). "Ablation of Cypher, a PDZ-LIM domain Z-line protein, causes a severe form of congenital myopathy." J Cell Biol **155**(4): 605-612.

CHAPTER 5

SINGLE CELL DETERMINATION OF CARDIAC MICROTISSUE STRUCTURE AND FUNCTION USING LIGHT SHEET MICROSCOPY

5.1. Introduction

Native cardiac tissue is comprised of heterogeneous cell populations that work cooperatively for proper tissue function; thus, engineered tissue models have moved toward incorporating multiple cardiac cell types in an effort to recapitulate native multicellular composition and organization. Cardiac tissue models comprised of stem cell-derived cardiomyocytes require inclusion of non-myocytes to promote stable tissue formation, yet the specific contributions of the supporting non-myocyte population on the parenchymal cardiomyocytes and cardiac microtissues have yet to be fully dissected. This gap can be partly attributed to limitations in technologies able to accurately study the individual cellular structure and function that comprise intact 3D tissues. The ability to interrogate the cell-cell interactions in 3D tissue constructs has been restricted by conventional optical imaging techniques that fail to adequately penetrate multicellular microtissues with sufficient spatial resolution. Light sheet fluorescence microscopy (LSFM) overcomes these constraints to enable single cell-resolution structural and functional imaging of intact cardiac microtissues. Multicellular spatial distribution analysis of heterotypic cardiac cell populations revealed that cardiomyocytes and cardiac fibroblasts were randomly distributed throughout 3D microtissues. Furthermore, calcium imaging of live cardiac microtissues enabled single-cell detection of cardiomyocyte calcium activity, which showed that functional heterogeneity correlated with spatial location within the tissues. This study demonstrates that LSFM can be utilized to determine single-cell spatial and functional interactions

of multiple cell types within intact 3D engineered microtissues, thereby facilitating the determination of structure-function relationships at both tissue-level and single-cell resolution.

5.2. *Materials and Methods*

5.2.1. Cardiac fibroblast cell culture

Human cardiac fibroblasts (CFs) were purchased from Cell Applications (lot #s 2584 & 3067; San Diego, CA) and cultured according to manufacturer's recommendations: fibroblasts were seeded onto non-coated TCPS plates at density of 1×10^4 cells/cm² and cultured in Cardiac Fibroblast Medium (Cell Applications) for up to 10 passages. CFs were passaged by incubating with 0.25% Trypsin-EDTA for 5min when cultures reached ~80% confluence.

5.2.2. Cardiomyocyte differentiation

Human induced pluripotent stem cells (hiPSCs) (WTC11 cells modified with GCaMP6f reporter in the AAVS1 safe harbor locus (Huebsch et al. 2015, Mandegar et al. 2016); generously donated by Dr. Bruce Conklin) were seeded onto Matrigel-coated (80µg/mL; Corning, Corning, NY) plates at a concentration of 3×10^4 cells/cm² in mTeSR1 medium (Stem Cell Technologies, Vancouver, CA) supplemented with 10µM ROCK inhibitor (Y-27632, SelleckChem, Houston, TX) for the first 24h. Differentiation of hiPSCs to cardiomyocytes was performed using a serum-free, chemically defined protocol (Lian et al. 2012, Lian et al. 2013). Briefly, once hiPSCs reached 100% confluence (~3-4 days; denoted as differentiation day 0), cells were fed with 12µM CHIR (SelleckChem) in RPMI1640 medium (Thermo Fisher, Waltham, MA) with B27 supplement without insulin (RPMI/B27-; Life Technologies, Grand Island, NY). After 24h, CHIR was removed by feeding with RPMI/B27- and on day 3, cells received a 48h-treatment with 5µM IWP2

(Tocris, Bristol, UK) in RPMI/B27-. Medium was then switched to RPMI1640 medium containing B27 supplement with insulin (RPMI/B27+; Life Technologies) and fed every 3 days thereafter. On day 15 of differentiation, hiPSC-CMs were re-plated onto Matrigel-coated plates at a density of 1×10^5 cells/cm² in RPMI/B27+ with 10 μ M ROCK inhibitor (see Appendix A for detailed protocol). Selection of CMs was achieved by lactate purification with two 2-day feedings with no-glucose Dulbecco's Modified Eagle Medium (Thermo Fisher) supplemented with 1X Non Essential Amino Acids (NEAA; Corning), 1X Glutamax (*L*-glut; Life Technologies), and 4mM Lactate) (Tohyama et al. 2013). After lactate selection, cultures were returned to RPMI/B27+ media and re-fed every 3 days thereafter with fresh media.

5.2.3. Cardiac microtissue formation

Lactate-purified hiPSC-CMs and primary human CFs were dissociated with 0.25% Trypsin for 10min to obtain a single-cell suspension, mixed at a 3:1 CM:CF ratio, and seeded into an array of inverted 400 μ m pyramidal microwells at a density of ~2000 cells per microwell (Hookway et al. 2016, Hookway et al. 2019). Cells self-assembled into 3D tissues over the course of 24h and were then transferred from the microwells to rotary orbital suspension culture at a density of ~4000 microtissues per 10cm Petri dish (~ 8×10^5 cells/mL) and maintained in RPMI/B27+ medium (Hookway et al. 2016) until analysis. See Chapter 2 for detailed protocol.

5.2.4. Immunofluorescence staining

Microtissues were fixed in 10% neutral-buffered formalin for 1h at RT and then washed 3x with PBS. Samples were permeabilized in 1.5% Triton X-100 (Sigma-Aldrich, St. Louis, MO) for 1h and blocked overnight at 4°C in 2% normal donkey serum and 0.1% Tween-20. Tissues

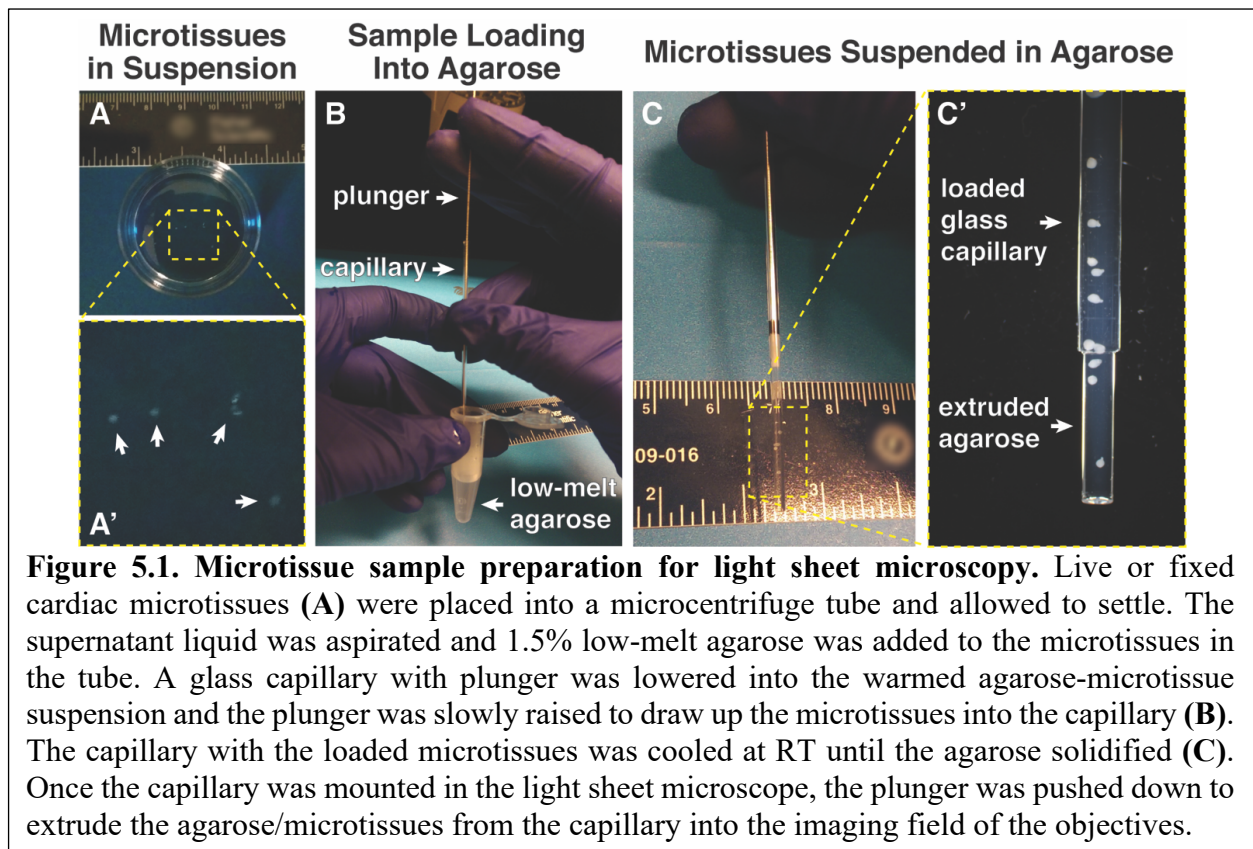
were incubated in primary antibody against GATA4 (1:50 dilution; Santa Cruz Biotechnology, Dallas, TX) overnight at 4°C, and counterstained with Alexa Fluor 555 (1:400; Thermo Fisher) and Hoechst (1:1000; Thermo Fisher) overnight at 4°C (Table 5.1 for antibody information).

Table 5.1. Wholemout immunostaining antibody information.

Antibody	Company	Catalog #	Dilution
GATA4	Santa Cruz Biotechnology	sc-25310	1:50
Alexa Fluor 555	Thermo Fisher	A-31572	1:400
Hoechst	Thermo Fisher	62249	1:1000

5.2.5. Structural light sheet microscopy

Cardiac microtissues stained for GATA4 and labeled with Hoechst were suspended in size 2 glass capillaries (Zeiss; ~1mm inner diameter) in 2% low-melt agarose (made up in PBS; IBI



Scientific, Dubuque, IA) immediately prior to imaging (Figure 5.1). The Zeiss z.1 light sheet microscope used for imaging was equipped with two PCO.edge sCMOS cameras, 10x 0.2 NA illumination lens, 20x 1.0 NA detection lens, and 488/647nm lasers for dual imaging. Cardiac microtissue samples ($n \geq 9$ per condition) were each imaged at three angles (120° rotations between views), and then stitched with multi-view reconstruction to provide isotropic resolution throughout the microtissue. Volumetric reconstruction and size analyses of the microtissues were performed using custom Matlab (R2019a) scripts (adapted from (Holekamp et al. 2008)).

5.2.6. Cell classification and spatial quantification

Imaris image analysis software (version 9.3.1) was used to identify labeled cell nuclei within the microtissues. Classification of cell identity was performed by determining co-localization of DAPI+ and GATA4+ nuclei. CMs were identified as GATA4+ nuclei whereas CFs were classified as cells with GATA4- nuclei. The spatial coordinates for each CM and CF were used to determine the multicellular arrangement within the microtissues. The numbers of nearest CM or CF neighbors (within a $20\mu\text{m}$ radius) for each CM were calculated using a custom python script to create 3D spatial maps of CM homotypic and heterotypic interactions. The nearest-neighbor calculation was performed across multiple CM+CF microtissues ($n=8$) to determine the distribution of proximal interactions. This empirical distribution was compared against a simulated distribution of randomly-dispersed CMs and CFs. CMs and CFs were simulated as $10\mu\text{m}$ -diameter hard spheres randomly dispersed inside a larger spherical volume, matching the empirical parameters of microtissue size (average CM+CF microtissue diameter of $165\mu\text{m}$; Figure 5.2) and multicellular composition (average of 400 CMs and 127 CFs per heterotypic microtissue; Figure 5.3). The simulation was performed using a custom python script to generate a random sequential

packing of hard spheres for the total number of cells within a volume (517), followed by proportional random assignment of cell identity as either CM (400/517) or CF (127/517) to each sphere (He et al. 1999). Code available at <https://github.com/david-a-joy/cm-microtissue-struct>.

5.2.7. Functional light sheet microscopy

5-10 live cardiac microtissues were suspended in size 2 glass capillaries in 2% low-melt agarose made up in Tyrode's solution (137mM NaCl, 2.7mM KCl, 1mM MgCl₂, 0.2mM Na₂HPO₄, 12mM NaHCO₃, 5.5mM D-glucose, 1.8mM CaCl₂; Sigma-Aldrich). Calcium handling properties were assessed in live cardiac microtissues by recording fluorescence intensity of GCaMP6f calcium indicator while tissues were maintained at 37°C. 3D calcium imaging stacks were imaged at ~120ms per frame and each z-spacing was 0.86µm per frame. Single optical sections (3-4µm light thickness) were excited at 488nm and imaged at ~20Hz for 52 seconds (1000 total frames). Regions of interest (ROIs) were manually selected for individual CMs, and normalized fluorescence intensity change ($\Delta F/F$) profiles were calculated for each calcium transient. A custom Matlab script was used to perform K-means clustering (k=2) on the calcium transient profiles to determine synchronously-active CM calcium profiles.

5.2.8. Statistics

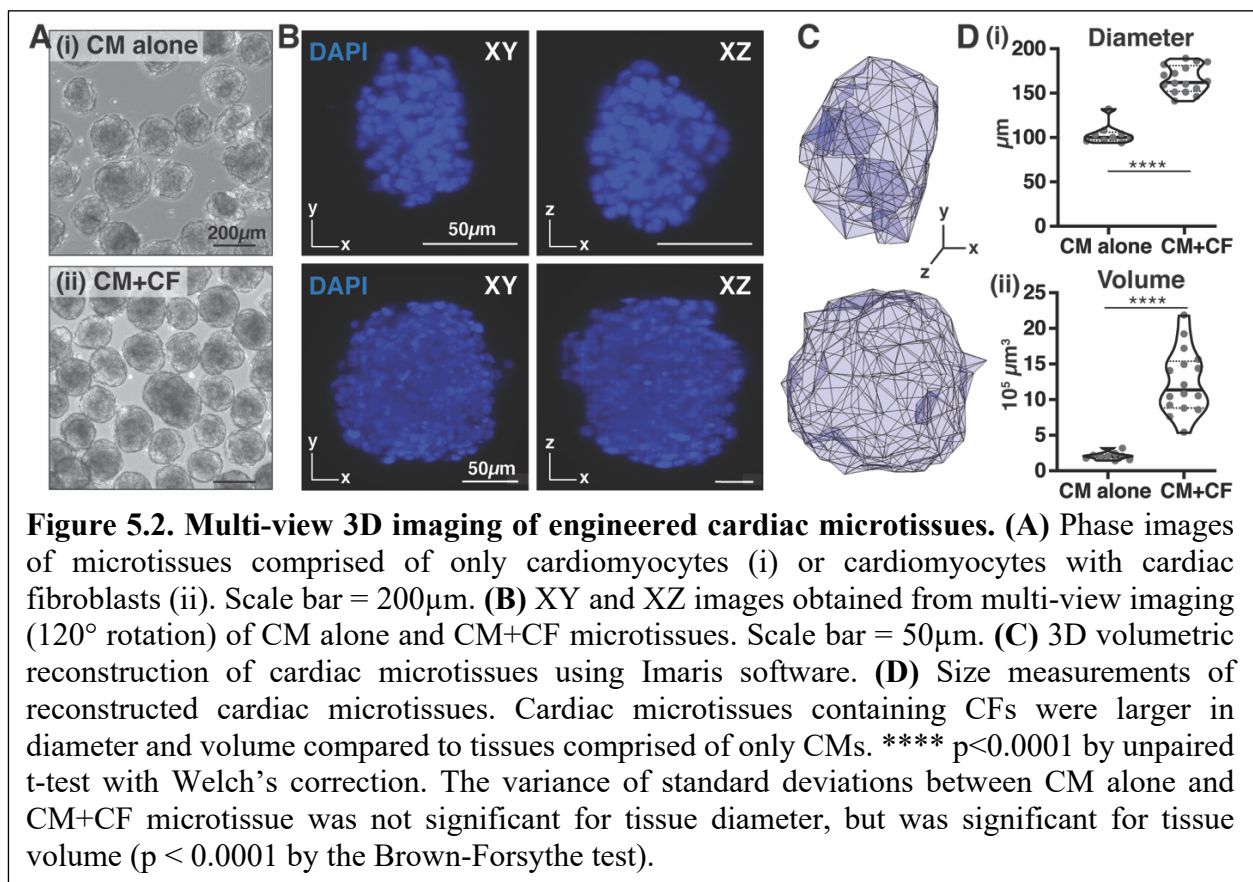
The mean and standard deviations for cardiac microtissue size analyses (Figure 5.2) were calculated for independent CM alone (n = 9) and CM+CF (n = 16) tissues. Statistical testing of diameter and volume means was performed using unpaired t-test with Welch's correction and variance of diameter and volume standard deviations was analyzed using the Brown-Forsythe test. A two-sided Kolmogorov-Smirnov (K-S) statistical test was performed to determine significance

between the empirical vs. simulated distributions of homotypic and heterotypic nearest neighbors (Figure 5.4E). The Brown-Forsythe statistical test was used to determine significance between the variance of inter-beat intervals between CM alone and CM+CF microtissues (Figure 5.5). All statistical tests were performed using SciPy (Virtanen et al. 2019) (version 1.3.1) with significance determined at $p < 0.05$.

5.3. Results

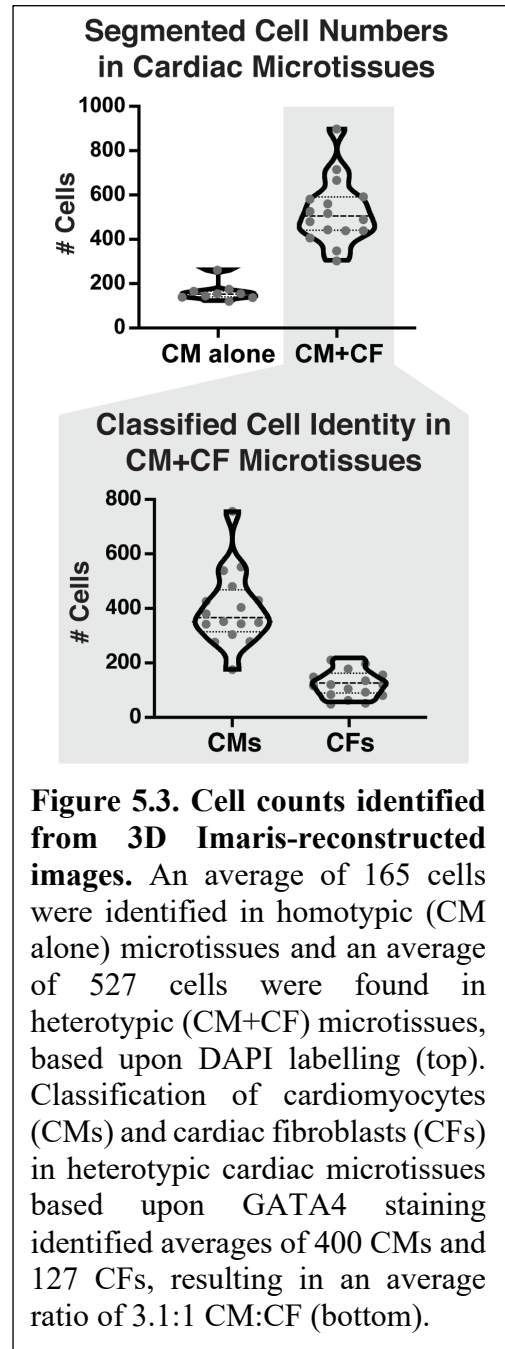
5.3.1. Multi-view light sheet imaging enables high resolution 3D reconstruction of cardiac microtissues

Cardiac microtissues comprised of either hiPSC-cardiomyocytes alone (CM alone; Figure 5.2A(i)) or hiPSC-CMs with cardiac fibroblasts (CM+CF; Figure 5.2A(ii)) were imaged at



multiple views (120° apart; lateral resolution = 0.5μm x 0.5μm; axial resolution = 3-4μm) in order to obtain improved and consistent resolution across the entire microtissue (Figure 5.2B). The resultant higher resolution imaging enabled accurate 3D volumetric renderings of individual microtissues (Figure 5.2C), which permitted calculation of tissue size and shape. Despite seeding the same number of total cells for both homotypic and heterotypic tissues, cardiac microtissues that contained CFs were ~60% larger in diameter and ~6-fold greater in volume than the CM alone microtissues (average diameter of 165μm vs. 103μm with p-value = 1.80×10^{-10} ; average volume of $12.5 \times 10^5 \mu\text{m}^3$ vs $2.1 \times 10^5 \mu\text{m}^3$ with p-value = 1.08×10^{-7} ; Figure 5.2D), though CM alone cardiac microtissues were more consistent in their size as compared to CM+CF microtissues (respective volume standard deviations of $\pm 0.5 \times 10^5 \mu\text{m}^3$ compared to $\pm 4.3 \times 10^5 \mu\text{m}^3$; p-value = 0.002 by Brown-Forsythe test of volume variance, with

statistical significance determined at $p = 0.05$). Identification of DAPI-labeled cells by Imaris image analysis revealed an average of 165 cells in the CM alone microtissues compared to 527 cells in the heterotypic CM+CF microtissues (Figure 5.3).



5.3.2. Localization of labeled cells allows for cell identity classification and intercellular spatial analyses

Multi-view imaging for different fluorescent channels was performed to identify CMs (GATA4+ nuclei; Figure 5.4A(ii)) from all cells (GATA4- nuclei; Figure 5.4A(i)) and individual cells were segmented using Imaris image analysis software to identify the *in situ* location of individual cells (Figure 5.4B). Therefore, the classification of cell identity with respect to 3D spatial location within the microtissue was determined by combining localization information for the different cell types. CMs were identified as cells with GATA4+ nuclei while CFs were classified as cells with GATA4- nuclei (Figure 5.4C). Furthermore, counts of classified CMs and CFs across analyzed heterotypic cardiac microtissues revealed that the seeding ratio of 3:1 CMs:CFs was maintained through culture and image analysis (Figure 5.3). Taken together, the image analysis pipeline of multi-view reconstruction, cell localization, and identity classification resulted in 3D spatial mapping of CMs and CFs in each microtissue.

The interrogation of heterogeneous cellular packing within cardiac microtissues could be derived from the 3D spatial mapping of CMs and CFs. Heterotypic (CM+CF) cardiac microtissues were utilized in order to study intercellular interactions between different pairings of cell types (i.e. homotypic (CM-CM) versus heterotypic (CM-CF) interactions). The local density of homotypic and heterotypic neighbors was determined for each individual CM (Figure 5.4D). On average, each CM was located adjacent to 6-8 CMs and 1-2 CFs within a 20 μ m radius. Furthermore, looking at the spatial distribution of the interactions across 3D microtissues revealed that homotypic interactions (yellow-to-red heatmap range; Figure 5.4D(i)) were greater in the center of the tissue compared to the edge, while heterotypic CM-CF interactions were generally consistent throughout the microtissues (blue-green heatmap range; Figure 5.4D(ii)). To assess the

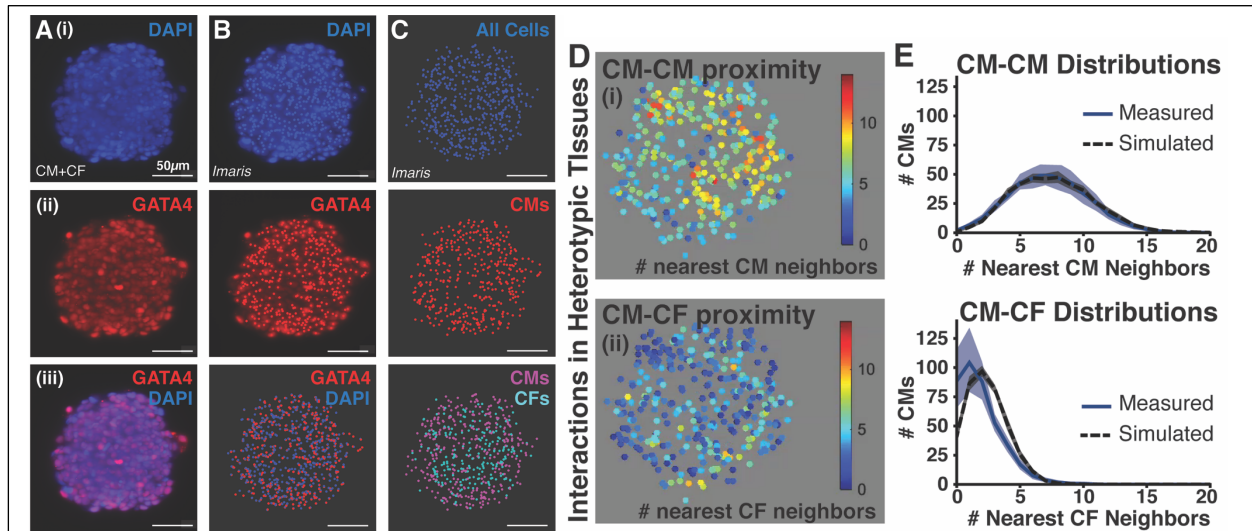


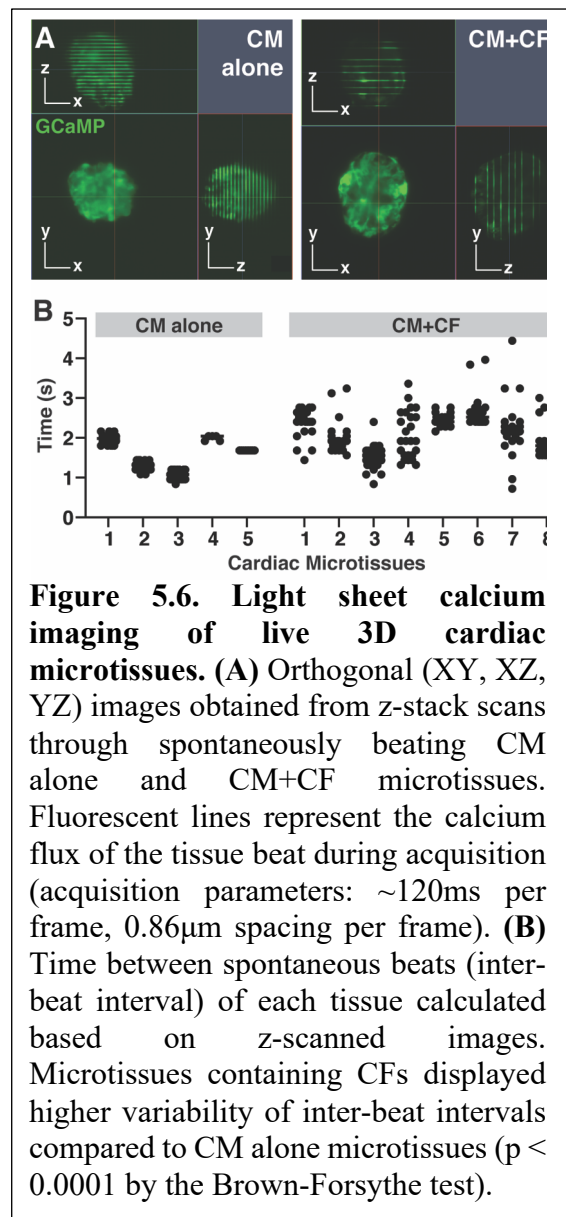
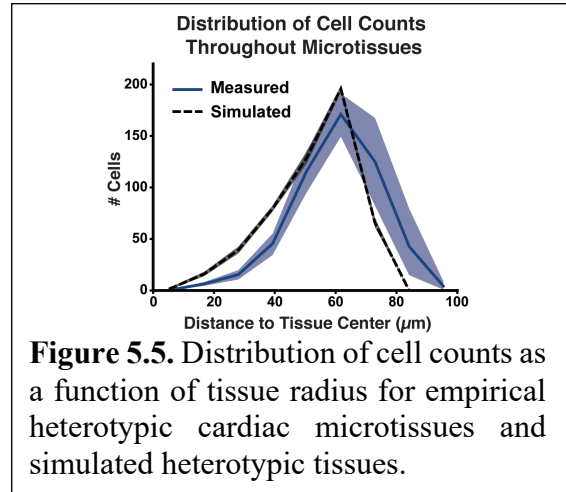
Figure 5.4. *In situ* cell classification enables cell-specific spatial quantification of heterotypic CM+CF microtissues. (A) Maximum intensity projections of multi-view images were obtained for microtissues with labeled nuclei (DAPI; i), GATA4 staining (ii), and merged channels (iii). Scale bar = 50µm. (B) Nuclear localization (with Imaris image analysis software) within maximum intensity projection multi-view images of a microtissue with DAPI-labeling (i), GATA4-staining (ii), and merged (iii). (C) Cell classification based on nuclear localization of DAPI (marking all cells) and GATA4 (identifying CMs). GATA4+ nuclei were classified as CMs (ii) whereas GATA4- nuclei were classified as CFs (iii). (D) Number of nearest homotypic (CM-CM; i) and heterotypic (CM-CF; ii) neighbors for each CM in the heterotypic CM+CF microtissue. (E) Measured distributions of numbers of CM (i) and CF (ii) nearest neighbors matched that of a simulated tissue model of randomly-distributed CMs and CFs, indicating that CFs were randomly distributed throughout CMs in the empirical microtissues.

extent to which CMs and CFs were distributed in a random or biased manner throughout the microtissues, the empirical distributions of nearest homotypic and heterotypic neighbors were compared to a simulated model of well-mixed, randomly-dispersed heterotypic tissues that matched empirical tissue size and cellular composition (Figure 5.4E). The simulated distribution curves indicated that CMs should be surrounded by 6-8 CMs and 2-3 CFs on average. The empirical and simulated nearest-neighbor distributions were not significantly different as determined by two-sided K-S test, indicating that the CFs in the imaged heterotypic microtissues were randomly dispersed among the CMs. The K-S value for homotypic (CM-CM) distribution analysis was 0.0264 and the K-S value for heterotypic (CM-CF) distribution analysis was 0.1630, where $K-S > 1.224$ indicates a statistically significant difference between the two distributions (p

< 0.05). Furthermore, radial distribution of cells throughout the empirical imaged tissues did not differ significantly from the simulated tissue model (K-S = 0.2386; Figure 5.5). Therefore, Imaris analysis detected cells at the microtissue center just as well as at the tissue edge, indicating that the accuracy of cell detection did not diminish despite attenuation of imaging resolution with increasing tissue depth.

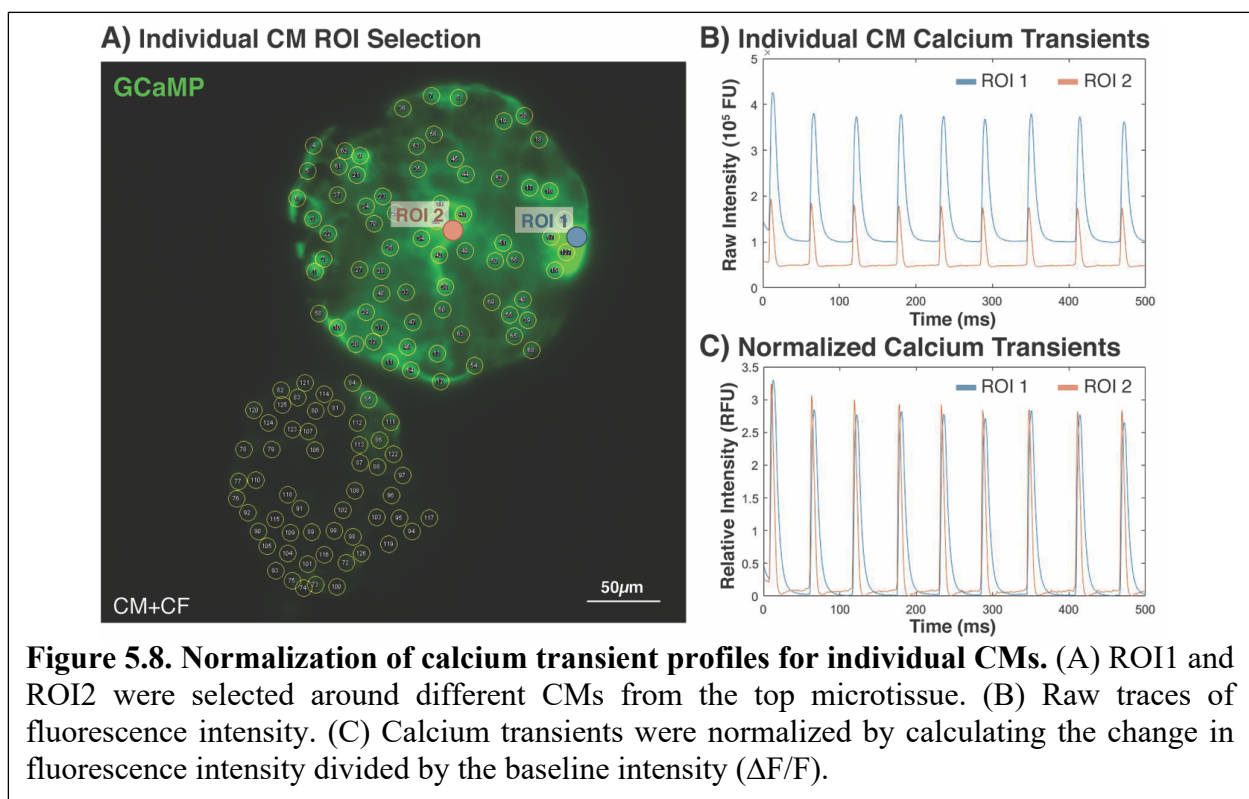
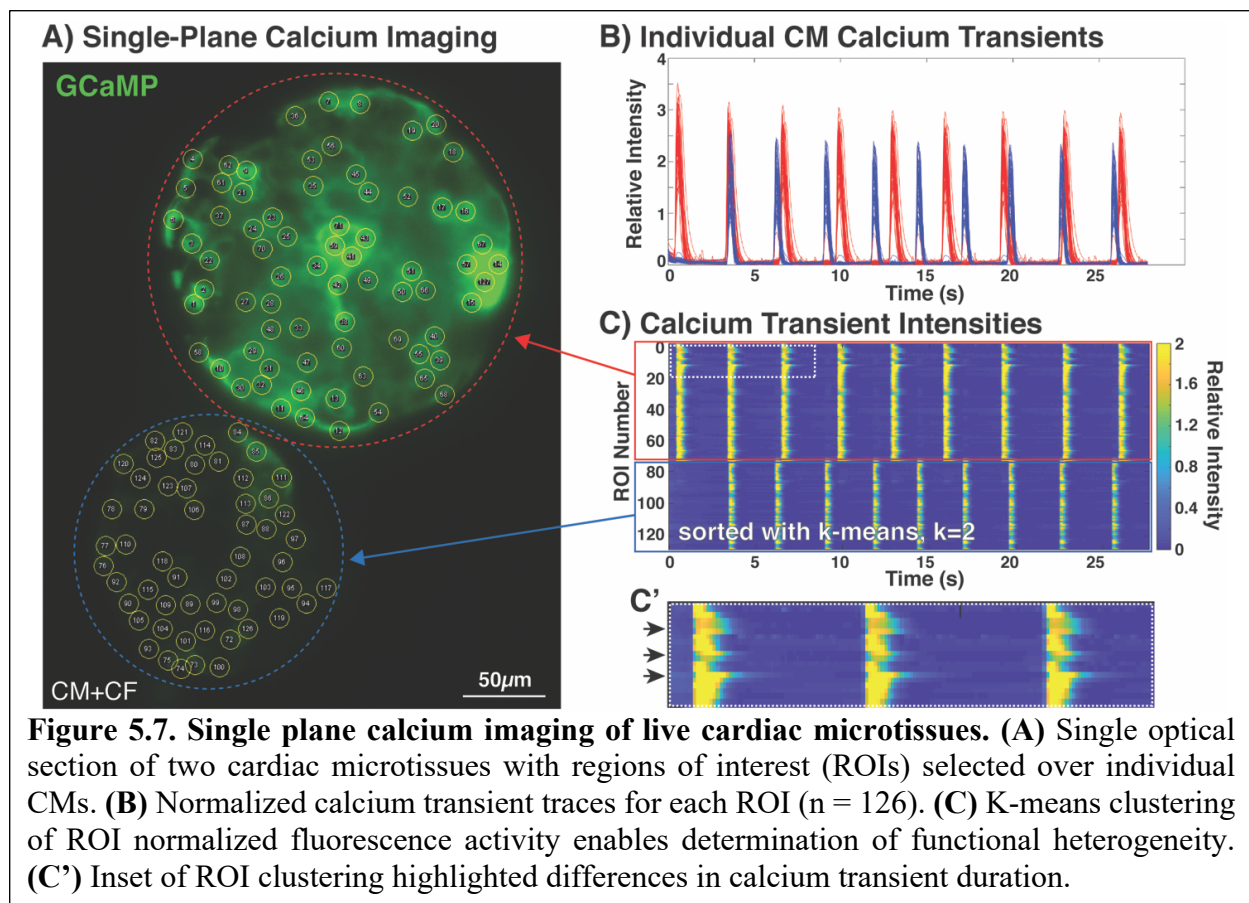
5.3.3. Live light sheet calcium imaging enables detection of functional heterogeneity between engineered cardiac microtissues

In order to study functional synchrony within individual tissues as a result of multicellular composition, calcium imaging of live cardiac microtissues was performed. Microtissues comprised of hiPSC-CMs expressing a genetically-encoded calcium indicator, GCaMP6f, enabled direct visualization of synchronicity of calcium handling activity throughout tissues, as well as individual CM calcium fluxes within single optical sections. The periodicity of spontaneous calcium



propagation was determined by z-stack imaging through cardiac microtissues. Combining the known z-scan rate with the measured distance between beats (fluorescent lines indicating GCaMP6f signal) in the orthogonal (XZ/YX) views of the image (Figure 5.6A) enabled the determination of inter-beat time interval for each microtissue (Figure 5.6B). Microtissues comprised of only CMs beat more periodically than the microtissues containing CFs, as exhibited by the smaller variation in the CM alone inter-beat intervals compared to the more widespread values of the CM+CF tissues (inter-beat interval standard deviation of ± 0.095 ms for CM alone microtissues and ± 0.447 ms for CM+CF tissues; p -value = 6.865×10^{-9} by Brown-Forsythe test of inter-beat interval variance, with statistical significance determined at $p = 0.05$). The orthogonal views of z-stack calcium activity displayed distinct lines of GCaMP6f fluorescence that transected the entirety of the CM alone microtissue (Figure 5.6A), suggesting that CMs within the single z-plane were typically firing in synchrony and therefore the variation in inter-beat interval periodicity was due to time rather than space. The GCaMP6f lines transecting the CM+CF microtissues exhibited some breaks in the fluorescence, likely indicating the presence of CFs in those particular locations.

In order to quantitatively determine the synchronicity of calcium transients of individual CMs within the microtissues, a time series of a single optical section within the microtissues was captured at ~ 20 Hz. The two CM+CF microtissues in the same optical field of view beat spontaneously but independently from one another. ROIs for individual CMs were selected in both tissues (Figure 5.7A) and the normalized fluorescence intensity traces of each ROI were plotted; calcium traces from the top tissue are depicted in red and the lower tissue traces are depicted in blue (Figure 5.7B, Figure 5.8). Unbiased k-means clustering grouped CMs with similar calcium transients. The clustered calcium traces partitioned entirely with respect to the microtissues they



originated from, indicating that CMs from the two tissues fired at independent times and rates from one other (Figure 5.7C). However, although CMs within the individual tissues fired synchronously, differences in calcium transient duration varied, even among CMs in close proximity to one another (Figure 5.7C', arrows) sustained longer calcium traces than their neighbors. Therefore, this analysis platform demonstrates that regional analysis of individual CM calcium transients can be used to assess functional heterogeneity as it relates to spatial location.

5.4. Discussion

This study interrogated the structural and functional information of intact 3D engineered cardiac microtissues at single-cell resolution. The methods described establish a powerful toolkit to better dissect *in situ* multicellular heterogeneity and the impacts of organization on function. Light sheet fluorescence microscopy was used to map 3D tissue structure by segmenting, localizing, and classifying distinct cardiac cell populations. Use of LSM also enabled imaging of multiple live cardiac tissues in a rapid manner to assess functional tissue synchrony as well as detect individual cell functional variation at different depths and spatial locations within intact engineered tissues.

Constructing a tissue-level representation from cells imaged at single-cell resolution provided an accurate model of engineered microtissue surface terrain and volumetric shape information. Although spatial resolution was greatest at the exterior edges of the tissues and gradually declined towards the center, single-plane imaging at different depths of individual tissues confirmed the presence of cells distributed throughout the interior. The addition of clearing and refractive index-matching processes could improve the attenuation of resolution with depth of imaging (Chung et al. 2013, Boothe et al. 2017, Dekkers et al. 2019). However, despite decreased

spatial resolution at the center of imaged microtissues, detection of cells by computational segmentation did not change based on tissue radius, thereby highlighting the ability of LSM to accurately capture 3D multicellular density *in situ*.

3D volumetric reconstruction of cardiac microtissues allowed for tissue-scale size analyses. Conventional methods to quantify tissue size include 2D cross-sectional measures of tissue slices as well as standard light microscopy image analysis tools, but these approaches are limited to measures along one plane. 3D reconstructions from the imaged cellular constituents therefore retain more accurate size and shape information. The heterotypic CM+CF cardiac microtissues were larger than the homotypic CM microtissues despite identical initial seeding conditions, suggesting that CFs impact tissue formation and culture. In the native heart, CFs interact with CMs directly via physical adhesion molecules and indirectly via secretion and organization of the surrounding extracellular matrix (ECM) (Camelliti et al. 2006, Zhang et al. 2012, Zeng et al. 2013, Cartledge et al. 2015, Rother et al. 2015). These CF-mediated methods of intercellular interactions could potentially account for the larger heterotypic microtissue size distinction by more strongly promoting the adhesion of cells in the initial tissue formation phase, ultimately leading to larger numbers of cells assembling into the microtissue constructs. The distinct tissue-level structural differences between microtissue compositions was further analyzed at single-cell resolution by quantifying multicellular organization within the microtissues, in order to determine whether the addition of a stromal population changed the CM interaction properties.

Identification of cell number and identity was performed on the heterotypic (CM+CF) microtissues to compare to the initial seeding conditions. Although CMs and CFs were mixed at a 3:1 ratio and seeded at a total of 2000 cells per tissue, an average of only ~500 cells were identified in the heterotypic microtissues, but the ratio of CMs to CFs was retained at an average of 400 CMs

to 127 CFs (~3:1 CM:CF). The lower-than-expected cell numbers were likely due to lack of total incorporation of all 2000 cells during the initial tissue formation step—which is to be expected (Nguyen et al. 2014, Hookway et al. 2016, Hookway et al. 2019). However, the maintained ratio of the heterogeneous cardiac cell populations allowed for the interrogation of intra-tissue spatial interactions. Cell identity was classified based on positive or negative staining for GATA4, a nuclear cardiac marker, along with DAPI labeling of individual nuclei in order to identify CMs. Specific phenotypic markers for CFs are particularly challenging (Furtado et al. 2016, Pinto et al. 2016), therefore, a subtractive method was used to distinguish CFs from CMs in the microtissues. Alternatively, constitutive expression of a fluorescent protein could be used to label non-myocytes prior to tissue formation, thereby improving longitudinal analyses of multicellular, heterotypic interactions. Based on cell identity classification and spatial localization of cells within heterotypic microtissues, CFs appeared to be randomly distributed among the CMs. Furthermore, random-dispersion simulations confirmed that pockets slightly enriched for heterotypic (CM-CF) interactions arise spontaneously in randomly mixed cardiac microtissues, suggesting a mechanism for multicellular CF organization driven by stochastic inhomogeneity in the initial cell mixture. This multicellular spatial analysis is important as it can be used to determine cell-specific localization biases within complex organizational tissue structures. Furthermore, this platform for quantifying spatial organization can be extended to interrogate the multicellular interactions of more complex engineered microtissue constructs, such as those that contain more three or more tissue-specific cell types (Richards et al. 2017).

The ability to dissect structure-function-phenotype relationships at the single-cell level within engineered tissue constructs would advance understanding of how multicellular spatial arrangements impact functional heterogeneity. With increased access to and improved robustness

of single cell RNA sequencing technologies, studying tissue transcriptional phenotypes at the single cell level has become increasingly widespread (Butler et al. 2018, Svensson et al. 2018), yet most assessments of tissue function are still analyzed at the bulk tissue-level. This study, however, used LSM to describe novel methods for imaging live cardiac tissue functional properties at single-cell resolution. Since GCaMP6f was used to visualize calcium transients, no exogenous dye was needed for imaging, though this method is compatible with the use of fluorescent calcium and action potential dyes. In order to assess tissue-level functional synchrony before focusing in on individual cell activity, calcium imaging of live cardiac microtissues was first acquired by scanning through the microtissue at a fixed z-stack rate. The orthogonal imaging views (XZ, YZ) displayed fluorescent lines when the tissues beat during the z-stack acquisition, which allowed the periodicity of beat rate to be determined. While the individual tissues had different intrinsic average beat rates, the variance of inter-beat intervals (time between sequential beats) was lower in the CM alone microtissues compared to the inter-beat interval variance of CM+CF microtissues. Since cardiac tissue calcium dynamics are too fast to acquire full volumetric renderings via z-scanning, time series acquisition of single optical sections acquired at multiple z-positions throughout the tissue was needed to determine 3D connectivity network of calcium activity. Fixed plane calcium imaging also allowed for the assessment of calcium handling function at single-cell resolution within the engineered cardiac microtissues.

Although the CM calcium activity between independent tissues differed with respect to spontaneous beat rate, the calcium transients of individual CMs were largely synchronous within any single cross-section of heterotypic cardiac microtissues. Unbiased k-means clustering of individual CM calcium transients identified cells that behaved most similarly to one another. CM function was linked to spatial location by correlating the grouped calcium transients back to the

specific CMs from which the traces were derived. Therefore, this method is uniquely poised to answer questions related to spatially-distinct functional heterogeneity within engineered constructs. For example, a pacemaker-like cell population within cardiac tissue could be detected by identifying the cells that originate calcium or action potential propagations. The ability to dissect the heterogeneity of cellular structure-function would be a powerful tool for the study of certain cardiac diseases. For example, conductive disorders, such as long QT syndrome (LQTS) and catecholaminergic polymorphic ventricular tachycardia (CPVT), induce abnormal heart rhythms due to ion channelopathies (Napolitano et al. 2012). Spatial mapping of 3D engineered tissue models of LQTS or CPVT, created from primary and/or iPSC-derived cells, could be used to examine the mechanisms responsible for the dysregulation of action potential and calcium transient propagation associated with the pathology.

Current limitations in the functional imaging acquisition pipeline preclude 3D calcium imaging of the entire microtissues at single-cell resolution. While single planes within tissues can be imaged at 20Hz, it takes several seconds to image an entire z-stack at the fastest acquisition rate. This acquisition speed limitation could potentially be overcome by acquiring high-speed single plane time series every few micrometers apart within the tissue followed by post-imaging stitching of these frames, ultimately constructing a 3D network of functional propagation—a method known as post acquisition synchronization (Weber et al. 2017). Another challenge is that additional in-depth quantitative assessments of calcium handling properties could not be determined using the Zeiss z.1 microscope. The calcium response of cardiac tissues to electrical stimulation at increasing frequencies reveals the relative maturity level of cardiomyocyte contractile machinery. However, electrical stimulation could not be performed due to steric constraints of the metallic chamber used in the light sheet microscope; therefore, using a non-

metallic chamber could potentially circumvent this limitation. Other methods of stimulation, such as optogenetic (Bjork et al. 2017, Li et al. 2017) as opposed to voltage- or current-driven, could also be incorporated to control CM contractility and eliminate intrinsic differences in beat rate between independent tissues.

Altogether, this study demonstrates the ability to interrogate the structural and functional properties of intact, dense, 3D microtissues at single-cell resolution. Analogous to how single-cell RNA sequencing has led to significant advances in understanding the phenotypic heterogeneity within complex multicellular environments, single-cell imaging enabled by LSM will improve the coupling of spatial organization and functional heterogeneity within engineered tissues. Ultimately, the convergence of parallel advances in complementary single-cell technologies will lead to a more comprehensive view of the individual contributions of heterotypic cells to integrated properties at the tissue-level.

5.5. Conclusions

This study built on the previous idea of linking single-cell measures to tissue-level properties. However, light sheet fluorescence microscopy allowed for these single-cell measures to be acquired *in situ*, enabling the dissection of structural, functional, and phenotypic properties of individual heterotypic cells within intact 3D cardiac microtissues. Here we detailed the methods for classifying multiple cell types within a tissue based on cell type-specific markers and the types of multicellular organization quantification made possible because of the identified cell types and positional information. We further demonstrated that calcium transients of individual cardiomyocytes can be visualized within an interior plane of the tissue, enabling the study of functional heterogeneity within cardiac microtissues. The main caveat of this study was that the

light sheet microscope we used did not have the fastest acquisition speed, topping out at 10 frames per second. When compared to the microscope that we use for bulk calcium imaging, which reaches 100 frames per second, the slower speed of the LSMF meant that calcium transient shape information could not be readily analyzed (and therefore kinetic parameters could not be quantified). In response, a colleague, Dr. Ana C. Silva, traveled to Janelia Research Campus to use their SiMView (Simultaneous Multiview Light Sheet Microscope) to image calcium handling function within intact cardiac microtissues at much faster speeds.

5.6. *Bibliography*

- Bjork, S., et al. (2017). "Evaluation of Optogenetic Electrophysiology Tools in Human Stem Cell-Derived Cardiomyocytes." Front Physiol **8**: 884.
- Boothe, T., et al. (2017). "A tunable refractive index matching medium for live imaging cells, tissues and model organisms." Elife **6**.
- Butler, A., et al. (2018). "Integrating single-cell transcriptomic data across different conditions, technologies, and species." Nat Biotechnol **36**(5): 411-420.
- Camelliti, P., et al. (2006). "Structural and functional coupling of cardiac myocytes and fibroblasts." Adv Cardiol **42**: 132-149.
- Cartledge, J. E., et al. (2015). "Functional crosstalk between cardiac fibroblasts and adult cardiomyocytes by soluble mediators." Cardiovasc Res **105**(3): 260-270.
- Chung, K., et al. (2013). "Structural and molecular interrogation of intact biological systems." Nature **497**(7449): 332-337.
- Dekkers, J. F., et al. (2019). "High-resolution 3D imaging of fixed and cleared organoids." Nat Protoc **14**(6): 1756-1771.
- Furtado, M. B., et al. (2016). "View from the heart: cardiac fibroblasts in development, scarring and regeneration." Development **143**(3): 387-397.
- He, D., et al. (1999). "Computer simulation of random packing of unequal particles." Phys Rev E Stat Phys Plasmas Fluids Relat Interdiscip Topics **60**(6 Pt B): 7098-7104.
- Holekamp, T. F., et al. (2008). "Fast three-dimensional fluorescence imaging of activity in neural populations by objective-coupled planar illumination microscopy." Neuron **57**(5): 661-672.

- Hookway, T. A., et al. (2016). "Aggregate formation and suspension culture of human pluripotent stem cells and differentiated progeny." Methods **101**: 11-20.
- Hookway, T. A., et al. (2019). "Phenotypic Variation Between Stromal Cells Differentially Impacts Engineered Cardiac Tissue Function." Tissue Eng Part A **25**(9-10): 773-785.
- Huebsch, N., et al. (2015). "Automated Video-Based Analysis of Contractility and Calcium Flux in Human-Induced Pluripotent Stem Cell-Derived Cardiomyocytes Cultured over Different Spatial Scales." Tissue Eng Part C Methods **21**(5): 467-479.
- Li, Q., et al. (2017). "Electrophysiological Properties and Viability of Neonatal Rat Ventricular Myocyte Cultures with Inducible ChR2 Expression." Sci Rep **7**(1): 1531.
- Lian, X., et al. (2012). "Robust cardiomyocyte differentiation from human pluripotent stem cells via temporal modulation of canonical Wnt signaling." Proc Natl Acad Sci U S A **109**(27): E1848-1857.
- Lian, X., et al. (2013). "Directed cardiomyocyte differentiation from human pluripotent stem cells by modulating Wnt/beta-catenin signaling under fully defined conditions." Nat Protoc **8**(1): 162-175.
- Mandegar, M. A., et al. (2016). "CRISPR Interference Efficiently Induces Specific and Reversible Gene Silencing in Human iPSCs." Cell Stem Cell **18**(4): 541-553.
- Napolitano, C., et al. (2012). "Sudden cardiac death and genetic ion channelopathies: long QT, Brugada, short QT, catecholaminergic polymorphic ventricular tachycardia, and idiopathic ventricular fibrillation." Circulation **125**(16): 2027-2034.
- Nguyen, D. C., et al. (2014). "Microscale generation of cardiospheres promotes robust enrichment of cardiomyocytes derived from human pluripotent stem cells." Stem Cell Reports **3**(2): 260-268.

- Pinto, A. R., et al. (2016). "Revisiting Cardiac Cellular Composition." Circ Res **118**(3): 400-409.
- Richards, D. J., et al. (2017). "Inspiration from heart development: Biomimetic development of functional human cardiac organoids." Biomaterials **142**: 112-123.
- Rother, J., et al. (2015). "Crosstalk of cardiomyocytes and fibroblasts in co-cultures." Open Biol **5**(6): 150038.
- Svensson, V., et al. (2018). "Exponential scaling of single-cell RNA-seq in the past decade." Nat Protoc **13**(4): 599-604.
- Tohyama, S., et al. (2013). "Distinct metabolic flow enables large-scale purification of mouse and human pluripotent stem cell-derived cardiomyocytes." Cell Stem Cell **12**(1): 127-137.
- Virtanen, P., et al. (2019) SciPy 1.0--Fundamental Algorithms for Scientific Computing in Python. arXiv e-prints
- Weber, M., et al. (2017). "Cell-accurate optical mapping across the entire developing heart." Elife **6**.
- Zeng, Q. C., et al. (2013). "Cardiac fibroblast-derived extracellular matrix produced in vitro stimulates growth and metabolism of cultured ventricular cells." Int Heart J **54**(1): 40-44.
- Zhang, P., et al. (2012). "Cross talk between cardiac myocytes and fibroblasts: from multiscale investigative approaches to mechanisms and functional consequences." Am J Physiol Heart Circ Physiol **303**(12): H1385-1396.

CHAPTER 6

MODULATING CARDIOMYOCYTE-CARDIAC FIBROBLAST INTERACTIONS IN ISOGENIC HETEROTYPIC CARDIAC MICROTISSUES

6.1. Introduction

Robust differentiation protocols for the derivation of cardiomyocytes (CMs) and endothelial cells (ECs) from human pluripotent stem cells (hPSCs) have been established for a number of years, while the derivation of cardiac fibroblasts (CFs) was not described until recently. Looking to the developmental origins of native CFs provided a framework to develop differentiation processes for different subtypes of CFs: Zhang et al. mimicked the epicardial-derived nature of the largest CF population in the heart that populates the ventricles (Zhang et al. 2019), while Zhang et al. pushed their cardiac progenitor cells through a second heart field state before deriving CFs, more similar to the endocardial-derivation of native CFs that end up in the atria and valves (Zhang et al. 2019).

The creation of these different CF subtype differentiations enabled the formation of entirely stem cell-derived, and therefore the possibility of isogenic, cardiac microtissues. We found that the different subtypes of hPSC-CFs similarly supported heterotypic cardiac microtissue function. In order to gain a deeper mechanistic understanding of the interactions between CMs and CFs, we knocked down gap junction connexin 43 in the CFs before forming isogenic heterotypic cardiac microtissues and found that silencing GJA1 attenuated microtissue calcium handling ability. Further utilizing these strategies of modulating cardiac cell types in conjunction with 3D microtissue models of defined heterotypic pairings will improve understanding of the multicellular interactions in the heart necessary for tissue homeostasis and proper function.

6.2. *Materials and Methods*

6.2.1. *Cardiomyocyte differentiation*

WTC11-GCaMP6f hiPSCs (Mandegar et al. 2016) were differentiated into cardiomyocytes (CMs) following the GiWi protocol (Lian et al. 2012, Lian et al. 2013). Briefly, hiPSCs were seeded onto Matrigel-coated (80 μ g/mL) plates at a density of 3×10^4 cells/cm² in mTeSR medium with 10 μ M Rock inhibitor. Once cells reached 100% confluence (~3 days), medium was changed to RPMI1640 with B27 supplement without insulin (R/B-) supplemented with 12 μ M CHIR99021 (differentiation day 0). Exactly 24 hours later, cells were fed with fresh R/B- and on day 3, medium was changed to R/B- supplemented with 5 μ M IWP2. On days 7,10, and 13, cells were fed with RPMI1640 with B27 supplement containing insulin (R/B+). On day 15, cells were replated onto Matrigel-coated plates at a density of 2×10^5 cells/cm² in R/B+ containing 15% FBS and 10 μ M Rock inhibitor (see Appendix A for detailed protocol). Medium was changed to fresh R/B+ on day 16. Enrichment of CMs occurred by feeding cells with lactate purification medium (Tohyama et al. 2013) (no-glucose Dulbecco's Modified Eagle Medium with 1X Non Essential Amino Acids, 1X Glutamax, and 4mM Lactate) on days 17 and 20, and cells were returned to R/B+ on day 23 and used for cardiac microtissues between days 25 and 28.

6.2.2. *Differentiation of hiPSC-cardiac fibroblasts from epicardial cells*

Epicardial-derived cardiac fibroblasts (EpiC-CFs) were derived by first following an established protocol differentiating epicardial cells from hiPSCs (Bao et al. 2017). Briefly, day 6 cells from the GiWi CM differentiation were singularized with Accutase and seeded onto Matrigel-coated plates at a density of 2×10^4 - 8×10^4 cells/cm² in LaSR medium (advanced DMEM/F12 with

0.06g/L L-ascorbic acid 2-phosphate sesquimagnesium salt hydrate and 12.5 mL GlutaMAX) supplemented with 5 μ M ROCK inhibitor. On days 7 and 8, cells were treated with 3 μ M CHIR99021 in LaSR medium and on days 9-11, cells were fed with fresh LaSR medium. On day 12, epicardial cells were singularized with Accutase for 5 minutes at 37°C and replated in LaSR medium supplemented with A8301 (R&D Systems) and 5 μ M ROCK inhibitor. Epicardial cells were fed daily with LaSR supplemented with A8301 until they reached 90-100% confluency. Epicardial cells were then passaged using Versene into fresh LaSR medium plus A8301 for up to five passages. Cells were validated to be >90% WT1-positive by flow cytometry. To derive CFs from the epicardial cells, the 90-100% confluent epicardial cells were fed daily with LaSR medium plus 5ng/mL bFGF for 10 days. CFs were dissociated with Accutase and replated into TCPS plates at ~7,000 cells/cm² in FibroGRO medium (Millipore Sigma). SHF-CFs were validated to be >80% double-positive for TE-7 and vimentin by flow cytometry.

6.2.3. Differentiation of hiPSC-cardiac fibroblasts from second heart field-like progenitors

Second heart field-derived cardiac fibroblasts (SHF-CFs) were differentiated following the GiFGF protocol, as previously published (Zhang et al. 2019). Briefly, hiPSCs were seeded at 1.5x10⁴ cells/cm² in mTeSR1 medium; once they reached 100% confluency, they were treated with 12 μ M CHIR99021 in R/B- medium (day 0). 24 hours later, media was changed to fresh R/B- (day 1). From days 2-20, cells were fed every 2 days with cardiac fibroblast basal media (CFBM) supplemented with 75ng/mL bFGF. On day 20, CFs were singularized with Accutase for 10 minutes and replated at ~7,000 cells/cm² onto TCPS plates in FibroGRO medium. Following this, FibroGRO media was changed every two days until the fibroblasts reached approximately 80-90%

confluency when they were passaged with Accutase. SHF-CFs were validated to be >80% double-positive for TE-7 and vimentin by flow cytometry.

6.2.4. Primary human cardiac fibroblast culture

Primary cardiac fibroblasts isolated from human fetal tissue (fCFs; Cell Applications lot # 2584) were cultured according to manufacturer recommendations. Briefly, cells were seeded and passaged at a density of 1×10^4 cells/cm², and fed with FibroGRO Medium every 2-3 days, for up to 10 passages.

6.2.5. DOX-inducible GJA1 knockdown in hiPSCs via CRISPRi

The generation of the GJA1 CRISPRi line (made by Ashley R.G. Libby and David A. Joy) first involved TALEN-mediated insertion of the CRISPRi cassette pAAVS1-NDi-CRISPRi (Gen2) (Addgene) into the AAVS1 locus of the Allen Institute's WTC11-LaminB hiPSC line. Following antibiotic selection of clones that received the CRISPRi cassette, CRISPRi gRNAs were generated targeting GJA1 using the Broad Institute GPP Web Portal and cloned into the gRNA-CKB (Addgene) following the previously described protocol (Libby et al. 2018). Guide RNA vectors were nucleofected into the LaminB CRISPRi hiPSC line using a P3 Primary Cell 96-well Nucleofector Kit (Lonza) and the 4D Nucleofector X Unit (Lonza) following manufacturer's instructions. Nucleofected cells were allowed to recover in mTeSR medium supplemented with 10 μ M Rock inhibitor and then underwent antibiotic selection with 10 μ g/mL blasticidin (ThermoFisher Scientific), as previously described (Mandegar et al. 2016, Libby et al. 2018). Knockdown efficiency was evaluated by addition of doxycycline (DOX) to the daily feeding media for 5 days, collection of mRNA, and subsequent quantification of gene expression by qPCR.

6.2.6. GJA1 knockdown in hiPSC-cardiac fibroblasts

CFs were differentiated from the GJA1 CRISPRi hiPSC line following the second heart field derivation process (see section 6.2.3). To induce knockdown in the CFs, DOX was started on differentiation day 0 and added at every feed thereafter. mRNA from differentiating cells was collected on days 0, 3, 6, 10, and 20 from the differentiations that received DOX-treatment as well as from day 20 cells that did not receive DOX (control group).

6.2.7. Cardiac microtissue formation

Lactate-purified CMs and CFs (EpiC-CFs, SHF-CFs, fCFs, or hPSC-CF_{KD}) were dissociated with 0.25% Trypsin for 5-10 minutes and then mixed together at a ratio of 3:1 CMs:CFs in R/B+ medium with 10 μ M Rock inhibitor. The heterotypic cell mixtures were seeded into 400 μ m inverted pyramidal agarose microwells at a density of 2000 cells per microwell and incubated overnight to allow cells to self-assemble into 3D microtissues. 18-24 hours later, the microtissues were removed from the microwells and transferred to low-attachment plates in R/B+ medium. Microtissues were maintained in rotary suspension culture at a density of 8000 tissues per 10cm plate for 10 days, and fed every 2-3 days with R/B+ medium. See Chapter 2 for detailed protocol.

6.2.8. Calcium imaging

Cardiac microtissues cultured for 10 days were incubated in Tyrode's solution (137 mM NaCl, 2.7 mM KCl, 1 mM MgCl₂, 0.2 mM Na₂HPO₄, 12 mM NaHCO₃, 5.5 mM D-glucose, 1.8mM CaCl₂) for 30 minutes at 37°C immediately prior to imaging. A Zeiss Axio Observer Z1 inverted microscope equipped with a Hamamatsu ORCA-Flash 4.0 camera was used for image

acquisition. Electrical field stimulation of 1Hz was applied to the samples by placing electrodes in the Tyrode's bath containing the microtissues (MyoPacer, IonOptix). Calcium transient videos were acquired using Zen Professional software (v.2.0.0.0) at 10ms exposure and 100 frames per second. Circular regions of interest (ROI; 65-pixel diameter) were selected at the center of each microtissue and mean fluorescence intensity values were plotted against time. Metrics of calcium transient kinetics, such as amplitude, time-to peak, upstroke and downstroke velocities, and beat rate, were analyzed using a custom python script.

6.2.9. Statistics

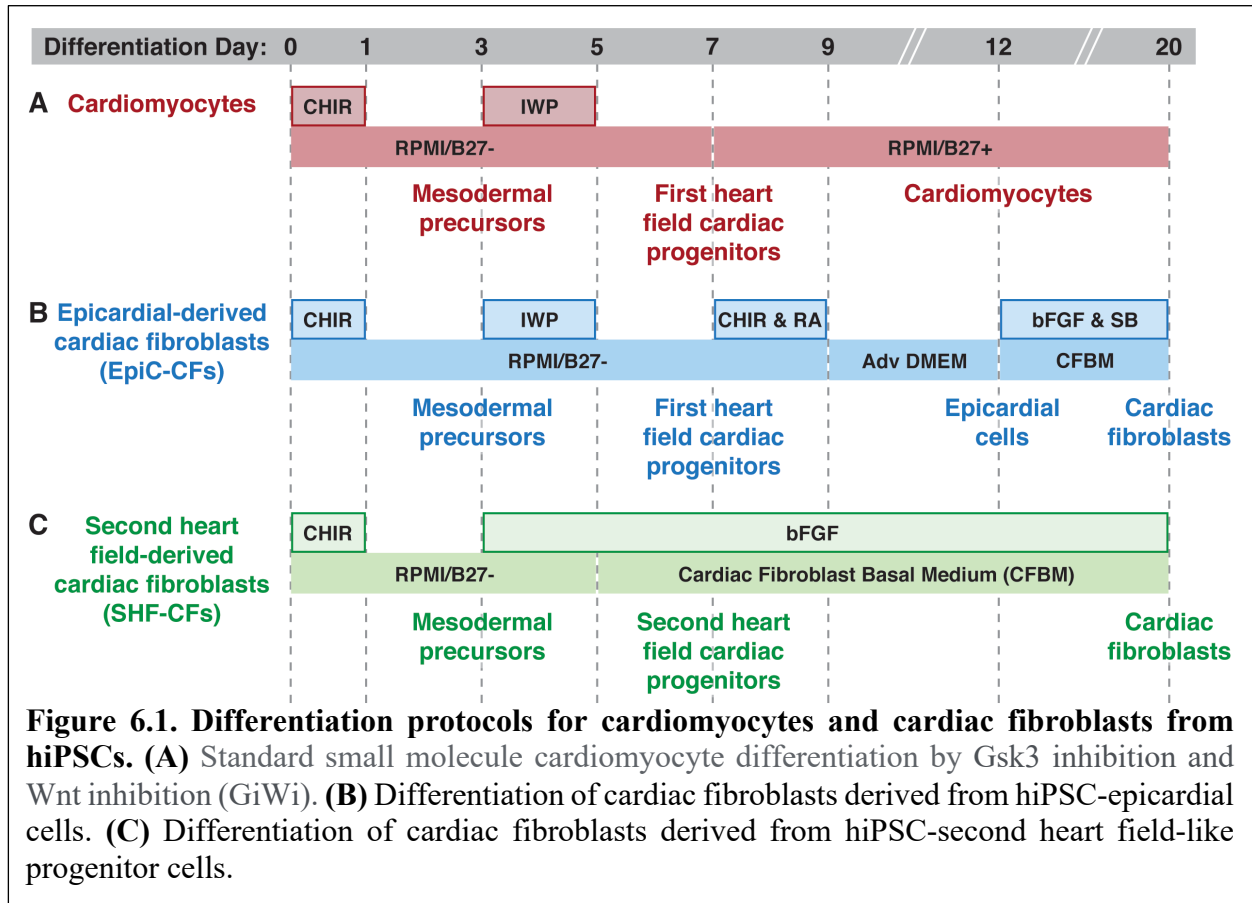
For the calcium analysis of hPSC-CFs, one-way analysis of variance (ANOVA) followed by Tukey's post hoc analysis was performed to compare mean of the four tissue groups, where each group contained a minimum of 67 biological replicates. For the calcium analysis of GJA1 KD-CFs, unpaired t-test was performed to compare mean of the two tissue groups, where each group contained a minimum of 15 biological replicates. For all comparisons, statistical significance was determined at $p < 0.05$. All statistical analysis was performed using GraphPad Prism 8.0 software.

6.3. Results

6.3.1. Derivation of subtype-specific cardiac fibroblasts from human pluripotent stem cells

The standard GiWi cardiomyocyte differentiation protocol (Figure 6.1A) was adapted in order to derive cardiac fibroblasts from hPSCs. Two derivation pathways were followed that mimicked the developmental processes of different subtypes of CFs. Epicardial-derived CFs (EpiC-CFs) were generated by first pushing the cardiac progenitor cells (first heart field-like

cardiac progenitors) to an epicardial cell fate before coaxing them to CFs with basic fibroblast growth factor (bFGF) (Figure 6.1B) while CFs more akin to endocardial-derived CFs were produced by pushing the mesodermal precursor cells to a second heart field-like cardiac progenitor state before exposing them to bFGF to generate CFs (SHF-CFs; Figure 6.1C).



6.3.2. Cardiac fibroblasts promote robust cardiac microtissue assembly

Engineered cardiac microtissues were formed from a heterotypic mixture of cardiomyocytes and cardiac fibroblasts in order to study how EpiC-CFs and SHF-CFs supported CM function compared to primary human fetal CFs (fCFs). The same pool of enriched CMs was used for all microtissue groups, indicating that any differences in tissue formation and function were due to the different sources of fibroblasts and their ability to interact with CMs. The highly-

pure population of enriched CMs did not form into tissues after 24 hours, instead resulting only in a few small clumps of aggregated cells (Figure 6.2B,C). In contrast, all microtissues that contained CFs self-assembled into 3D spheroids within 24 hours of seeding into microwell molds (Figure 6.2B,C), indicating that a stromal component is necessary to facilitate robust microtissue assembly. The heterotypic cardiac microtissues compacted after removal from the microwell molds, as demonstrated by the more distinct tissue boundaries and increasingly spheroidal shape 3 days after tissue formation (Figure 6.2D) compared to 1 day after (Figure 6.2C), and stably persisted throughout the 10 days of

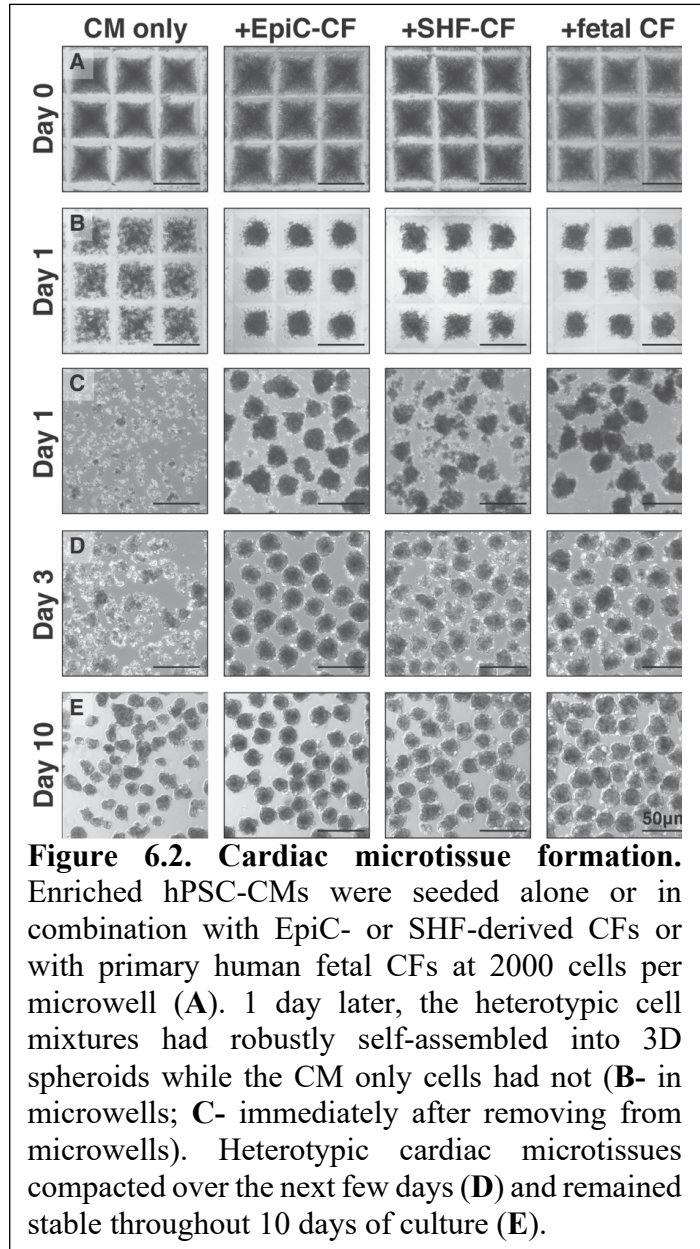
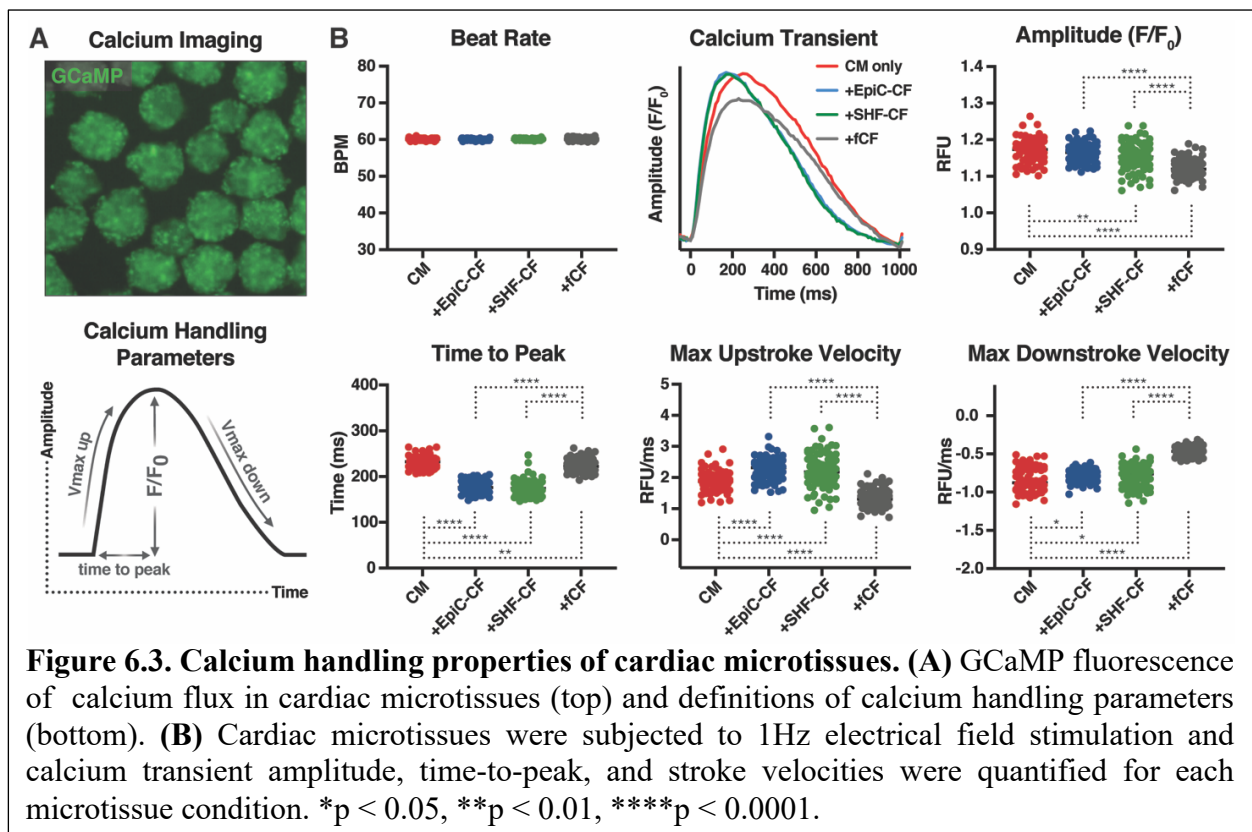


Figure 6.2. Cardiac microtissue formation. Enriched hPSC-CMs were seeded alone or in combination with EpiC- or SHF-derived CFs or with primary human fetal CFs at 2000 cells per microwell (A). 1 day later, the heterotypic cell mixtures had robustly self-assembled into 3D spheroids while the CM only cells had not (B- in microwells; C- immediately after removing from microwells). Heterotypic cardiac microtissues compacted over the next few days (D) and remained stable throughout 10 days of culture (E).

microtissue culture. The CM only microtissues appeared more stable with increased culture duration, likely because those that persisted throughout culture contained the small fraction of non-myocyte cells that carried over from the CM differentiation and enrichment.

6.3.3. Cardiac fibroblast source does not impact heterotypic cardiac microtissue calcium handling

Calcium handling properties of the engineered cardiac microtissues were assessed in order to determine whether different cardiac fibroblast subtypes alter CM function. Day 10 microtissues (Figure 6.2E) were subjected to 1Hz electrical field stimulation in order to eliminate intrinsic differences in beat rate between the individual tissues (Figure 6.3). Video-based imaging of the fluorescence intensity of the genetically-encoded calcium sensor GCaMP6f in the CMs enabled quantification of the kinetic parameters of the microtissues' calcium transients. There was no statistical significance between any of the calcium handling properties from microtissues made with EpiC-CFs compared to those made with SHF-CFs, indicating that the hPSC-CF subtypes equally supported hPSC-CM function. The amplitude values of the calcium transients from the +EpiC-CF and +SHF-CF microtissues were similar to that of the hPSC-CM only microtissues and



slightly higher than the values of the microtissues containing primary fCFs (Figure 6.3). The microtissues comprised of the hPSC-CFs displayed the fastest upstroke kinetic properties, taking the shortest time to reach the peak of the calcium transient and exhibiting the fastest maximum upstroke velocities. The maximum downstroke velocities followed the same trend as the amplitude values, where the CM only, CM+EpiC-CF, and CM+SHF-CF microtissues exhibited similar velocity values and were all faster than the CM+fCF microtissues. Overall, these data indicate the different subtypes of hPSC-CFs behave similarly to one another and to primary human fetal CFs.

6.3.4. GJA1 knockdown in cardiac fibroblasts attenuates calcium handling function

GJA1 CRISPRi hiPSCs were differentiated to CFs following the second heart field-like derivation process (Figure 6.1C). Doxycycline (DOX) treatment to induce knockdown of gap junction GJA1 was started at differentiation day 0 and fresh DOX was added to the media at every

feed. mRNA samples from 2 biological replicates (independent differentiations) were collected on days 0, 3, 6, 10, and 20 of the differentiation and compared to day 20 hPSC-CFs that never received Dox treatment. Rapid knockdown was achieved in a matter of days, with <20% mRNA expression at differentiation day 3 and <1% expression at day 20

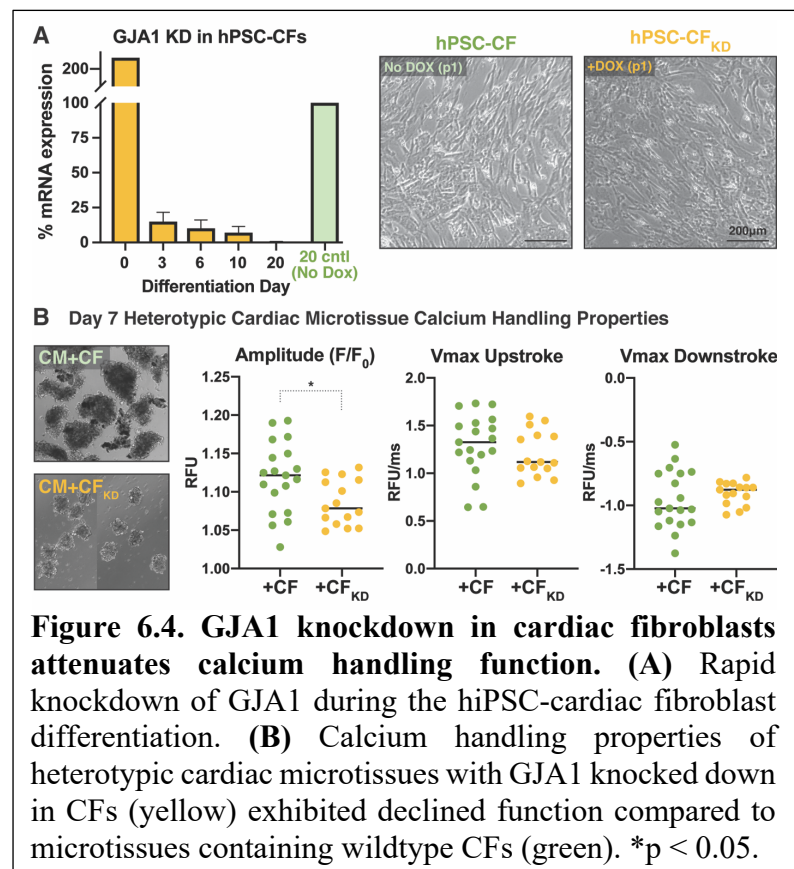


(Figure 6.4A). Cardiac microtissues were formed from enriched CMs mixed with either hPSC-CFs that did not receive DOX treatment (control) or those that did and therefore had GJA1 knocked down (+CF_{KD}). Calcium imaging was performed 7 days after microtissue formation, and cardiac microtissues containing GJA1 knockdown in the CFs displayed significantly decreased amplitude values as well as slower upstroke and downstroke maximum velocities (though the variance was rather large), indicating decreased calcium handling ability (Figure 6.4B).

6.4. Conclusions

In this study, we were finally able to generate engineered cardiac microtissues with entirely stem cell-derived cellular constituents. Two descriptions of cardiac fibroblast differentiations were published within a few months of each other that derived CFs from hPSCs through different cardiac progenitor states, one from second heart field-like progenitors (Zhang et al. 2019) and the other from first heart field epicardial cells (Zhang et al. 2019). These differentiation protocols not only enabled the study of entirely isogenic tissues, but also allowed us to study how different subtypes of CFs behave within engineered heterotypic cardiac microtissues.

This question motivated a collaboration between our lab and the labs of Sean Palecek, PhD and Timothy Kamp, MD, PhD at the University of Wisconsin, Madison. Using hPSC-CFs from the Palecek Lab (epicardial-derived CFs; EpiC-CFs) and the Kamp lab (second heart field-derived CFs; SHF-CFs), we formed cardiac microtissues and analyzed the ability of the different hPSC-CFs to support calcium handling function compared to one another and compared to primary human fetal CFs. Overall, we found that all microtissue groups behaved similarly, which was to be expected based on comprehensive characterization of the different CF populations performed by our collaborators, who determined that the different hPSC-CF subtypes were phenotypically

similar to each other and to fCFs more so than primary adult CFs. The CM only microtissues exhibited similar functional properties to the microtissues with +hPSC-CFs likely because the CM only microtissues that were able to stably persist throughout the 10 days of culture contained the small non-myocyte carry-over from the CM differentiation and enrichment. Though the differences were slight, the heterotypic cardiac microtissues containing the hPSC-derived CFs demonstrated faster kinetic properties compared to microtissues containing primary fetal cardiac fibroblasts, perhaps indicating that the ‘age-matching’ or ‘source-matching’ between heterotypic hPSC-cell types facilitated improved performance. Lastly, our previous studies (Chapter 3) demonstrated that non-cardiac-specific hiPSC-derived fibroblasts (teratoma- and embryoid body-outgrowth cells) did not support heterotypic cardiac microtissue formation and function (though primary human CFs did), therefore, the cardiac-specific derivation process of these hPSC-CFs was necessary for the robust formation and function of engineered cardiac microtissues. Furthermore, the ability to generate different subtypes of CFs mirrors a number of current studies aiming to generate different subtypes of CMs (i.e. ventricular, atrial, nodal). Once robust CM subtype differentiations are established, isogenic CM and CF subtypes can be paired in cardiac microtissues in order to potentially study chamber-specific functional phenotypes.

One of the main benefits of using hPSC-derived CFs in our engineered microtissues (besides isogenic matching) was that we could leverage hiPSC genome editing strategies. Inducible knockdown of specific genes via CRISPRi in the CFs enabled us to study how key players in CM-CF interactions affected tissue function. Connexin 43 is implicated as one of the most prominent gap junctions electrically connecting CMs and CFs in the heart. When we knocked down GJA1 in the hPSC-CFs and generated microtissues from these modulated CFs, we found that the cardiac microtissues made with CF_{KD} demonstrated declined calcium handling ability

compared to tissues made with the same hPSC-CFs that did not receive the inducible GJA1 knockdown treatment. This finding was recently confirmed in another cardiac heterotypic interactions study (Giacomelli et al. 2020). Giacomelli et al. silenced connexin 43 in hPSC-CFs (with short hairpin RNA) and combined the modulated cells with hPSC-CMs and hPSC-ECs in spheroidal cardiac microtissues. They found that contraction duration decreased with the use of CF_{KD} and other CM maturation properties, such as sarcomere organization, were adversely altered.

In conclusion, this strategy of modulating one or multiple cell types in fully-defined, isogenic microtissue constructs enables a mechanistic study of key interactors between heterotypic cell types, further contributing to our understanding of native multicellular interactions, which are difficult to probe *in vivo*.

6.5. *Bibliography*

- Bao, X., et al. (2017). "Directed differentiation and long-term maintenance of epicardial cells derived from human pluripotent stem cells under fully defined conditions." Nat Protoc **12**(9): 1890-1900.
- Giacomelli, E., et al. (2020). "Human-iPSC-Derived Cardiac Stromal Cells Enhance Maturation in 3D Cardiac Microtissues and Reveal Non-cardiomyocyte Contributions to Heart Disease." Cell Stem Cell.
- Lian, X., et al. (2012). "Robust cardiomyocyte differentiation from human pluripotent stem cells via temporal modulation of canonical Wnt signaling." Proc Natl Acad Sci U S A **109**(27): E1848-1857.
- Lian, X., et al. (2013). "Directed cardiomyocyte differentiation from human pluripotent stem cells by modulating Wnt/beta-catenin signaling under fully defined conditions." Nat Protoc **8**(1): 162-175.
- Libby, A. R., et al. (2018). "Spatiotemporal mosaic self-patterning of pluripotent stem cells using CRISPR interference." Elife **7**.
- Mandegar, M. A., et al. (2016). "CRISPR Interference Efficiently Induces Specific and Reversible Gene Silencing in Human iPSCs." Cell Stem Cell **18**(4): 541-553.
- Tohyama, S., et al. (2013). "Distinct metabolic flow enables large-scale purification of mouse and human pluripotent stem cell-derived cardiomyocytes." Cell Stem Cell **12**(1): 127-137.
- Zhang, H., et al. (2019). "Generation of Quiescent Cardiac Fibroblasts From Human Induced Pluripotent Stem Cells for In Vitro Modeling of Cardiac Fibrosis." Circ Res **125**(5): 552-566.

Zhang, J., et al. (2019). "Functional cardiac fibroblasts derived from human pluripotent stem cells via second heart field progenitors." Nat Commun **10**(1): 2238.

CHAPTER 7

FUTURE CONSIDERATIONS

7.1. Altering the timing of cardiac heterotypic interactions

The methodology we followed in forming our fully-defined heterotypic tissue models relied on the input of highly-purified or enriched populations of cell types in order to accurately dictate the relative proportions of cell types in the tissues. Robustly achieving high efficiency hPSC differentiations remains an ongoing challenge and typically requires an exogenous selection step, such as fluorescence-activated or magnetic-activated cell sorting. Throughout the studies presented here, we employed a metabolic method of enriching for hPSC-derived cardiomyocytes (CMs), which involved replacing glucose in the culture medium with lactate. Since only cardiomyocytes can survive this metabolic shift, the other non-myocyte contaminants in the differentiation died, resulting in cultures that were generally comprised of 85-95% cardiac troponin T-positive cells. However, since this metabolic enrichment process only works with committed cardiomyocytes, by the time the cardiomyocytes were enriched and were ready for use in tissues, the cells were at day 25 of differentiation at the earliest (and typically between 30-35 days of differentiation). Therefore, all of our heterotypic cardiac microtissue studies used these relatively aged cardiomyocytes at the outset of tissue formation.

Seminal work looking at electrical conditioning of cardiac microtissues has found that the most mature cardiac tissue condition at the endpoint was the one that received the longest electrical stimulation but also was made from early cardiomyocytes (day 12) as opposed to late cardiomyocytes (day 28) (Ronaldson-Bouchard et al. 2018). This study suggests a state of cardiomyocyte plasticity, during which the cells are more receptive to external cues. Therefore, it

would be interesting to look at the effects of heterotypic ‘conditioning’ on different stages of cardiomyocytes in our self-assembled tissue constructs, in order to determine whether early exposure of cardiomyocytes to non-myocytes will result in more substantial phenotypic and functional differences. Doing so while also selecting for cardiomyocytes at early differentiation time points remains challenging. One promising direction to follow is differentiating cells in an hPSC line that contains antibiotic (blasticidin) resistance under the cardiac-specific MYH6 gene. Blasticidin treatment can be started as early as differentiation day 7, and preliminary results in our hands have shown drastic improvement in cardiomyocyte selection, from 50% cTnT+ cells to 90% cTnT+ cells after 5-7 days of treatment.

7.2. Increasing the heterotypic complexity of engineered cardiac microtissues

The bi-typic nature of the cardiac microtissue studies in this dissertation stripped the multicellular tissue components down to the simplest, and therefore best controlled, form. Physiologically-relevant cell pairings were utilized in order to extract cell type-specific differences in the ways in which cardiac fibroblasts (CFs) versus endothelial cells (ECs) supported cardiomyocyte fate and function, but in order to build an engineered tissue model that more accurately mimics the native myocardium, more than two cardiac cell types need to be incorporated into future tissue constructs. More groups across the field of cardiac tissue engineering are starting to build tri-culture microtissues, with one study recently demonstrating that the function of self-assembled 3D cardiac spheroids was improved in tissues made from CMs+CFs compared to CMs+ECs, and even further improved in tissues made from CMs+CFs+ECs compared to just CMs+CFs (Giacomelli et al. 2020).

Furthermore, incorporation of an immune cell population into heterotypic cardiac microtissues is starting to gain traction, especially in the current landscape of the global SARS-CoV-2 pandemic. Resident macrophages in the heart are thought to have cardioprotective and ultimately anti-inflammatory effects under pathological conditions (Fujiu and Nagai 2013, Fujiu et al. 2014, Swirski et al. 2016). Adding these immune cells into CM+CF or CM+CF+EC microtissues will enable studies dissecting the specific impacts that immune cells have in maintaining tissue homeostasis or in disease states, for example in microtissues made from CMs and activated CFs.

7.3. Concluding remarks

The results of this dissertation significantly contribute to the fields of tissue engineering and cardiac biology by establishing an engineered microtissue platform to extensively characterize the changing interactions between multiple cardiac cell types in 3D. We not only studied how non-myocyte or stromal cell identity impacts cardiomyocyte fate and cardiac tissue function, but we also combined advanced technologies in unique ways to examine how changes in single-cell properties affect tissue-level parameters. We brought it all together by engineering entirely-isogenic cardiac microtissues with genome editing capabilities to further dissect the mechanisms of electromechanical interactions between heterotypic cardiac cell types.

7.4. Bibliography

Fujiu, K. and R. Nagai (2013). "Contributions of cardiomyocyte-cardiac fibroblast-immune cell interactions in heart failure development." Basic Res Cardiol **108**(4): 357.

Fujiu, K., et al. (2014). "Cardioprotective function of cardiac macrophages." Cardiovasc Res **102**(2): 232-239.

Giacomelli, E., et al. (2020). "Human-iPSC-Derived Cardiac Stromal Cells Enhance Maturation in 3D Cardiac Microtissues and Reveal Non-cardiomyocyte Contributions to Heart Disease." Cell Stem Cell.

Ronaldson-Bouchard, K., et al. (2018). "Advanced maturation of human cardiac tissue grown from pluripotent stem cells." Nature **556**(7700): 239-243.

Swirski, F. K., et al. (2016). "Development and Function of Arterial and Cardiac Macrophages." Trends Immunol **37**(1): 32-40.

APPENDIX A

CARDIOMYOCYTE ENRICHMENT PROTOCOL

The following protocol provides step-by-step instructions that we have optimized for the replating of committed hPSC-derived cardiomyocytes (~day 15) and lactate purification to metabolically enrich for the cardiomyocyte fraction of the heterogeneous differentiation.

Materials & Reagents:

10cm tissue culture polystyrene (TCPS) plates

Growth Factor Reduced Matrigel: diluted to 80 μ g/mL in Knockout DMEM

0.25% Trypsin

Fetal bovine serum (FBS)

ROCK inhibitor

RPMI1640 medium + B27 supplement with insulin

Conical tubes

100 μ m sterile filters

Hemocytometer

DPBS without calcium/magnesium

Sodium L-lactate powder

1M HEPES

100X Glutamax

100X Non Essential Amino Acids

DMEM w/o glucose and sodium pyruvate

Preparation:

1. In a 50mL conical tube, add 2.2412g of lactate to 18mL of 1M HEPES solution in sterile conditions. Invert the tube up and down to dissolve the lactate.
2. Allow solution to settle for a couple of minutes at room temperature. Dissolve all clumps. Filter through a 22 μ m filter.
3. Store as 1mL aliquots of 1M lactate solution at -20°C.
4. Prepare lactate purification medium (final lactate concentration of 4mM):

In 500mL DMEM w/o glucose and sodium pyruvate, add:

5mL 100X Non Essential Amino Acids,

5mL 100X Glutamax

2mL of 1M lactate solution

5. Filter lactate purification medium through a 22 μ m filter.

Methods: Replating hPSC-CMs for the purpose of enrichment should be done with committed CMs, typically differentiation day 15, though it can be performed a day or two earlier (if differentiation efficiency is high) or up to 5 days later.

1. Coat 10cm TCPS plates with ~5mL of 80 μ g/mL Growth Factor Reduced Matrigel and store at 37°C for at least 2 days (don't let the Matrigel dry out on the plates).
2. Add 0.25% Trypsin to the CM differentiation plates (2mL per 6-well or 1mL per 12-well) and incubate for 20 minutes. Gently triturate after 10 minutes.
3. Collect cells and quench with 20% FBS with 10 μ M ROCK inhibitor. Make sure to rinse out well-plates to ensure all cells are collected.
4. Centrifuge quenched cell at 200g for 3 minutes.
5. Aspirate supernatant.

6. Resuspend in R/B+ with 15% FBS and 10 μ M ROCK inhibitor.
7. Filter cells through 100 μ m pore size filters.
8. Count cells with hemocytometer.
9. Aspirate Matrigel from the 10cm plates and wash with PBS.
10. Seed 10-15 million CMs per 10cm plate in R/B+ with 15% FBS and 10 μ M ROCK inhibitor (10mL media per plate). Gently shake plates side-to-side and front-to-back to evenly distribute cells within the plate.

NOTE: Exact seeding density depends on differentiation efficiency at the time of replating. Patchy beating in the wells indicates a lower differentiation efficiency, and therefore should be seeded at the higher end of the range (because more non-myocytes will be removed during the enrichment step), while robust beating/higher efficiency differentiations can be replated at a lower density because there are less non-myocytes to remove.

11. 24 hours after seeding, feed with R/B+ (10mL per plate).
12. 48 hours later, feed cells with lactate purification medium (10mL per plate). This first treatment lasts for 3 days.
13. 3 days after first lactate purification feed, refresh the lactate purification medium (10mL per plate). This second treatment lasts for 2 or 3 days (depending on efficiency at time of replate: lower efficiency = 3 day treatment, higher efficiency = 2 day treatment).
14. Return cells to R/B+ after second lactate purification treatment.
15. Feed cells every 3 days thereafter with R/B+.
16. When using enriched CMs for experiments, dissociate with 0.25% Trypsin for 5-10 minutes. Save a portion of cells (~500k) for flow cytometry for cTnT to determine the differentiation efficiency of the enriched cells.

Publishing Agreement

It is the policy of the University to encourage open access and broad distribution of all theses, dissertations, and manuscripts. The Graduate Division will facilitate the distribution of UCSF theses, dissertations, and manuscripts to the UCSF Library for open access and distribution. UCSF will make such theses, dissertations, and manuscripts accessible to the public and will take reasonable steps to preserve these works in perpetuity.

I hereby grant the non-exclusive, perpetual right to The Regents of the University of California to reproduce, publicly display, distribute, preserve, and publish copies of my thesis, dissertation, or manuscript in any form or media, now existing or later derived, including access online for teaching, research, and public service purposes.

DocuSigned by:

Oriane Matheys

A667CF7C28454C2...

Author Signature

12/1/2020

Date